NAVAL POSTGRADUATE SCHOOL

THESIS

MULTI ANGLE IMAGING WITH SPECTRAL REMOTE SENSING FOR SCENE CLASSIFICATION

by

Sunyaruk Prasert

March 2005

Thesis Advisor:	Richard C. Olsen
Second Reader:	William J. Welch

Approved for public release; distribution is unlimited

THIS PAGE INTENTIONALLY LEFT BLANK

REPORT DOCUMENTATION PAGE			Form Approved OMB No. 0704-0188
Public reporting burden for this collection of information is estimated to average 1 hour per response, including the time for reviewing instruction, searching existing data sources, gathering and maintaining the data needed, and completing and reviewing the collection of information. Send comments regarding this burden estimate or any other aspect of this collection of information, including suggestions for reducing this burden, to Washington headquarters Services, Directorate for Information Operations and Reports, 1215 Jefferson Davis Highway, Suite 1204, Arlington, VA 22202-4302, and to the Office of Management and Budget, Paperwork Reduction Project (0704-0188) Washington DC 20503.			
1. AGENCY USE ONLY *(Leave blank)*	**2. REPORT DATE** March 2005	**3. REPORT TYPE AND DATES COVERED** Master's Thesis	
4. TITLE AND SUBTITLE: Multi Angle Imaging with Spectral Remote Sensing for Scene Classification			**5. FUNDING NUMBERS**
6. AUTHOR(S) Sunyaruk Prasert			
7. PERFORMING ORGANIZATION NAME(S) AND ADDRESS(ES) Naval Postgraduate School Monterey, CA 93943-5000			**8. PERFORMING ORGANIZATION REPORT NUMBER**
9. SPONSORING /MONITORING AGENCY NAME(S) AND ADDRESS(ES) N/A			**10. SPONSORING/MONITORING AGENCY REPORT NUMBER**
11. SUPPLEMENTARY NOTES The views expressed in this thesis are those of the author and do not reflect the official policy or position of the Department of Defense or the U.S. Government.			
12a. DISTRIBUTION / AVAILABILITY STATEMENT Approved for public release; distribution is unlimited			**12b. DISTRIBUTION CODE**

13. ABSTRACT (maximum 200 words)

Scene classification is studied here using the tool of texture analysis of multi-angle high-spatial resolution panchromatic and multi-spectral imagery. This study analyses the BRDF (Bidirectional Reflectance Distribution Function) impact and effectiveness of texture analysis on terrain classification within Fresno County area in state of California. QuickBird panchromatic (0.61 meter) and multispectral (2.44 meter) imagery collected in July 2003 are examined to determine the impact of adding multi-angles and filtered texture information to the standard MSI classification approaches. Four images were collected, with view angles from -64° to +64°, including a nadir view. Texture filter function and maximum likelihood classifier are used in this study. Both texture analysis and the results of classifications using multi-angle (BRDF) information are promising. Fine discrimination of similar soil classes was produced by the BRDF variations in the high-spatial resolution panchromatic image. Texture analysis results depended on the directionality of the gray level co-occurrence matrix (GLCM) calculation. Combining the different modalities of analysis did not improve the overall classification, perhaps illustrating the consequences of the Hughes paradox (Hughes, 1968).

14. SUBJECT TERMS Bidirectional Reflectance Distribution Function, BRDF, Texture Analysis, QuickBird, Multi Angle Imaging, Multispectral, Panchromatic, Scene Classification	**15. NUMBER OF PAGES** 115
	16. PRICE CODE

17. SECURITY CLASSIFICATION OF REPORT	**18. SECURITY CLASSIFICATION OF THIS PAGE**	**19. SECURITY CLASSIFICATION OF ABSTRACT**	**20. LIMITATION OF ABSTRACT**
Unclassified	Unclassified	Unclassified	UL

NSN 7540-01-280-5500 Standard Form 298 (Rev. 2-89)
Prescribed by ANSI Std. 239-18

THIS PAGE INTENTIONALLY LEFT BLANK

Approved for public release; distribution is unlimited

MULTI ANGLE IMAGING WITH SPECTRAL REMOTE SENSING FOR SCENE CLASSIFICATION

Sunyaruk Prasert
Flight Lieutenant, Royal Thai Air Force
B.S., Virginia Military Institute, 1998

Submitted in partial fulfillment of the
requirements for the degree of

MASTER OF SCIENCE IN INFORMATION TECHNOLOGY MANAGEMENT

from the

NAVAL POSTGRADUATE SCHOOL
March 2005

Author: Sunyaruk Prasert

Approved by: Richard C. Olsen
Thesis Advisor

William J. Welch
Second Reader

Dan C. Boger
Chairman, Department of Information Sciences

THIS PAGE INTENTIONALLY LEFT BLANK

ABSTRACT

Scene classification is studied here using the tool of texture analysis of multi-angle high-spatial resolution panchromatic and multi-spectral imagery. This study analyses the BRDF (Bidirectional Reflectance Distribution Function) impact and effectiveness of texture analysis on terrain classification within Fresno County area in state of California. QuickBird panchromatic (0.61 meter) and multispectral (2.44 meter) imagery collected in July 2003 are examined to determine the impact of adding multi-angles and filtered texture information to the standard MSI classification approaches. Four images were collected, with view angles from -64° to +64°, including a nadir view. Texture filter function and maximum likelihood classifier are used in this study. Both texture analysis and the results of classifications using multi-angle (BRDF) information are promising. Fine discrimination of similar soil classes was produced by the BRDF variations in the high-spatial resolution panchromatic image. Texture analysis results depended on the directionality of the gray level co-occurrence matrix (GLCM) calculation. Combining the different modalities of analysis did not improve the overall classification, perhaps illustrating the consequences of the Hughes paradox (Hughes, 1968).

THIS PAGE INTENTIONALLY LEFT BLANK

TABLE OF CONTENTS

LIST OF FIGURES

LIST OF TABLES

THIS PAGE INTENTIONALLY LEFT BLANK

ACKNOWLEDGMENTS

This thesis could not have been finished without much effort and help from others. The author is aware that anyone working with international students must be very patient since the communication barrier is not inextricable. The author would like to thank several people. Thanks to the Royal Thai Government for providing him the opportunity to study at the Naval Postgraduate School. Thanks to Matthew D. Humphrey, a former NPS graduate who did not know that a few years after he turned in his thesis, an alumni from the same school, Virginia Military Institute, would follow in his footsteps. Thanks to Angela M. Puetz for providing image registrations; these processes take much time. Thanks to Professor William J. Welch for his cooperation in being a second reader. Finally, the author would like to thank to Professor Richard C. Olsen for providing the chances to join his valuable scientific experiments. The author truly appreciates the science and life lessons, logics, and invaluable time Professor Olsen dedicated to him.

THIS PAGE INTENTIONALLY LEFT BLANK

I. INTRODUCTION

Image classification, a primary goal in much of remote sensing is an important tool in environmental studies. New commercial satellites provide multi-spectral (4-color) imagery, which can be used to conduct scene classification, along with the high-spatial resolution panchromatic sensors. These systems can form multiple images during an imaging pass, over a significant angular range (elevation from -60° to +60°). In such imagery, BRDF (Bidirectional Reflectance Distribution Function) effects, previously not greatly appreciated, become important. With the advances in the computational capabilities of commercial remote sensing software, the applications of analysis approaches for several large images simultaneously are now practicable.

Johann H. Lambert introduced the concept of reflectance from surfaces in the 18th century. It was not until 1965, however, that the first consideration of BRDF effects in imaging was presented by Nicodemus. BDRF studies have been limited by computational costs, and the cost of such imagery. At the time of the present study, the cost of acquiring high-spatial resolution satellite imagery is still fairly high, and the acquisition of multiple images of a given scene is a fairly expensive process. One such test has now been conducted, however, and it is these data that are considered in this study.

Texture-based filtering of high-resolution and multi-angle imagery is an established analysis tool that requires further investigation. Haralick et al. developed texture as an imagery analysis tool in 1973, but computers of that era were unable to cope with large images. Jensen et al (1986) applied texture analysis on modern data sets, combining spectral and texture analysis for the first time. Humphrey (2003), under the direction of Professor Olsen, followed a similar track in his work over the Elkhorn Slough area. The present study will extend the work by Humphrey in a new image area, with the additional input of multi-angle imagery to examine the consequences of BRDF effects.

This study attempts to address two major questions in imagery analysis. How does the addition of multiple views to a data collection improve the terrain classification process, in particular with respect to standard 4-color multispectral imaging, and what analysis procedure makes the best use of the additional remote sensing information? The second question includes texture analysis as a primary tool.

To attempt to answer these questions, 0.61 meter resolution panchromatic and 2.44 meter resolution multispectral QuickBird imagery were analyzed using ENVI and ERDAS image processing software. The area examined within this study is located in Fresno County, California, which is rich in various terrains, numerous agricultural fields, and several urban areas.

The development of this study begins with a review of previous works concerning energy-matter interactions, bidirectional effects, hotspot, POLDER data analysis, and texture introduction (Chapter II). The methodology section (Chapter III) describes the area, the classification tools used for the study, and the investigative methodology utilized. Finally, the analysis and conclusion sections discuss the results of the investigation and presents the conclusions derived from this study (Chapters IV and V).

II. BACKGROUND

A. ENERGY-MATTER INTERACTIONS WITH SURFACES

As electromagnetic energy reaches the earth‘s surface, it must be reflected, absorbed, or transmitted. The proportions accounted for by each process depend upon the nature of the surface and mediums, the wavelength of the energy, and the angle of illumination. (Campbell, 2002) The following section briefly reviews the description on each interaction, and then describes reflectance in more detail, which is the main topic of this thesis.

B. TRANSMISSION

Transmission is the process by which incident radiation passes through matter without measurable attenuation. The substance is transparent to the radiation. Transmission through material media of different densities causes the radiation to be refracted or deflected from a straight-line path with an accompanying change in its velocity and wavelength. The frequency always remains constant. (Avery and Berlin, 1992)

C. ABSORPTION

Absorption is the process by which radiant energy is absorbed and converted into other forms of energy, i.e., heat energy, which is subsequently emitted at a longer thermal infrared wavelength. The absorption of the incident radiant energy may take place in the atmosphere or on the terrain. (Jensen, 2000) For this to occur on the terrain, the substance must be opaque to the incident radiation. (Avery and Berlin, 1992)

D. REFLECTANCE

Reflectance is the process whereby radiation “bounces off” an object such as the top of a cloud, a water body, or the terrestrial Earth. Reflection exhibits fundamental characteristics that are important in remote sensing. First, the incident radiation, the reflected radiation, and a vertical to the surface from which the angles of incidence and reflection are measured, all lie in the same plane. Second, the angle of incidence and the angle of reflection (exitance) are approximately equal. (Jensen, 2000)

Figure 1 shows the various types of reflecting surfaces. If the surface is smooth relative to wavelength (average surface height is several times smaller than the wavelength of radiation striking the surface), specular reflection occurs. (Campbell, 2002)

If the surface has a large surface height relative to the size of the wavelength of the incident energy, the reflected rays go in many directions, depending on the orientation of the smaller reflecting surfaces. This reflectance is called diffuse reflection, or scattering. It does not yield a mirror image, but instead produces diffused radiation. (Jensen, 2000)

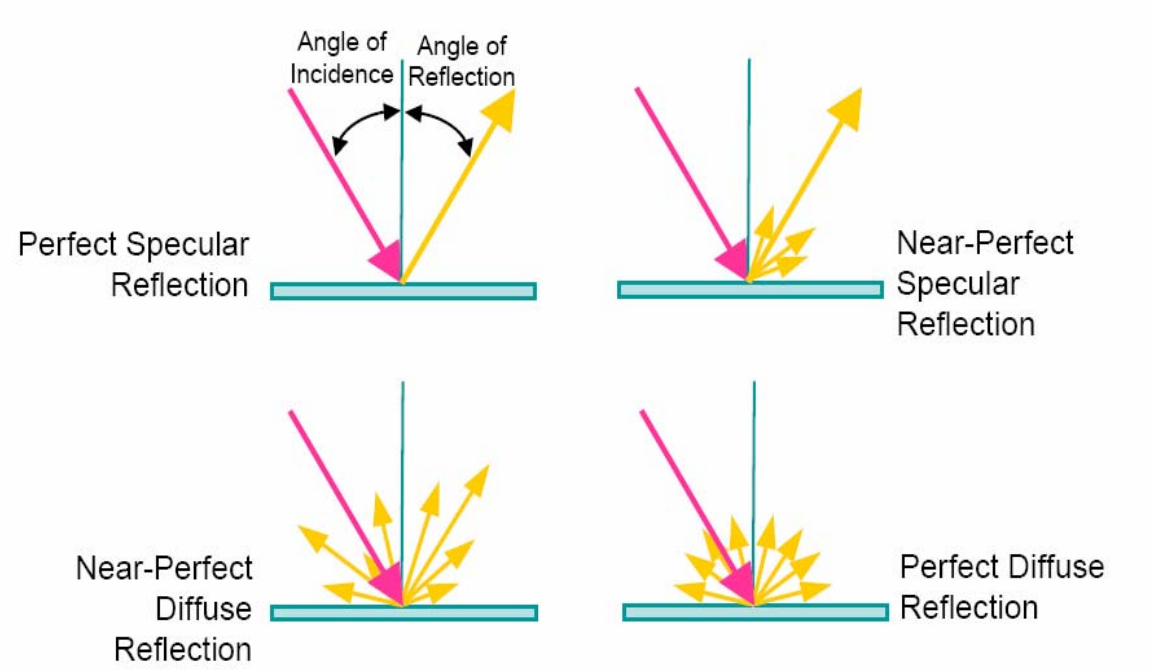

Figure 1. Various Types of Reflecting Surfaces (From: http://www.pixoneer.co.kr/main/ pro/pg_steamer/Education_Module.pdf, 4 September 2004)

The work of Johann H. Lambert (1728-1777) derives the idealized concept of a perfectly diffuse reflecting surface. One of Lambert's laws of illumination states the perceived brightness (radiance) of perfectly diffuse surface does not change with the angle of view. (Campbell, 2002) Lambert defined a perfectly diffuse surface. The commonly designated Lambertian surface is one for which the radiant flux leaving the

surface is constant for any angle of reflectance to the surface. (Jensen, 2000) Lambert's law is a definition of an ideal. No physical principle must be followed, but it approximates what is observed in reflection from a rough surface where many randomizing events can occur before the light leaves the surface. (http://www.4physics.com/tn3/lambertian.htm, 4 September 2004)

E. BRDF (BIDIRECTIONAL REFLECTANCE DISTRIBUTION FUNCTION)

One of the most general means to characterize the reflection properties of a surface is by use of the bi-directional reflection distribution function (BRDF); a function which defines the spectral and spatial reflection characteristic of a surface. (http://math.nist.gov/~FHunt/appearance/brdf.html, 20 August 2004)

"We are firmly convinced of the primary important of the bidirectional reflectance-distribution function, f_r, as the basic parameter for describing (geometrically) the reflecting properties of a surface element." (Nicodemus, 1970)

The BRDF is originally defined by Nicodemus (1965) as the ratio of the reflected radiance $dL_r(\text{w}\cdot\text{m}^{-2}\cdot\text{sr}^{-1}\cdot\text{nm}^{-1})$ in a particular direction (θ_r,φ_r) to the incident irradiance $dE_i(\text{w}\cdot\text{m}^{-2}\cdot\text{nm}^{-1})$ from direction (θ_i,φ_i). (Figure 2 and Figure 3)

$$f_r(\theta_i,\varphi_i;\theta_r,\varphi_r;\lambda) \equiv \frac{dL_r(\theta_i,\varphi_i,\theta_r,\varphi_r;\lambda)}{dE_i(\theta_i,\lambda)}\,(\text{sr})^{-1}$$

The units of the BRDF are inverse solid-angle (sr^{-1}).

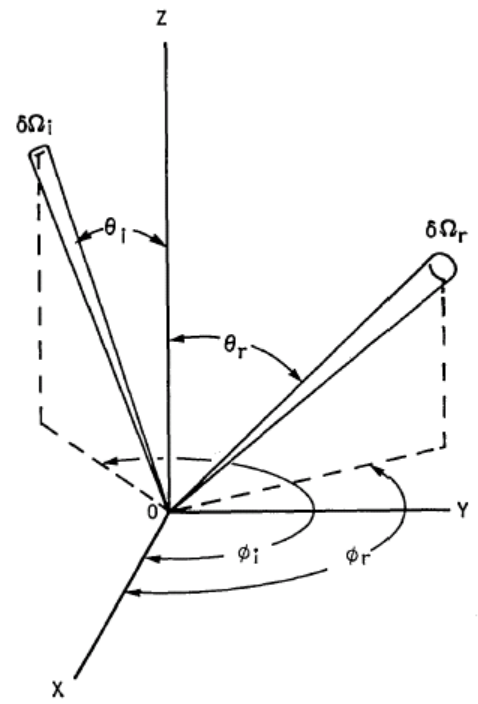

Figure 2. Original Geometry of Incident and Reflected Elementary Beams. Z axis is chosen along the normal to the surface element at 0. (From: Nicodemus, 1965)

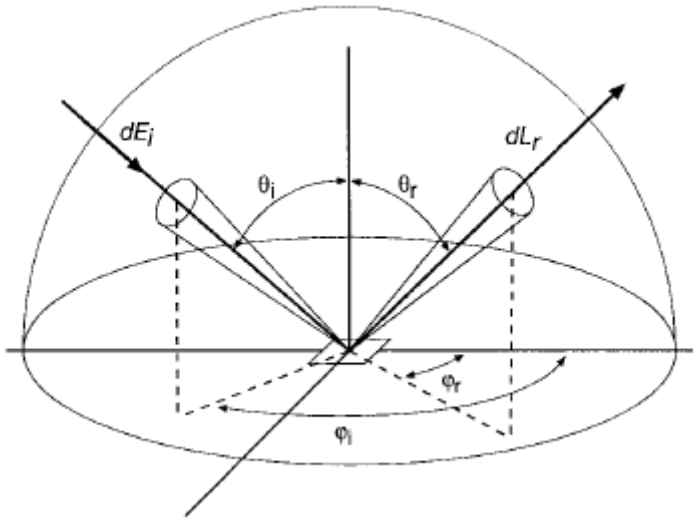

Figure 3. BRDF Parameters (From: Sandmeier et al., 1999)

The reflectance of a surface depends on both the direction of the irradiating flux and the direction along which the reflected flux is detected. Thus, remember that the distribution of reflected flux from a surface depends on the geometry of the measurement. In particular, flux from a small radiant source depends on (1) the angle of incidence, θ_i,

of the flux at the surface, (2) the azimuthal angle φ_i of the plane of incidence with respect to a direction across the surface, (3) the angle to the surface normal from which the flux is detected, θ_r, (4) the azimuthal angle φ_r of the plane of reflection, (5) the solid angle subtended by the source at a point on the surface, and (6) the solid angle subtended by the entrance pupil of the sensor at the surface. (Slater, 1980)

The BRDF may be interpreted as a boundary condition relating the upwelling radiance distribution at a reflecting surface. (Gerstl and Simmer, 1986) Figure 4 shows a pictorial representation of a typical BRDF, taken from the well-known paper by Nicodemus that provides a good physical description of these concepts. On the right figure, the incident light came from the left, and then reflected back on various directions in various intensities. The figures on the left show the illustrations as seen from the nadir views in various layers.

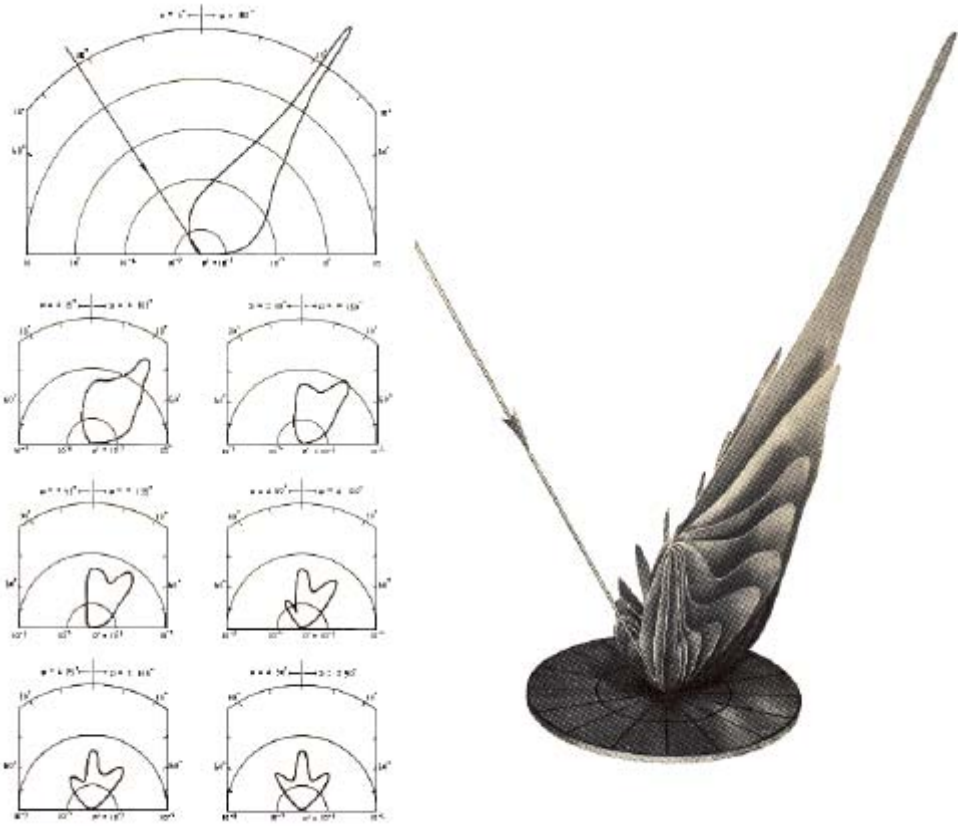

Figure 4. BRDF Visualization (From: Nicodemus, 1965)

Figure 5 is the example which shows the bidirectional reflectance effect on a grass lawn, observed under different viewing angles from a FIGOS (Field Goniometer System) mounted camera in the solar principal plane. The solar zenith angle is 35°, indicated with red arrows. Blue represents the view directions. The basic concept which can be grasped from these figures is one location with same angle of sun light, seen in various angles can cause different effects, and can be seen in everyday life.

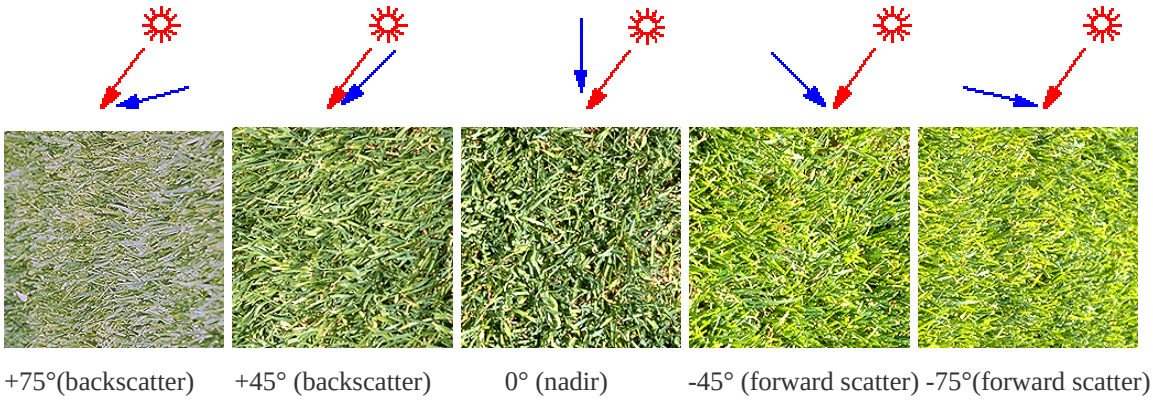

Figure 5. Phenomenon of Same Angle of Sun with Different Look Angles on Grass Lawn. (From: http://www.geo.unizh.ch/rsl/research/SpectroLab/goniometry/brdf_intro.shtml, 8 July 2004)

The nadir-normalized BRDF data of perennial ryegrass showed a strong spectral variability. In the visible blue (480 nm) and red (675 nm) chlorophyll absorption bands, BRDF effects were pronounced, whereas in the visible green and particularly in the low absorbing near infrared range, relatively low BRDF effects were observed. Thus, people using remote sensor data might think radiometrically, adjusting the brightness values associated with the blue and red bands, but not necessarily the near-infrared bands under investigation. (Jensen, 2000) The relationship between canopy optical properties and multiple scattering effects causes the spectral dependence of BRDF effects. In the high absorbing (i.e., low reflecting) wavelength ranges, multiple scattering effects are reduced due to the relatively low amount of radiation in the vegetation canopy. Thus, the contrast between shadowed and illuminated canopy components, and subsequently, the BRDF effects are enhanced. In the visible green and, particularly, in the near-infrared range, multiple scattering effects are strong and diminish the contrast in the canopy. As

Consequently, BRDF effects are rather small in the low absorbing (i.e., high reflecting) wavelength ranges. (Sandmeier and Itten, 1999)

Figure 6, anisotropy factors which are used to analyze the spectral variability in BRDF data, are depicted in the solar principal plane for four wavelength bands representing the colors red, blue and green and the near-infrared range. Anisotropy factors (ANIF) allow separation of spectral BRDF effects from the spectral signature of a target. They are calculated by normalizing bidirectional reflectance data, R to nadir reflectance, $R_{0.}$

Typical for vegetated surfaces, all four bands expose bowl shape, hot spot, and forward scattering components, but the extent of the BRDF features varies significantly among the four wavelengths. In the forward scattering direction, for example, the blue band exhibits much lower anisotropy factors than the green and red band due to transmittance effects. Consequently, the color of grass and other vegetated surfaces often show a touch of yellow in the forward scattering direction. In the hot spot direction where illumination and viewing angle are identical, the green reflectance is decreased relative to the reflectance of red and blue wavelengths. Thus, the hot spot appears white rather than green. (Sandmeier and Itten, 1999) The next section details hot spot.

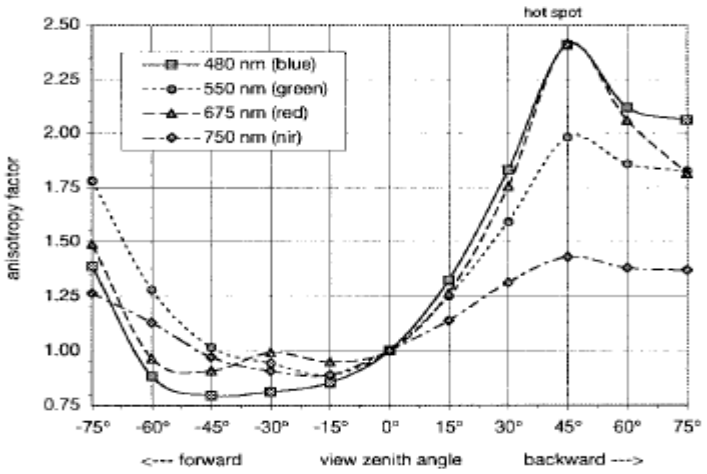

Figure 6. Anisotropy Factors of Grass Versus View Zenith Angle in the Solar Principal Plane for Four Spectral Bands. Sun zenith angle is 35º. Values for 30º view zenith angle are interpolated due to the sensor shadow. (From: Sandmeier and Itten, 1999)

Bidirectional effects affect remotely sensing observations in several ways. As soon as viewing and/or irradiance geometries within a single scene, or series of scenes, are altered, the spectral reflectance signature of the sensed objected changes according to their object-specific BRDFs. The bidirectional effect in remote sensing data is most obvious in the hotspot direction where illumination and viewing orientation are identical. Figure 7 demonstrates an oblique airphotograph showing the hotspot effect over a bare soil area.

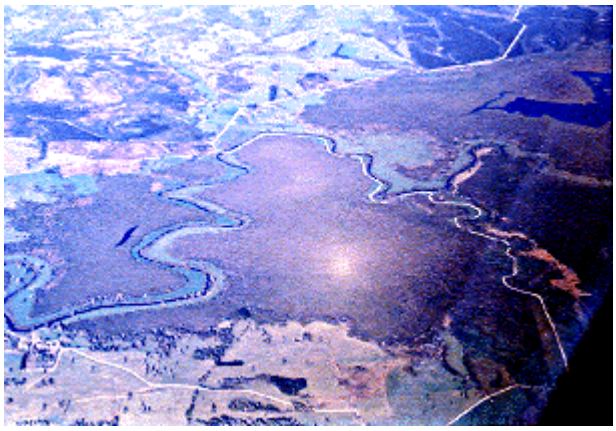

Figure 7. Hot Spot Effect in an Airphotograph (From: http://www.geo.unizh.ch/rsl/research/SpectroLab/goniometry/brdf_intro.shtml, 8 July 2004)

F. HOT SPOT

The surge in the brightness of a surface viewed in the backscatter direction has been known for over a century. It was first discovered by Seeliger (1887) in light scattered from the rings of Saturn. It was independently rediscovered in light from asteroids and the moon by Gehrels (1956), who called it the "opposition effect" because it occurs near astronomical opposition when the phase angle (the angle between the sun and the viewer as seen from the surface if the object) approaches zero. It is also sometimes called the "heiligenschein". In vegetation canopies, the opposition effect is known as the "hot spot". (Hapke, 1996) The widely accepted explanation for the hotspot effect is shadow hiding, in which particles at the surface (leaves, soil grains) cast shadows on adjacent particles. Those shadows are visible at large phase angles (the angle between the sun and view directions), but at zero phase angle they are hidden by the particles that cast them. (Breon, 2002) The hot spot phenomenon is generally interpreted

as a result of correlated probabilities of transmission in the incoming and reflected paths within the canopy and soils. On the other hand, a rough surface may also generate a reflectance maximum in the backscattering direction, even if the sun rays do not penetrate it. (Roujean et al., 1992)

The study of the hot spot is of interest for the remote sensing community for several reasons. The width of the peak in the shadow-hiding model depends on the ratio of the interparticle spacing to the extinction distance, which could be a discriminating structural parameter of vegetation canopies. (Gerstl and Simmer, 1986)

After ground conduct studies, scientists proceeded to the experiment on an airborne platform with the camera instrument. Breon et al. (2002) performed the measurement of hotspot with POLDER (POLarization and Directionality of the Earth's Reflectances) data using a different measurement principle. A brief description and analysis of POLDER follows.

G. POLDER

POLDER is a wide field of view imaging radiometer that has provided the first global, systematic measurements of spectral, directional and polarized characteristics of the solar radiation reflected by the Earth/atmosphere system. Its original observation capabilities have opened up new perspectives for discriminating the radiation scattered in the atmosphere from the radiation actually reflected by the surface. (http://smsc.cnes.fr/POLDER/, 21 August 2004)

A POLDER instrument is designed to collect accurate observations of the polarized and directional solar radiation reflected by the Earth-atmosphere system. The POLDER instrument concept is based on a charged coupled device (CCD) matrix array detector, a rotating filter wheel, and wide field of view optics, for both along track and cross track directions, with a maximum field of view of 114˚. Figure 8 demonstrates the configuration of a POLDER instrument. Its camera is composed of a two-dimensional CCD detector array, a wide field of view telecentric optics and rotating wheel carrying spectral and polarized filters. (http://smsc.cnes.fr/POLDER/GP_instrument.htm, 13 October 2004) This POLDER instrument has been installed in many platforms including helicopters and a C-130 airplane.

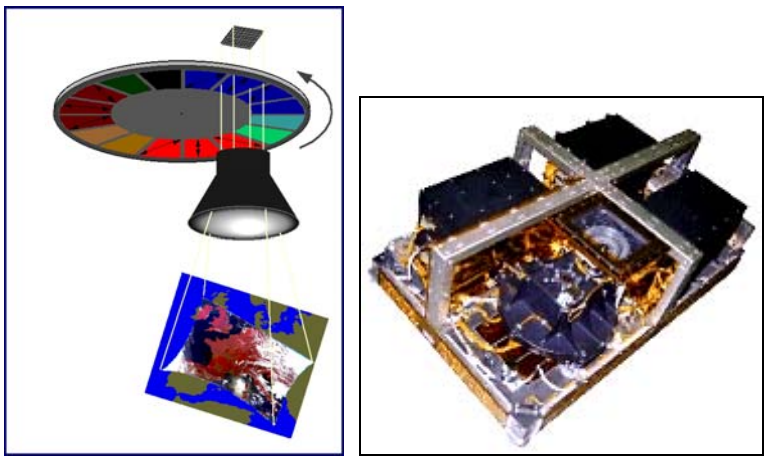

Figure 8. The Configuration of POLDER Instrument

The first consideration of POLDER data occurs during a helicopter flight, at a typical altitude of 300 m, and the POLDER instrument operating continuously. In the analysis, homogeneous sites within the POLDER field of view were those first selected, which was obtained by looking at the symmetry of the measurement with respect to the principal plane. Each pixel in the image corresponds to a different viewing geometry for a surface that is assumed invariant. Thus, the image simultaneously gives a representation of the complete directional signature. The measurements corresponding to the principal plane or any other azimuth can be extracted from the full image. (Breon et al., 1997)

Figure 9 demonstrates a typical example of a POLDER image acquired from 300 m altitude, over a homogeneous stand of Old Black Spruce, on June 7, 1994. The image is one "shot" of the CCD camera. Circles indicating zenith-viewing angles of 10, 20, 30, 40 and 50 degrees were added to this image. The lines are for the principal plane, the perpendicular plane as well as the 30º and 60º azimuth planes. The reflectance increases from black to white. The hot spot shows the larger reflectance in the lower right hand side of the figure. This image was acquired at 670 nm.

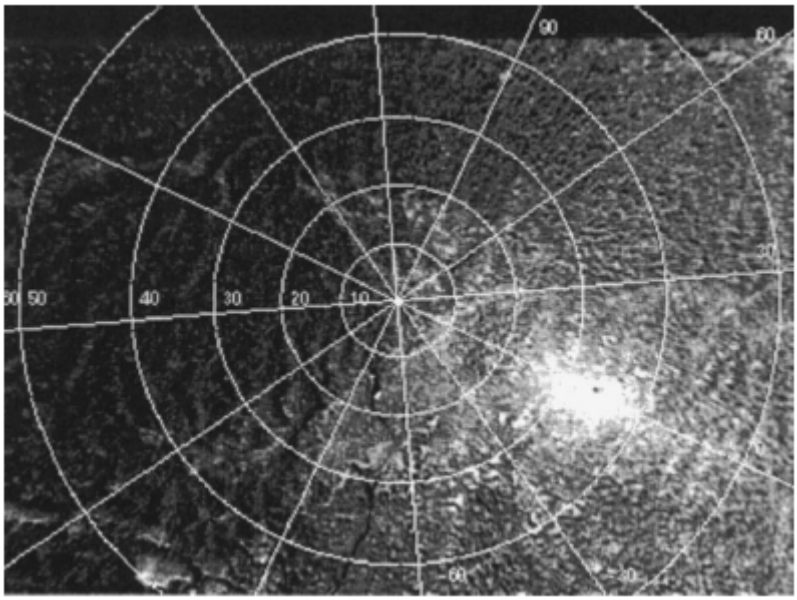

Figure 9. Example of POLDER Image Acquired from 300 m. Altitude

The hot spot feature is evident in the 4th quadrant of the image. For this measurement geometry, the POLDER measurement shows the directional signature of viewing angles up to 53˚. When the hot spot is in the diagonal of the image, the maximum viewing angle in the principal plane is 60˚. (Breon et al., 1997)

H. ANALYSIS OF POLDER FROM SPACE

The POLDER was onboard the Japanese ADEOS-I (Advanced Earth Observing Satellite) platform launched in 1996. It has measured the reflectance of the entire land-atmosphere terrestrial system in the period between November 1996 and June 1997. POLDER can observe a terrestrial target from different viewing angles during the same orbit. POLDER instrument resolution is 6 km at nadir and a swath width of 2400 km. POLDER radiometric measurements yield target reflectance and polarization properties as well as bidirectional reflectance and polarization distribution functions (BRDF and BPDF) from one or several orbits. (Breon et al., 1994) Unfortunately, on 30 June 1997, ADEOS-I was lost due to a solar panel cable breaking. Table 1 displays the characteristics of the POLDER instruments.

GENERAL CHARACTERISTICS OF THE POLDER INSTRUMENT ABOARD THE ADEOS SATELLITE

POLDER on ADEOS	
Size (m^3)	0.8 × 0.5 × 0.25
Weight	33 kg
Power consumption	42 W
Pixel coding	12 bits
Data rate	882 Kbit/s
Altitude	796 km
Period	100 min
Local cross. time	10:30
Inclination	98.59°

Table 1. Characteristics of Spaceborne POLDER

For POLDER data, the pixels in the image are viewed with various zenith angles and azimuths. The zenith angle at the surface varies between 0° at the image center, to 60° crosstrack and 50° forward and aft. In most cases, depending on the solar position with respect to the satellite, there is one pixel that is observed exactly (at the POLDER pixel angular resolution) in the backscattering geometry. This pixel occurs where the shadow of the satellite would be seen if it were much larger. The pixels surrounding this particular pixel are observed with slightly different viewing geometry. Figure 10 is a typical viewing geometry for a set of 7x7 POLDER pixels used to study the hot spot directional signature. The horizontal line is the principal plane that contains the Sun direction and local nadir. The solid circles indicate the view zenith angle by steps of 10º. The 13 clusters of dots correspond to 13 successive acquisitions within roughly 2 min. Each cluster is composed of 7x7 dots corresponding to 49 contiguous surface pixels of size $(6.2 \text{ km})^2$. (Breon et al., 2002)

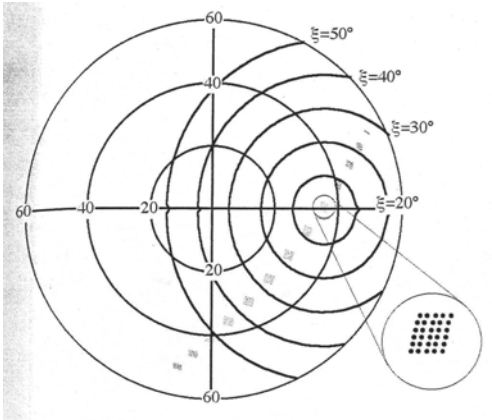

Figure 10. Typical Viewing Geometry for 7x7 POLDER Pixels

Figure 11 shows an example of the POLDER data retrieved from space. The image area includes Evergreen needleleaf, and closed shrublands. (Fernando Camacho de Coca, 2003)

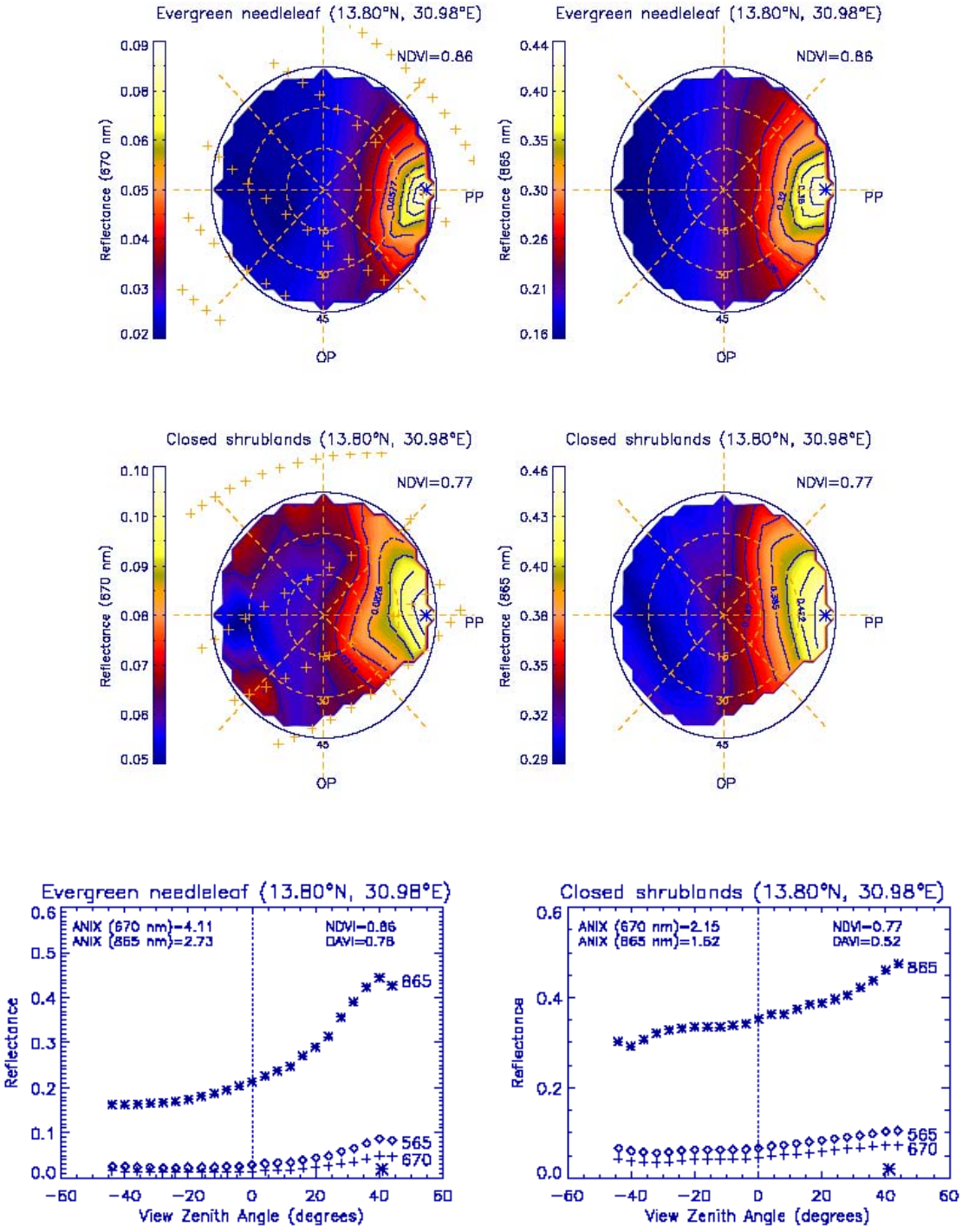

Figure 11. Example of POLDER Data

This figure shows example of POLDER BRDF at 670 nm (left) and 800 nm (right) for Evergreen needleleaf forest (top) and Closed shrublands (bottom). The star represents the sun position and the crosses (on the left side) the viewing geometry. The plots show the high anisotropic behavior of vegetation canopies. The BRDF is almost symmetrical regarding the principal plane, and very asymmetric regarding the orthogonal plane, showing the highest values in the hot spot domain. (Fernando Camacho de Coca, 2003)

Figure 12 shows the hot spot directional signature as observed from the POLDER spaceborne instrument. The measured reflectance is shown as a function of phase angle. A minus sign has been applied to the phase angle when $\theta_v \cos \varphi < \theta_s$, where θ_v is the view zenith angle and φ is the relative azimuth. The wavelength is 440, 670 nm and 865 nm from bottom to top. The text within the figures indicated the target type according to IGBP (International Geosphere-Biosphere Program) classification (top left) and the solar zenith θ_s (top right). The numbers indicate the retrieved hot spot half width for both 865 and 670 nm together with its uncertainty.

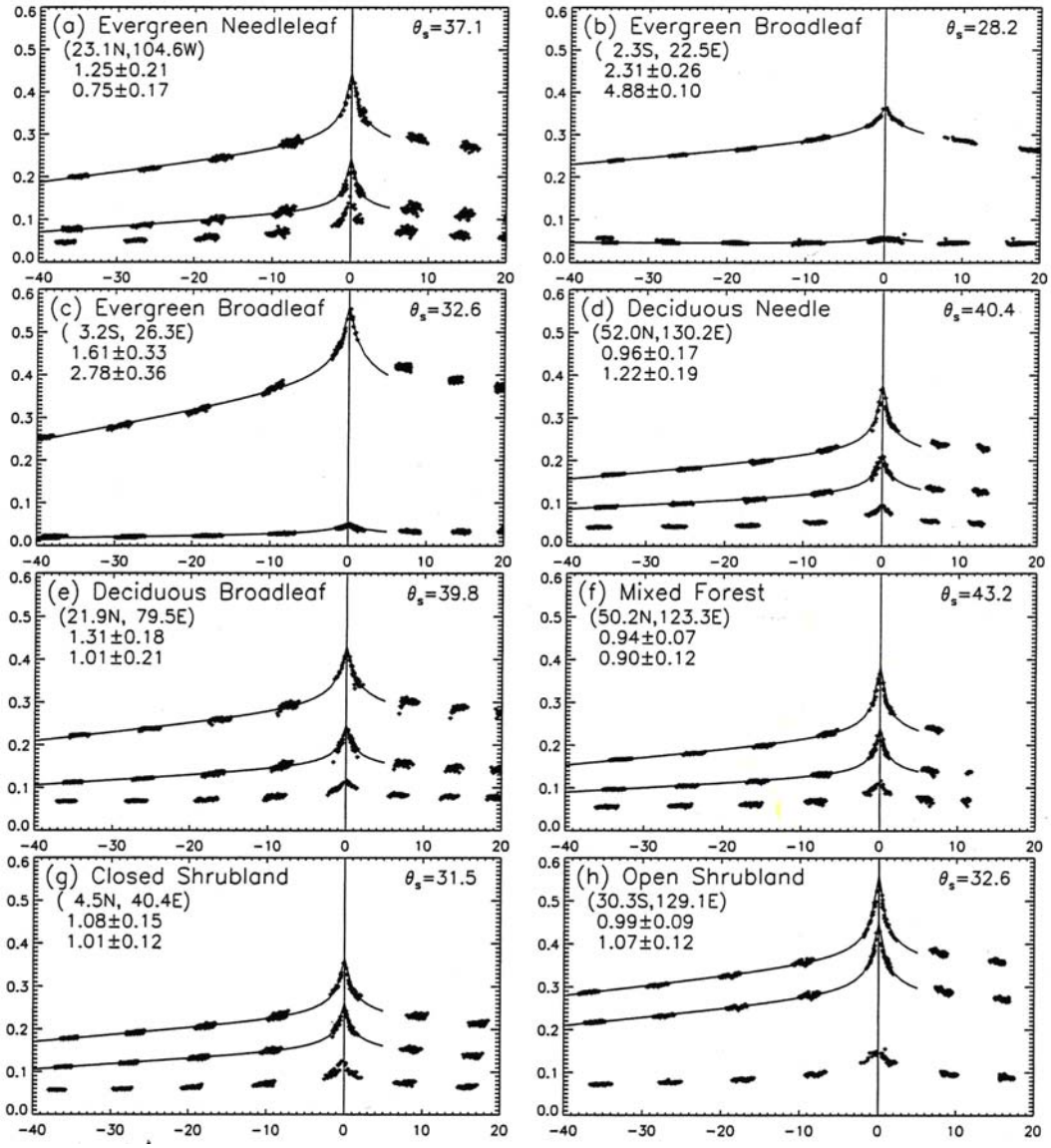

Figure 12. The Hotspot Directional Signature from Spaceborne POLDER Instrument

I. TEXTURE INTRODUCTION

Texture is the characteristic placement and arrangement of repetitions of tone or color in an image. In an aerial photograph, it is created by tonal repetitions of groups of objects that may be too small to be discerned individually. Sometimes two features that have very similar spectral characteristics exhibit different texture characteristics that allowed a trained interpreter to distinguish between them, often using the textural adjectives smooth (uniform, homogeneous), intermediate, and rough (coarse, heterogeneous).

It is important to understand that the texture in a certain portion of a photograph is strictly a function of scale. For example, in a very large-scale aerial photograph (1:500), it might be actually possible to see the leaves and branches in the canopy of a stand of trees and describe the area as having a coarse texture. However, as the scale of the imagery becomes smaller (1:5,000), the individual leaves and branches and even the tree crowns might coalesce, giving the impression that the stand now has an intermediate texture, i.e., it is not smooth but definitely not rough. When the same stand of trees is viewed at a very small scale (1:50,000), it might appear to be a uniform forest stand with a smooth texture. Thus, texture is a function of the scale of the imagery and the ability of the interpreter to perceive and describe it. (Jensen, 2000)

J. TEXTURAL FEATURES

Haralick et al. (1973) published the earliest application of texture measurements to digital remotely-sensed image data These authors proposed what has become known as the gray-level co-occurrence matrix (GLCM), which represents the distance and angular spatial relationships over an image sub-region of specified size. Each element of the GLCM is a measure of the probability of occurrence of two gray-scale values separated by a given distance in a given direction. (Mather, 1999) [Computer Processing of Remotely-Sensed Images, An Introduction]

Haralick's initial perspective of texture and tone is based on the concept that texture and tone bear an inextricable relationship to one another. Tone and texture are always present in an image, although one property can dominate the other at times. (Haralick, 1973) The basic intuitively perceived relationships between tone and texture are the following. When a small-area patch of an image has little variation—i.e., little variation of features of discrete gray tone—the dominant property of that area is tone. When a small-area patch has a wide variation of features of discrete gray tone, the dominant property of that area is texture.

One important property of tone-texture is the spatial pattern of the resolution cells composing each discrete tonal feature. When there is no spatial pattern and the gray-tone variation between features is wide, a fine texture results. As the spatial pattern becomes more definite and involves more and more resolution cells, a coarser texture results. It is assumed that the texture-context information in an image *I* is contained in the overall or

"average" spatial relationship, which the gray tones in image *I* have to one another. More specifically, it is also assumed that this texture-context information is adequately specified by the matrix of relative frequencies P_{ij} with which two neighboring resolution cell separated by distance *d* occur on the image, one with gray tone *i* and the other with gray tone *j*. Such matrices of gray-tone spatial-dependence frequencies are a function of the angular relationship between the neighboring resolution cells as well as a function of the distance between them. Figure 13 illustrates the set of all horizontal neighboring resolution cells separated by distance 1.

(1,1)	(1,2)	(1,3)	(1,4)
(2,1)	(2,2)	(2,3)	(2,4)
(3,1)	(3,2)	(3,3)	(3,4)
(4,1)	(4,2)	(4,3)	(4,4)

$L_y = \{1,2,3,4\}$

$L_x = \{1,2,3,4\}$

$$R_H = \{((k,l),(m,n)) \in (L_y x L_x) \times (L_y x L_x) \mid k-m = 0, \mid l-n \mid = 1\}$$
$$= \{((1,1),(1,2)\ ,\ ((1,2),\ (1,1))\ ,\ ((1,2),(1,3))\ ,\ ((1,3),(1,2))\ ,$$
$$((1,3),(1,4))\ ,\ ((1,4),(1,3))\ ,\ ((2,1),(2,2))\ ,\ ((2,2),(2,1))\ ,$$
$$((2,2),(2,3))\ ,\ ((2,3),(2,2))\ ,\ ((2,3),(2,4))\ ,\ ((2,4),(2,3))\ ,$$
$$((3,1),(3,2))\ ,\ ((3,2),(3,1))\ ,\ ((3,2),(3,3))\ ,\ ((3,3),(3,2))\ ,$$
$$((3,3),(3,4))\ ,\ ((3,4),(3,3))\ ,\ ((4,1),(4,2))\ ,\ ((4,2),(4,1))\ ,$$
$$((4,2),(4,3))\ ,\ ((4,3),(4,2))\ ,\ ((4,3),(4,4))\ ,\ ((4,4),(4,3))\}$$

Figure 13. Illustration Set of All Distance 1 Horizontal Neighboring Resolution Cells on 4x4 Image. (From: Haralick et al., 1973)

Next, Figure 14 (a) represents a 4x4 image with four gray tones, ranging from 0 to 3. Figure 14 (b) shows the general form of any gray-tone spatial-dependence matrix. For example, the element in the (2,1) position of the distance 1 horizontal P_H matrix is the total number of times two gray tones of value 2 and 1 occurred horizontally adjacent to each other. To determine this number, count the number of pairs or resolution cell in R_H

such that the second resolution cell of the pair has gray tone 1. Figures (c)-(f) calculate all four distance 1 gray-tone spatial-dependence matrices.

0	0	1	1
0	0	1	1
0	2	2	2
2	2	3	3

(a)

Gray Tone	Gray Tone			
	0	1	2	3
0	#(0,0)	#(0,1)	#(0,2)	#(0,3)
1	#(1,0)	#(1,1)	#(1,2)	#(1,3)
2	#(2,0)	#(2,1)	#(2,2)	#(2,3)
3	#(3,0)	#(3,1)	#(3,2)	#(3,3)

(b)

(c) 0^o $P_H = \begin{pmatrix} 4 & 2 & 1 & 0 \\ 2 & 4 & 0 & 0 \\ 1 & 0 & 6 & 1 \\ 0 & 0 & 1 & 2 \end{pmatrix}$

(d) 90^o $P_V = \begin{pmatrix} 6 & 0 & 2 & 0 \\ 0 & 4 & 2 & 0 \\ 2 & 2 & 2 & 2 \\ 0 & 0 & 2 & 0 \end{pmatrix}$

(e) 135^o $P_{LD} = \begin{pmatrix} 2 & 1 & 3 & 0 \\ 1 & 2 & 1 & 0 \\ 3 & 1 & 0 & 2 \\ 0 & 0 & 2 & 0 \end{pmatrix}$

(f) 45^o $P_{RD} = \begin{pmatrix} 4 & 1 & 0 & 0 \\ 1 & 2 & 2 & 0 \\ 0 & 2 & 4 & 1 \\ 0 & 0 & 1 & 0 \end{pmatrix}$

Figure 14. 4x4 Image with Four Gray Tones, Ranging from 0 to 3. (From: Haralick et al., 1973)

The initial assumption in characterizing image texture is that all the texture information is contained in the gray-tone spatial-dependence matrices. Hence, all the textural features suggested are extracted from these gray-tone spatial-dependence matrices. The equations, which define a set of 14 measures of textural features, are given in Appendix A of Textural Features for Image Classification. (Haralick et al., 1973) Only some of those features follow.

1) Angular Second Moment: a measure of homogeneity.

$$f_1 = \sum_i \sum_j \{p(i, j)\}^2$$

2) Contrast: a measure of the degree of local variation.

$$f_2 = \sum_{n=0}^{N_g-1} n^2 \{ \sum_{i=1}^{N_g} \sum_{\substack{j=1 \\ |i-j|=n}}^{N_g} p(i, j)\}$$

3) Correlation: a measure of the gray tone linear dependence.

$$f_3 = \frac{\sum_i \sum_j (i, j)\, p(i, j) - \mu_x \mu_y}{\sigma_x \sigma_y}$$

4) Entropy: a measure of the degree of variability.

$$f_4 = -\sum_i \sum_j p(i, j)\ \log(p(i, j))$$

5) Variance: a measure of the sum of squares.

$$f_5 = \sum_i \sum_j (i - \mu)^2\, p(i, j)$$

where μ_x, μ_y, σ_x, and σ_y are the means and standard deviations of p_x and p_y.

Notation: p(i,j) $(i,j)^{th}$ entry in a normalized gray-tone spatial-dependence matrix, = $\frac{P(i, j)}{R}$.

$p_x(i)$ i^{th} entry in the marginal-probability matrix obtained by summing the rows of $p(i,j)$, $= \sum_{j=1}^{N_g} P(i, j)$

N_g Number of distinct gray levels in the quantized image.

R Number of pairs of pixels used in the computation of the corresponding P.

Figure 15 shows the digital printout of two 64x64 image blocks taken from a satellite picture over the California coastline (NASA ERTS Image no. 1002-18134). Figure (a) is a representative sample of grasslands and Figure (b) is a representative sample of water bodies in the area. The value of the features f_1, f_2, f_3, obtained from gray-tone spatial-dependence matrices for a distance $d = 1$, are shown below the images.

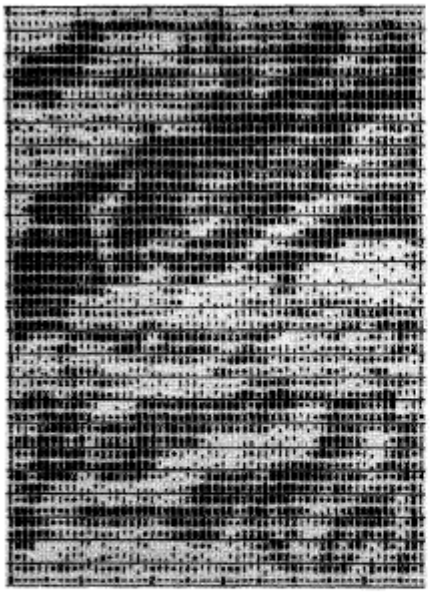

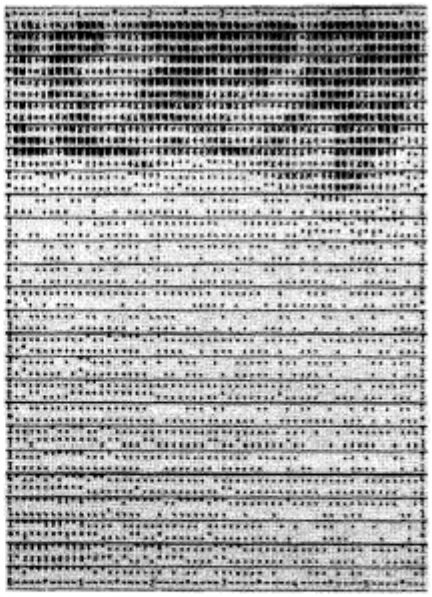

Grassland

Angle	ASM	Contrast	Correlation
0°	.0128	3.048	.8075
45°	.0080	4.011	.6366
90°	.0077	4.014	.5987
135°	.0064	4.709	.4610
Avg.	.0087	3.945	.6259

Water Body

ASM	Contrast	Correlation
.1016	2.153	.7254
.0771	3.057	.4768
.0762	3.113	.4646
.0741	3.129	.4650
.0822	2.863	.5327

(a) (b)

Figure 15. Textural Features for Two Different Land-Use Category Images. (From: Haralick et al., 1973)

Note that the ASM value of grassland image is consistently lower than ASM value of the water body. Meanwhile, the contrast feature for the grassland image has consistently higher values compared to the water-body image. For the correlation features, the water-body images have lower values compared to the grassland image. (Haralick et al., 1973)

THIS PAGE INTENTIONALLY LEFT BLANK

III. METHODOLOGY

A. QUICKBIRD REMOTE SENSING PLATFORM

QuickBird (Figure 16), launched on October 18, 2001 from Vandenberg AFB, California, was designed by all Aerospace & Technologies Corp., Kodak, and Fokker Space. QuickBird is owned and operated by DigitalGlobe Corporation. As of October 2004, QuickBird is the only spacecraft able to offer sub-meter resolution imagery, industry-leading geolocational accuracy, large on-board data storage, and an imaging footprint 2 to 10 times larger than any other commercial high-resolution satellite.

Figure 16. The QuickBird Satellite (After: DigitalGlobe)

QuickBird is deployed in a sun-synchronous Low Earth Orbit (LEO) at an altitude of 450 km. and an orbital inclination of 98 degrees. The sensor's orbit provides an orbital period of 93.4 minutes. The revisit frequency is 1 to 3.5 days depending on latitude at 70 centimeter resolution. (DigitalGlobe)

QuickBird has two sensors on board capable of collecting a 61-centimeter panchromatic (black and white) sensor and a 2.44-meter 4-band multispectral imagery. Both are collected every time an image is acquired. Moreover, the panchromatic (0.45-0.90 μm) and multispectral imagery can be fused to form a color 61-cm image in either three or four bands. The individual bands are broken down as followed: band#1 (blue) 0.45-0.52 μm, band#2 (green) 0.52-0.60 μm, band#3 (red) 0.63-0.69 μm, band#4 (near infrared) 0.76-0.90 μm. Figure 17 shows the spectral response of the QuickBird sensors. The satellite produces imagery that is spatially and spectrally very accurate, while

providing an industry-leading 16.5-kilometer (10.3-mile) wide swath width (http://www.sovereign-publications.com/digitalglobe.htm, 9 October 2004).

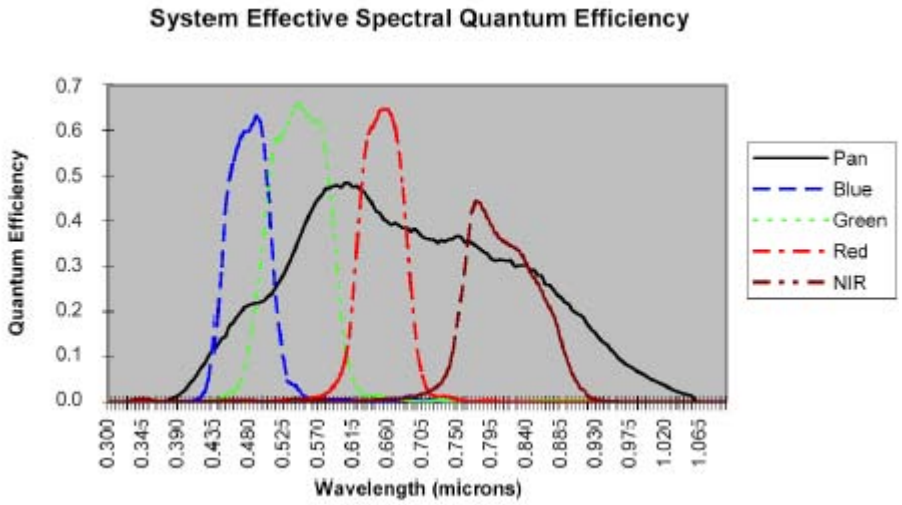

Figure 17. Spectral Response of QuickBird, (From: Remote Sensing from Air and Space, R. C. Olsen, 2003)

B. POSITION OF QUICKBIRD AND TIME INTERVAL BETWEEN IMAGES

Since the topic of this study is multi angle imaging, traditional nadir imaging is not the only concern. When QuickBird was taking the picture for this study, the orbit was at an altitude of 450 km above the earth's surface at a speed of 7.1 km/sec while the direction was approximately northeast toward southwest. The results are the image products from each individual angle with eight different lines (file) called line 1 to line 8, consecutively. Each line has a swath width of 16.5 km. and a length of 165 km. Lines 1, 3, 5, 7 are the overlapped areas with lines 2, 4, 6, 8, consecutively and not exploited in this study.

Table 2 summarizes position of QuickBird according to the line number. In line 4, the image was taken in the nadir position, which is the view from the traditional imaging satellite. In line 2, QuickBird was acquiring the image at a forward look position and the angle was 62.16°. Meanwhile, in line 6, QuickBird was in an after-look position with an angle of 48.64°. In line 8, QuickBird was also in an after-look position with an angle of 64.69°. Figure 18 shows an illustration of QuickBird's position.

Line number	Position and angle
2	Forward-look, 62.16°
4	Nadir
6	After-look, 48.64°
8	After-look, 64.69°

Table 2. Angles of QuickBird While Acquiring Images for Each Line

Figure 18. Image Shows Position of QuickBird Taking the Images (From: R. C. Olsen)

C. AREA OF INVESTIGATION

QuickBird images of the Fresno County, California (Figures 19 and 20) were utilized for this study. This particular area was chosen to move away from the coastal area where it is usually foggy, which prevents satellites from retrieving cloud and fog-free images. The destination area must consist of a variety of terrains, but not be too far from Monterey, California where most of the work was being done. The region of interest for this study covered the area around the Fresno Yosemite International Airport. Its center is located at 36°46'40 north latitude and 119°43'11 west longitude. Much of the area, besides the highways and residents housing, is devoted to the agricultural industry. The crops and fields within the image include almonds, grapes, cotton, tomatoes, lettuces, peaches, plums, and wheat farms. (http://www.exportcenter.net/FresnoCountyAgExportsReport20001revised.pdf, 9 October 2004). Some of the covered areas are water ponds, which are parts of the agricultural fields. Another reason this area was chosen was that one of Naval Postgraduate School faculty members, Professor David Trask, is a resident of Fresno area who can provide the explanations and ground images, if necessary.

The images were taken in July 2003, during the summer, which has the least possibility of cloudy skies. The times indicated in Figure 18 were the coordinated universal time (UTC), which was approximately 1036 AM local time.

Figure 19. Map of Fresno, California (From: http://www.mapquest.com, 25 January 2005)

Figure 20. Comparative Panchromatic Image of Interested Area (Nadir View)

D. ENVI SOFTWARE

The computational tool used in the development of this thesis was the Environment for Visualizing Images (ENVI) software created by Research Systems Incorporated (RSI), of the Kodak Company. ENVI is an Interactive Data Language (IDL) based image processing package that enables users to access and work with images in multiple formats and sources. For this study, only a small subset of ENVI functions were utilized including basic image manipulation tools, and the 13 embedded texture filters within the software. (Humphrey, 2003)

E. TEXTURE FILTERS

Many images contain regions characterized by variations in brightness rather than any unique value of brightness. Texture refers to the spatial variation of image tone as a function of scale. To be defined as a distinct textural area, the gray levels within the area must be more homogeneous as a unit than areas having a different texture. As mentioned previously, ENVI supports several textural filters based on either occurrence measures or co-occurrence measures. Five different texture filters are based on occurrence measures, and eight different texture filters are based on co-occurrence measures in ENVI. The texture filters within ENVI are based upon Haralick's work described in Chapter II.

F. OCCURRENCE-BASED FILTERS

The occurrence measures use the number of occurrences of each gray level within the processing window for the texture calculations (ENVI User's Guide, 2003). The default processing window of ENVI is 3 by 3 data matrices. Using larger windows resulted in greater edge effects where more pixels situated between two adjacent categories were being rejected. (Hsu, 1978) In this study, two different window sizes were chosen: 5 by 5, and 17 by 17. The five occurrence filters available are data range, mean, variance, entropy, and skewness.

G. CO-OCCURRENCE-BASED FILTERS

The co-occurrence measures use a gray-tone spatial dependence matrix to calculate texture values. This is a matrix of relative frequencies with which pixel values occur in two neighboring processing windows separately by a specified distance and direction. It shows the number of occurrences of the relationship between a pixel and its specified neighbor. The following matrices (Figure 21) demonstrate how the co-

occurrence texture filters measure the co-occurrence value. The window size of the following processing is 3x3, and shift values of X=1, Y=0 (directions) which means the pixels in the 3x3 base window and the pixels in a 3x3 window shifted by 1 pixel are used to create the co-occurrence matrix.

4	5	3
3	5	6
6	4	3

Base Window

3	5	6
5	6	3
4	3	6

Shift Window

Gray Level	3	4	5	6
3	0	0	2	1
4	2	0	0	0
5	0	0	0	2
6	1	1	0	0

Co-occurrence Matrix

Figure 21. Co-Occurrence Filter Matrices

The co-occurrence filtering process also utilized an angular distance (d) of one, and a gray level of quantization of 64. The eight co-occurrence filters are mean, variance, homogeneity, contrast, dissimilarity, entropy, second moment, and correlation. The co-occurrence filter measures use a gray-tone spatial dependence matrix to calculate texture values (ENVI User's Guide, 2003). Table 3 summarizes the texture filters.

Occurrence texture filters	Co-occurrence texture filters
Data Range	Mean
Mean	Variance
Variance	Homogeneity
Entropy	Contrast
Skewness	Dissimilarity
	Entropy
	Second Moment
	Correlation

Table 3. Texture Filters

H. SUPERVISED CLASSIFICATION

One of the essential analytical tools used for the extraction of quantitative information from remotely sensed image data are supervised classification procedures. In the supervised classification, the analyst defines the image small areas, called training sites, which are representative of each known terrain category, or class that appear fairly homogeneous on the image. Spectral values for each pixel in the training sites are used to define the decision space for that class. After the clusters for each training site are defined, the computer then classifies all the remaining pixels in the scene (Sabins, 1996).

I. REGIONS OF INTEREST CREATION (ROI)

The first step in the supervised classification is to select training sites called "regions of interest" (ROI) for each of the terrain categories. In this study, 28 different regions of interest were selected representing 28 different kinds of surface. The strategy is to identify homogeneous, representative samples of the different land cover types of interest. Then, the initial ROI's were exported into ENVI's n-Dimensional visualizer (ND-vis) for further refinement and additional separation into more accurately defined spectral classes. By exporting ROIs to a n-D visualizer, the goal is to see the distribution of the points within the selected ROIs and between the ROIs. This is one of ENVI's most useful options for checking the separability of the classes when using ROIs as input into supervised classification (ENVI User's Guide, 2003).

J. MAXIMUM LIKELIHOOD CLASSIFICATION

The classification algorithm utilized in this study is the maximum likelihood (ML) classifier. This type of classification is the most common supervised classification method used with remote sensing image data (Richards, 1999). The ML procedure is a supervised statistical approach to pattern recognition. The probability of a pixel belonging to each of a predefined set of classes is calculated, and the pixel is then assigned to the class for which the probability is the highest. (Brandt Tso, 2001)

The maximum likelihood is based on the Bayesian probability formula:

$$P(x, w) = P(w \mid x)P(x) = P(x \mid w)P(w)$$

where x and w are generally called "events". P(x, w) is the probability of co-existence (or intersection) of events x and w, $P(x)$ and $P(w)$ are the prior probabilities of events x and

w, and $P(w|\ x)$ is interpreted in the same manner. If event x_i is the ith pattern vector and w_j is information class j then, according to Bayesian probability formula, the probability that x_i belongs to class w_j is given by:

$$P(w_j \mid x_i) = \frac{P(x_i \mid w_j)P(w_j)}{P(x_i)}$$

ENVI utilizes the ML principles by using ROIs, previously processed through the n-D visualizer, which are imported into the ML classifier and serve as the training set of spectral classes for classification process. The ML classification assumes that the statistics for each class in each band are normally distributed and calculates the probability that a given pixel belongs to a specific class. Each pixel is assigned to the class that has the highest probability (ENVI User's Guide, 2003).

K. ERDAS SOFTWARE

Another computational tool used in the development of this thesis was the ERDAS software from Leica Geosystems. ERDAS Incorporated, a supplier of image processing software, was founded in 1978 as a commercial spin-off of research developed at Harvard University and the Georgia Institute of Technology. Its particular strengths are in land-use classification, ortho-modeling, making image maps and interfacing/data exchange with geographical information packages. For this study, only a small subset of ERDAS functions were utilized including basic image-to-image registration tools.

L. IMAGE-TO-IMAGE REGISTRATION

The imagery taken over the target area is provided in multiple data files. These files need to be recombined as mosaics, in order for the 4 images to be analyzed. This was done using ENVI, and comparison with an aerial map and road atlas. This was more difficult than normal with nadir view "quad" of four image files. The off-nadir views required several dozen image files be reconciled with the nadir view. Several iterations of image registration were needed.

Image-to-image registration is the translation and rotation alignment process by which two images of like geometry and of the same geographic area are positioned coincident with respect to one another so that corresponding elements of the same ground area appear in the same place on the registered images (Chen and Lee, 1992). Many

applications of remote sensing image data require two or more scenes of the same geographical region, acquired at the different dates, to be processed together (Richards, 1999). For example, it is simply possible to compare two images obtained on different dates to see if any change has occurred in them.

Two images can be registered to each other by registering each to a map coordinate base separately, or one image can be chosen as a master while the others, known as the slaves, are to be registered. In this study, an image acquired from line 4 was chosen, which is the nadir view as a master image, and images from lines 2, 6, 8 are slave images.

M. GENERAL PROCEDURES

This thesis attempted to study two portions of work. The first portion is texture analysis of multi-angle imaging, and the second is BRDF effects in these multi-angle images. After finishing the results of the first topic, those results were exploited for the second portion, which also tried to answer the research questions concerning additional retrieved information and how they improve the image classification process.

1. Part I: Texture Analysis

After the creation of mosaic images, the slave images were registered with the master image to acquire four identical areas with the different times each image was taken. Then, the texture filter function was applied using both the occurrence and co-occurrence filters contained within ENVI, resulting in the creation of two separate files for each mosaic, an occurrence filtered file and a co-occurrence filtered file. Note that each different filter produced unexpected results in some area of the image. The result also changed while using the same filter and when the angle of looking, or a combination of shift values was changed. Appendix A displays the complete set of non filtered and filtered images.

An early result, here, is the determination that texture is not invariant with angles, at least for a few of the scene elements. An early hope was hat texture might be invariant, which would make it a powerful tool in the analysis of off-nadir imagery.

2. Part II: BRDF Effect with Texture Analysis

Part II procedures are an implementation of Part I's product, but instead of focusing on only one area, which generated the difference-filtered result, the full scene

was considered. Several methods were also used to find the way to maximize, and show the BRDF effect on a set of images. The concept used in the ENVI software was to construct a multi-layer set of images termed a "metafile". This metafile consists of multiple layers of image, which represent various kinds of information. Figure 22 shows the example of the metafile. The top layer displayed in red represents a multispectral image, which was acquired from line 4. This layer provides multispectral information. The next group of layers displayed in blue represents a set of co-occurrence filtered panchromatic image when X:0, Y:1. The following group of layers displayed in yellow represents a set of co-occurrence filtered panchromatic image when X:1, Y:0. The group of layers displayed in green represents a set of co-occurrence filtered panchromatic image when X:1, Y:1. These three groups of layers provide filtered information. The bottom four layers displayed in grey represent a set of panchromatic images from various angles and these layers provide multi angle information.

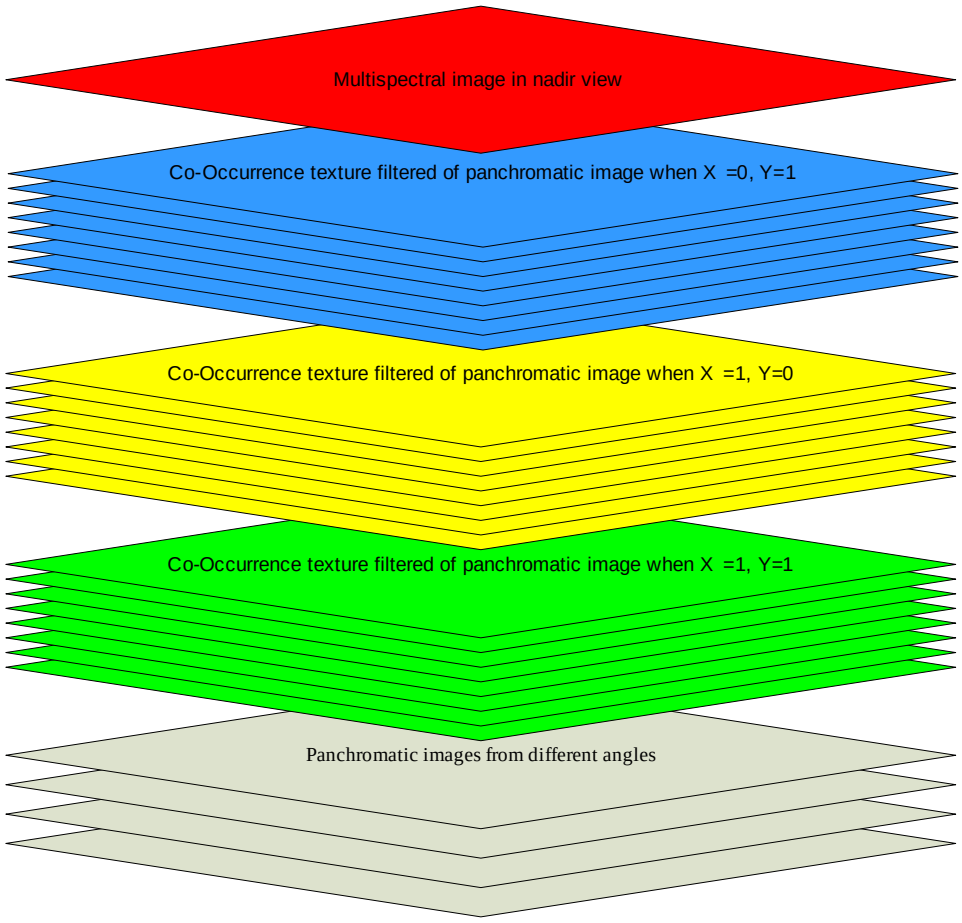

Figure 22. The Layers of Information which Represent Concept of Olsen's Methodology

The principal of supervised classification was exploited after constructing the metafile. The maximum likelihood (ML) classifications were applied with a set of 28 regions of interest (ROI). The ENVI's ML made it possible to select a group of spectral from the entire spectral in order to examine the results. Several combinations of interesting spectral were utilized in the ML classification. Both ENVI software and human eyes examined the Classification results. The next chapter discusses the analysis of classified images.

IV. ANALYSIS

According to the analysis to this point, this study consists of two phases: texture analysis and the BRDF effect in multi-angle imaging. The goal of the first phase was to analyze a small area of the same scene from various angles with various texture filters. The goal of the second phase was to analyze the full scene from various angles with the maximum likelihood classification. The final goal of the second phase is to find the usefulness of additional information from various angles of acquired images concerning the Bidirectional Reflectance Distribution Function (BRDF) effects.

A. TEXTURE ANALYSIS

The mosaic products of the Fresno area image from the QuickBird satellite from four angles were examined simultaneously by using ENVI software. By the nature of photographic principle, each image, which was taken from a different angle, produced a unique appearance. The following images (Figure 23) are the representations of an area containing water ponds, which are located northwest of the Fresno airport.

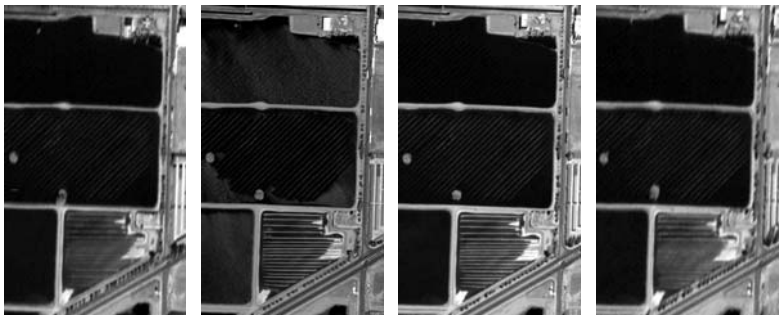

Figure 23. Scene#1, Line 2- Line 8 (Without any texture filter)

With the human eye alone, it is possible to distinguish the differences, and the similarity of those images. However, Haralick's texture filter principle was exploited by running the ENVI occurrence and co-occurrence texture filters. Some of the texture filtered products were promising. They discriminated the dissimilarity from the similarity. Figures 24 and 25, two occurrence texture filters, show the capability of enhanced discrimination of the water ponds. With the variance filter (Figure 24), the horizontal lines on the water pond's surface at the bottom of the figures are easily seen.

Also, only outlines of water ponds were displayed. Meanwhile, with the entropy filter (Figure 25), the lines on the top and middle water ponds were intensified and highlighted. The images from line 4, which were taken from the nadir view, show the unique result at the bottom left of the water ponds. This result might be caused by the slightly brighter reflectance, which was detected from the top view only, and then was enhanced by the entropy texture filter.

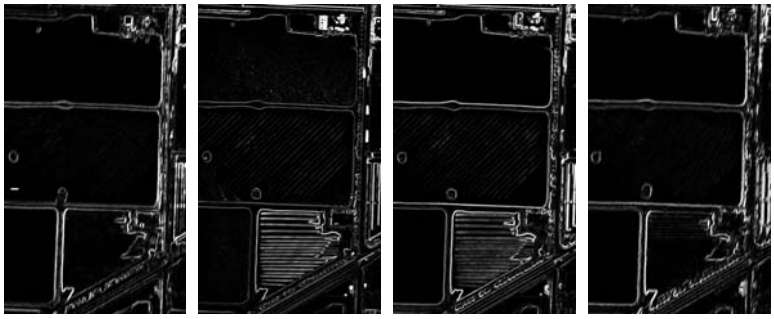

Figure 24. Line 2- Line 8 Window 5x5 Occurrence Texture Filter (Variance)

Figure 25. Line 2- Line 8 Window 5x5 Occurrence Texture Filter (Entropy)

The second type of texture filter used in this study was the co-occurrence based filter. The co-occurrence filter required the user to specify the value of X and Y, which are directions of matrix calculation. In this study, the directions of matrix calculation did affect the result. Most of the effects were discovered on the homogeneity and dissimilarity filtered image, while the least effects were on contrast-filtered image. The remaining co-occurrence filters produced fairly similar results. Figures 26 and 27 show the homogeneity co-occurrence filtered images, which illustrate the effect of direction of matrix calculation. When X=0 and Y=1, only the horizontally-plowed fields were displayed. When X=1 and Y=0, only the vertically-plowed grass fields were revealed.

Both horizontally and vertically plowed fields were revealed when X=1 and Y=1. Nevertheless, these combinations of X and Y shift have no effect on diagonal contours.

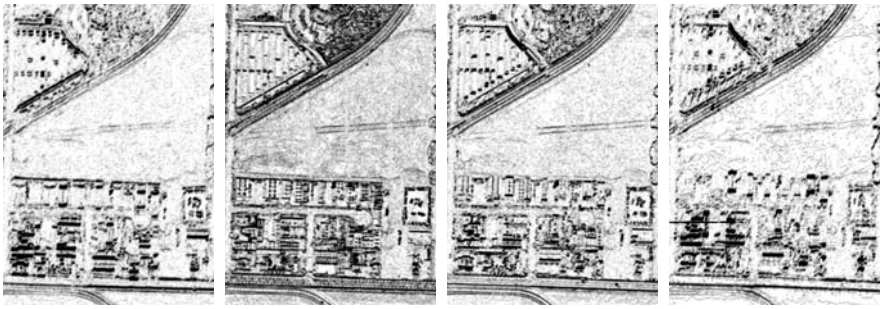

Figure 26. Line 2- Line 8 Window 5x5 Co-Occurrence Texture Filter, Shift X=0, Y=1 (Homogeneity)

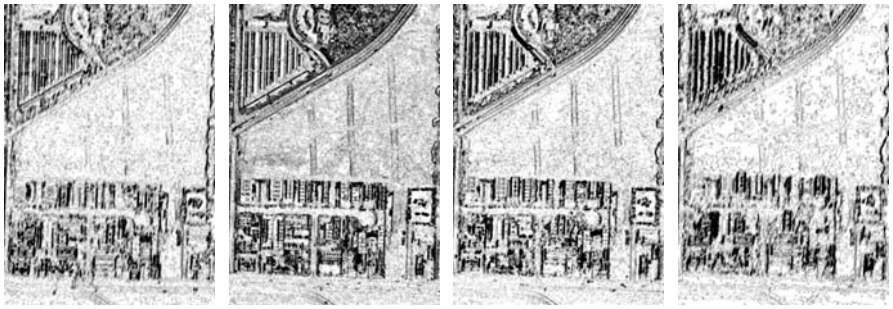

Figure 27. Line 2- Line 8 Window 5x5 Co-Occurrence Texture Filter, Shift X=1, Y=0 (Homogeneity)

B. BIDIRECTIONAL REFLECTANCE DISTRIBUTION FUNCTION (BRDF) ANALYSIS

After the texture filtered images were analyzed, a multispectral analysis approach was applied to the full Fresno image. This study noted that the reflectance of most materials varies with wavelength. Within a single band, material may appear to be the same, but by selecting the proper band combinations, various materials may be made to stand out against their background by exploiting color contrast. (Multispectral User's Guide, 1995) The combination of near infrared (NIR) as well as red and green bands is the first combination (false IR) of multispectral considered. Vegetation appears in various shades of red in the near infrared band due to chlorophyll. This feature discriminates healthy vegetation from dry soil area and is not easily seen in panchromatic (black and white) images. The following image (Figure 28) illustrates the multispectral (NIR, red, green) image in nadir view obtained from line 4. The healthy agricultural

areas of Fresno appear as bright red in this image. In the meantime, dry soils and grass fields appear in green and brown, consecutively.

Figure 28. Multispectral Image (MSI) from Nadir View (Full Scene)

Figure 29 illustrates the corresponding image in panchromatic band (black and white). Although the panchromatic band provides higher resolution (0.61 meter) capability, the difficulty in distinguishing various kinds of material still exists.

Figure 29. The Panchromatic Image from Nadir View

After exploring the comparative images between multispectral and panchromatic, a multispectral approach was followed with a combination of three panchromatic bands was exploited. These three bands were chosen from line 8 (after-look 64.69°, line 6 (after-look 48.64°), and line 4 (nadir view), consecutively. The colors are encoded as line 8, red; line6, green; and line 4, blue. Figure 30 displays the resulting image. The image appears as a colored image and not black and white as do their originals. Regions of different color, such as the brown area around runways at the airport, are caused by BRDF effects. The registration errors cause the displayed color fringes on the images.

Figure 30. Three Band Panchromatic Image

Using ENVI software made it possible to transform images from three band color space to HLS (hue, lightness, and saturation) color space. In this study, the above three band panchromatic images were transformed to HLS color space. This makes it possible to enhance the color contrast, and also to remove the overall intensity as a factor. The transformed product is called a "normalized intensity" image, whose result is displayed in Figure 31. The normalized intensity has enhanced the display of BRDF effect for the above three band panchromatic image. Appendix B displays the magnified portions compared with true and false color IR images.

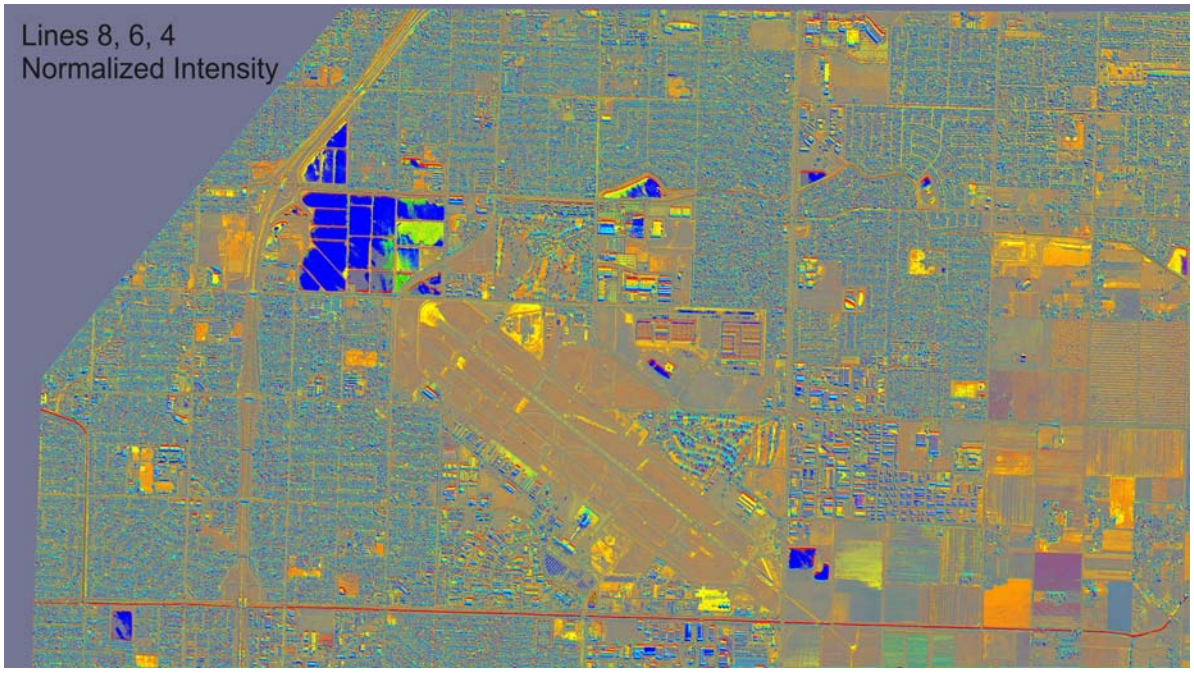

Figure 31. Normalized Intensity Panchromatic Image

Distinct kinds of surface were classified into five main classes by examining the normalized intensity panchromatic image. The five classes are runway/dry soil, vegetation, dry grass, water ponds, and harvested field. The purpose of dividing surfaces into classes is to plot a graph on reflectance scale versus the band number (angle of camera). As a result, it is possible to categorize which angle produces the maximum difference in reflectance. Figure 32 displays the plot.

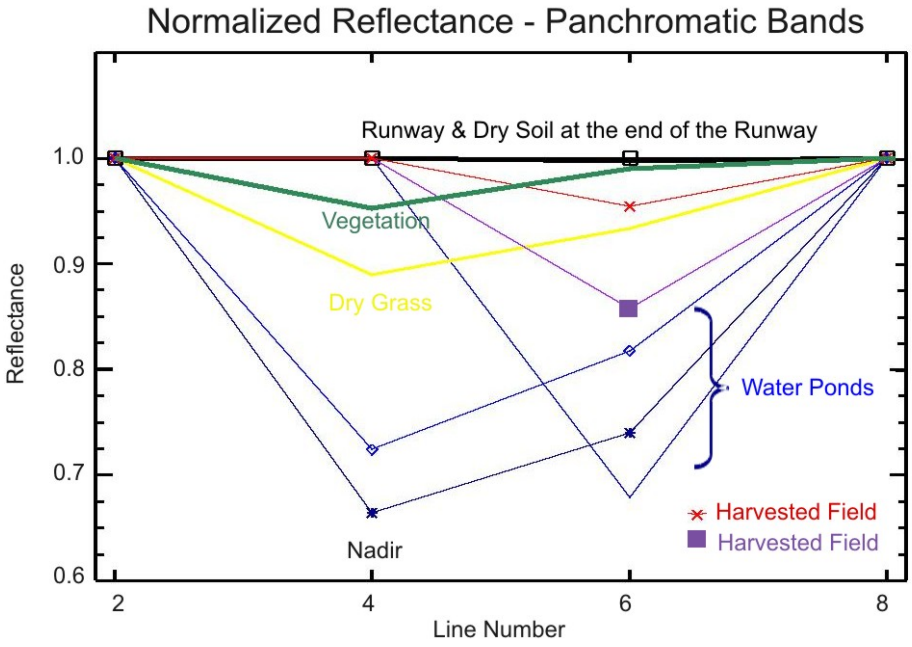

Figure 32. Plot of Reflectances versus Line Number

Figure 32, line 4, which is the nadir view, produced the maximum difference in reflectance for most surfaces. Meanwhile, line 6, the after-look angle, created the distinction in reflectance among the harvested field surface. This distinction did not occur in the nadir angle. This result may lead to promising outcomes in the future studies.

C. MAXIMUM LIKELIHOOD CLASSIFICATION RESULTS

At present, maximum likelihood is considered as the most powerful classifier based on statistic (mean, variance/covariance), and a (Bayesian) Probability Function is calculated from the inputs for classes established from training sites. Each pixel is then judged as to the class to which it most probably belongs. (http://rst.gsfc.nasa.gov/Sect1/Sect1_19.html, 17 February 2005)

This study performed the maximum likelihood classifier acting on several combinations of band from metafile as input. Multiband classes are derived statistically and each unknown pixel is assigned to a class using the ROIs function of ENVI. There were 16 different classes at the beginning of ROIs creation. During the process, these classes were deliberately granulated to 28 distinct categories. Appendix C shows the 25 color key. Modifying the number of classes produces a somewhat different end product.

Application of the ML classifier to subsets of the spectral from metafile illustrated the capability and differences in this approach to image analysis. ML classification of multispectral image from nadir view, as illustrated in Figure 33, shows that water, dry grass, vegetation, harvested field, and runway could be suitably distinguished. However, ML classification of the panchromatic band using multi angle, as illustrated in Figure 34, produces results which are similar overall.

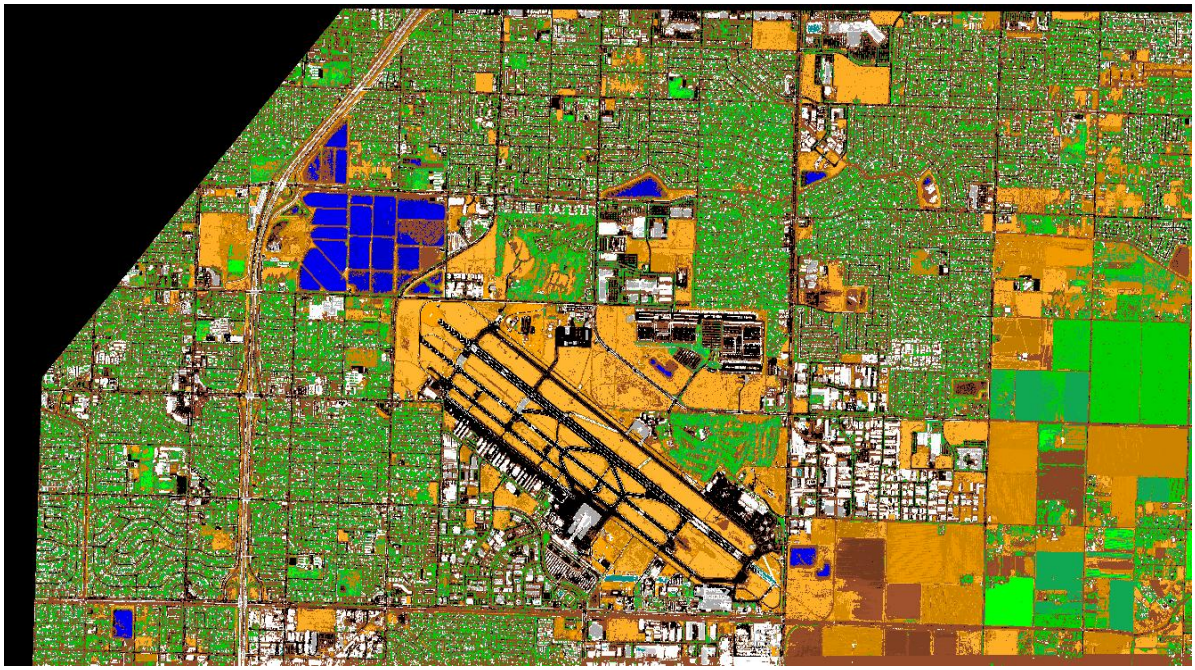

Figure 33. Nadir View- Multispectral Classification Result

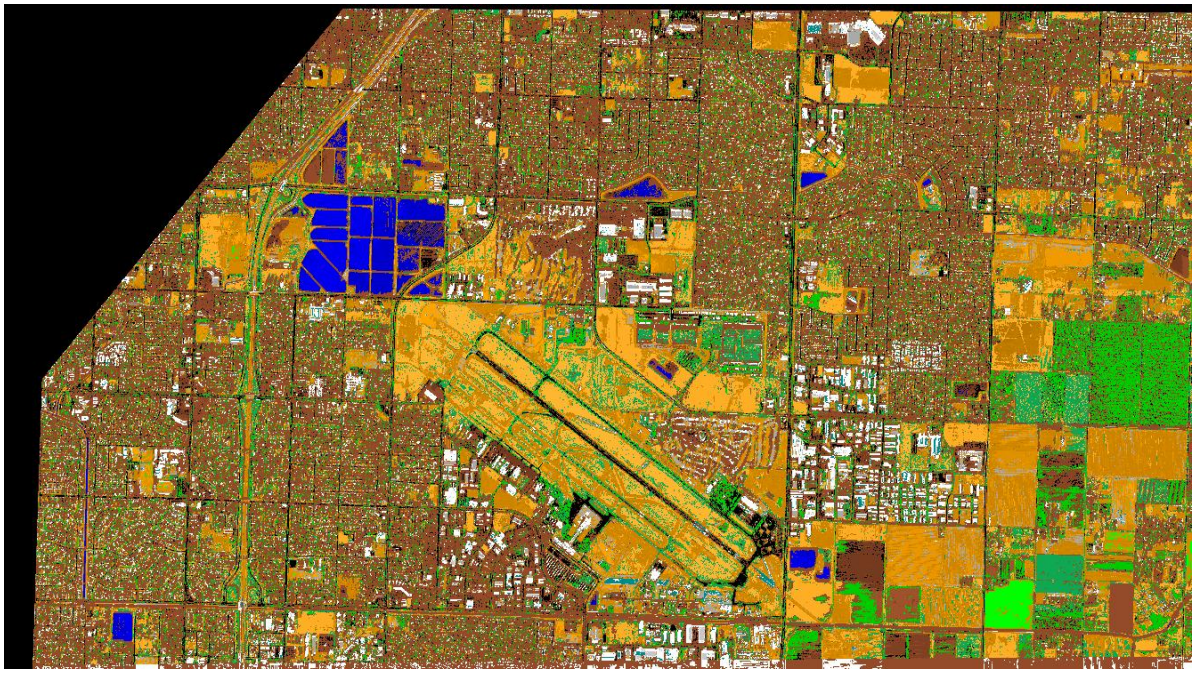

Figure 34. Panchromatic Band- Multi-Angle Classification Result

Figures 33 and 34 do show some differences. ML classification of panchromatic band reveals the soil class among the vegetation area, whose overall resulting image appears brownish. The first noticeable difference is in the middle right vegetation area of these figures. Figure 35 shows magnified portions with a comparison false color image. With the multispectral image, the ML classifier determined these fields to be either orchard or health crops. In the meantime, with the panchromatic band, the ML classifier indicates soil component in those fields, and this result is considered the BRDF effect.

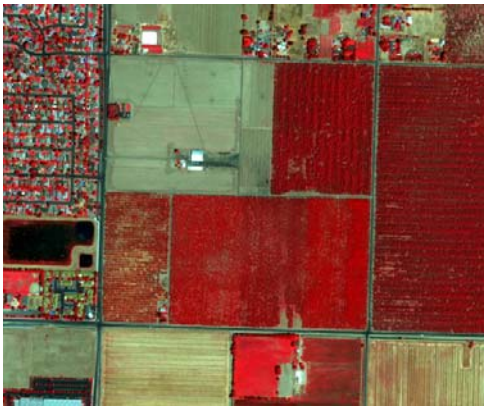

False Color IR

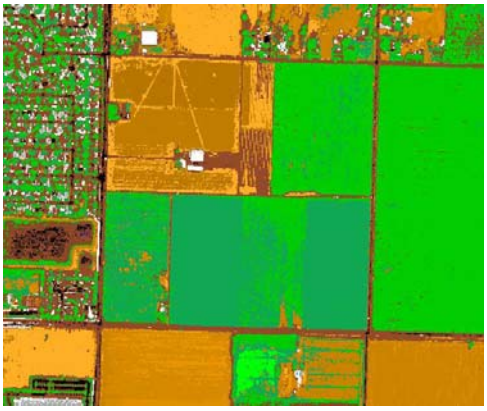

MSI Classification

Color Key

BRDF Classification

Figure 35. Classification Results

The second noticeable difference is located at overruns, the ends of runway, which were not classified as asphalt, but soil in the ML of the panchromatic band. The slight different reflectance on the asphalt surface lured the ML classifier to misinterpret a surface category. This discrepancy illustrates the ML of multi angle to be more sensitive on reflectance, which becomes less effectiveness than the ML of the traditional nadir multispectral approach. Appendix D shows the magnified portions with comparison true color images.

D. ML CLASSIFICATION ON COMBINATION OF MULTISPECTRAL AND PANCHROMATIC BANDS

The previous section explored ML classification on multispectral and panchromatic images individually. Each image was classified based on 28 distinct categories. This section utilized a subset of spectral in metafile to produce a merged file

of multispectral and panchromatic band together. Subsequently, a ML classifier was applied on the merged metafile of multispectral and panchromatic (BRDF) bands. Figure 36 displays the outcomes of ML classification with comparative true/false color images. The most perceptible difference is located in the middle right of each figure. The soil component in the vegetation area, which actually is part of the agricultural field, was misclassified on MSI plus 4 panchromatic results. The additional information has not improved the classification.

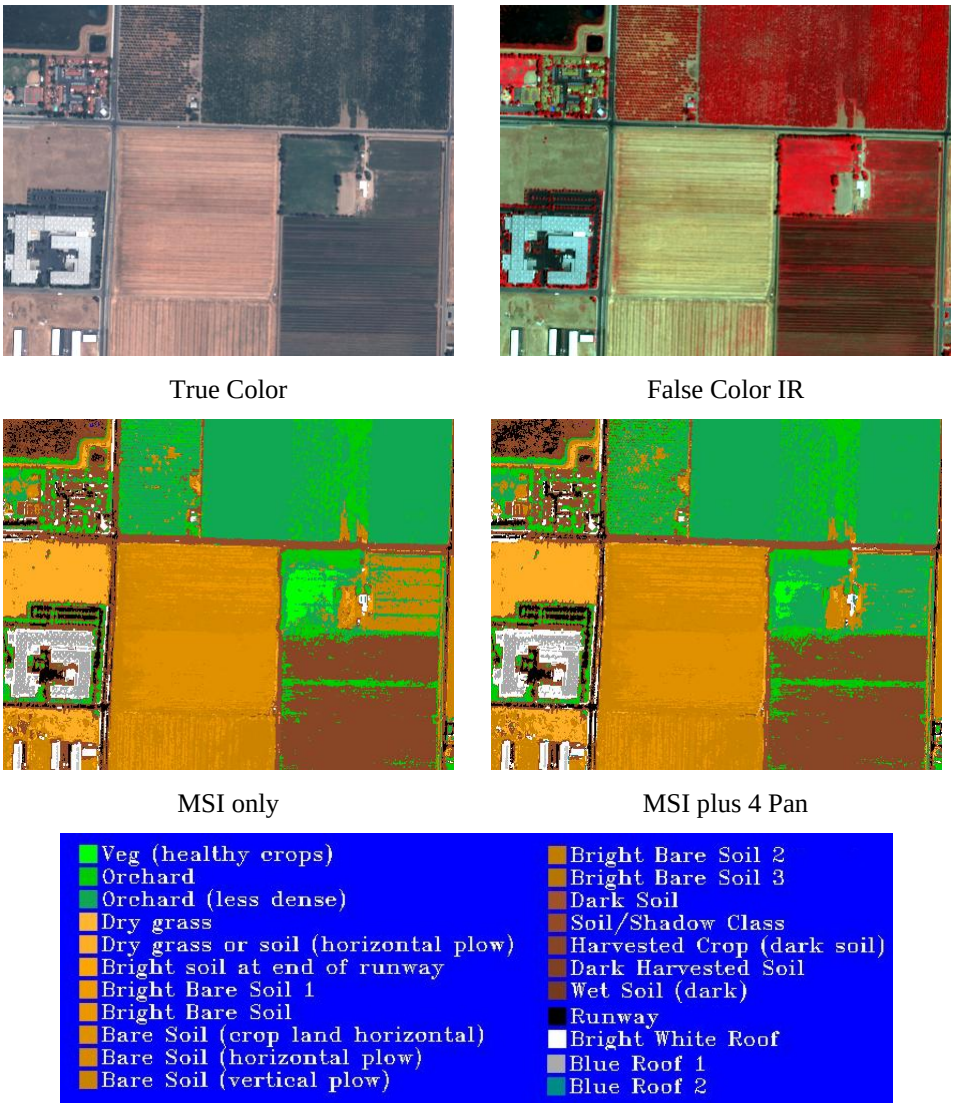

Figure 36. Comparison Figure of MSI and MSI Plus Panchromatic Classification

E. ML CLASSIFICATION ON PANCHROMATIC AND CO-OCCURRENCE TEXTURE FILTERED COMBINED

Immediately following the processing of classification on the combination of the multispectral and panchromatic band, several results became apparent. The information redundancy can lure the classifier to misclassify surface categories. A new approach to the experiment was attempted by combining some of the co-occurrence texture filter results. New combination inputs for ML classification are selected from the metafile. The combination consists of a panchromatic band from the nadir view and co-occurrence texture filter results for the nadir view. The classification output presented a similar result, seen above from the panchromatic band multi-angle classification result but they are not identical. Figure 37 presents the output of ML classification.

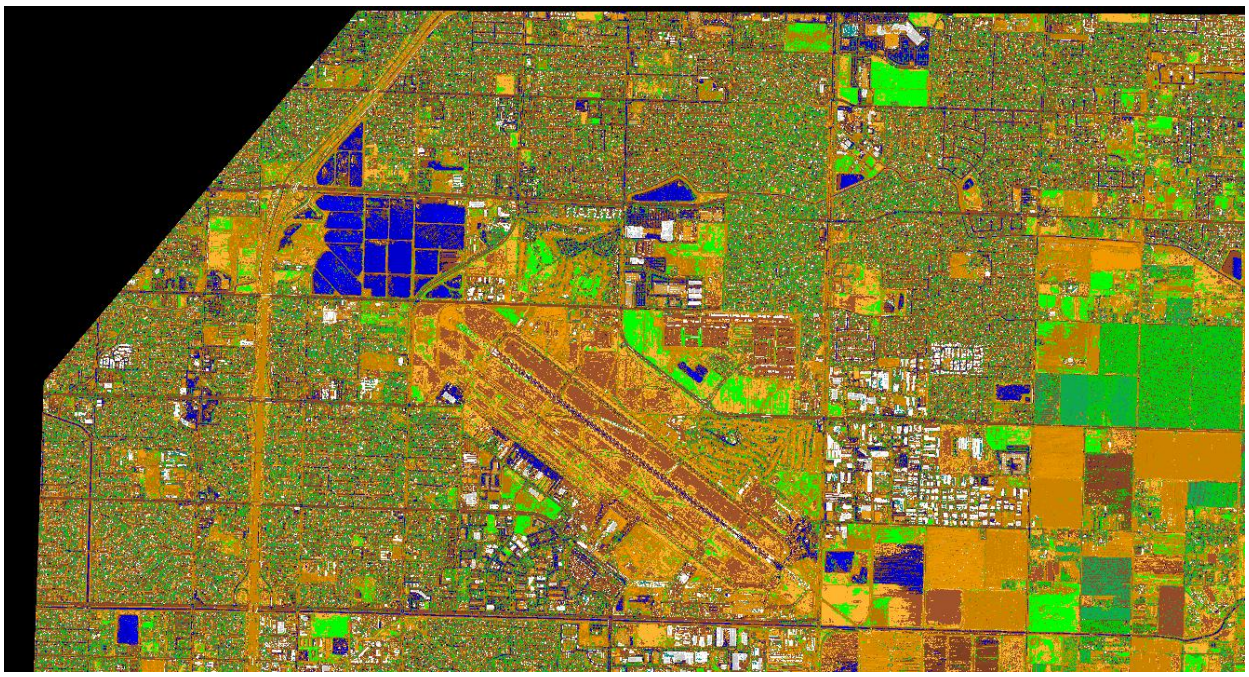

Figure 37. Panchromatic Band Nadir View Combined with Texture Co-Occurrence X=0, Y=1 Classification Result

The classifier has a dependence on the co-occurrence filter characteristics, previously mentioned in the beginning of Chapter IV. Both the view angle and the direction of calculation during image processing also influence the end product. The following set of images (Figure 38) illustrated the visible effect of the co-occurrence measure (homogeneity, dissimilarity, contrast). The combinations of X, Y shift, which

has revealed or unrevealed the horizontal/vertical contour, still produce those similar effects, but to a modest degree. When X=0 and Y=1, only horizontal contours were displayed. When X=1 and Y=0, only vertical contours were revealed. Both horizontal and vertical contours were revealed when X=1 and Y=1. These effects were weakened because eight filtered layers had been combined in the metafile for each X, Y shift. The "Merged" shift figure at the lower right shows a composition of all combinations. Wet soil has now disclosed its water component.

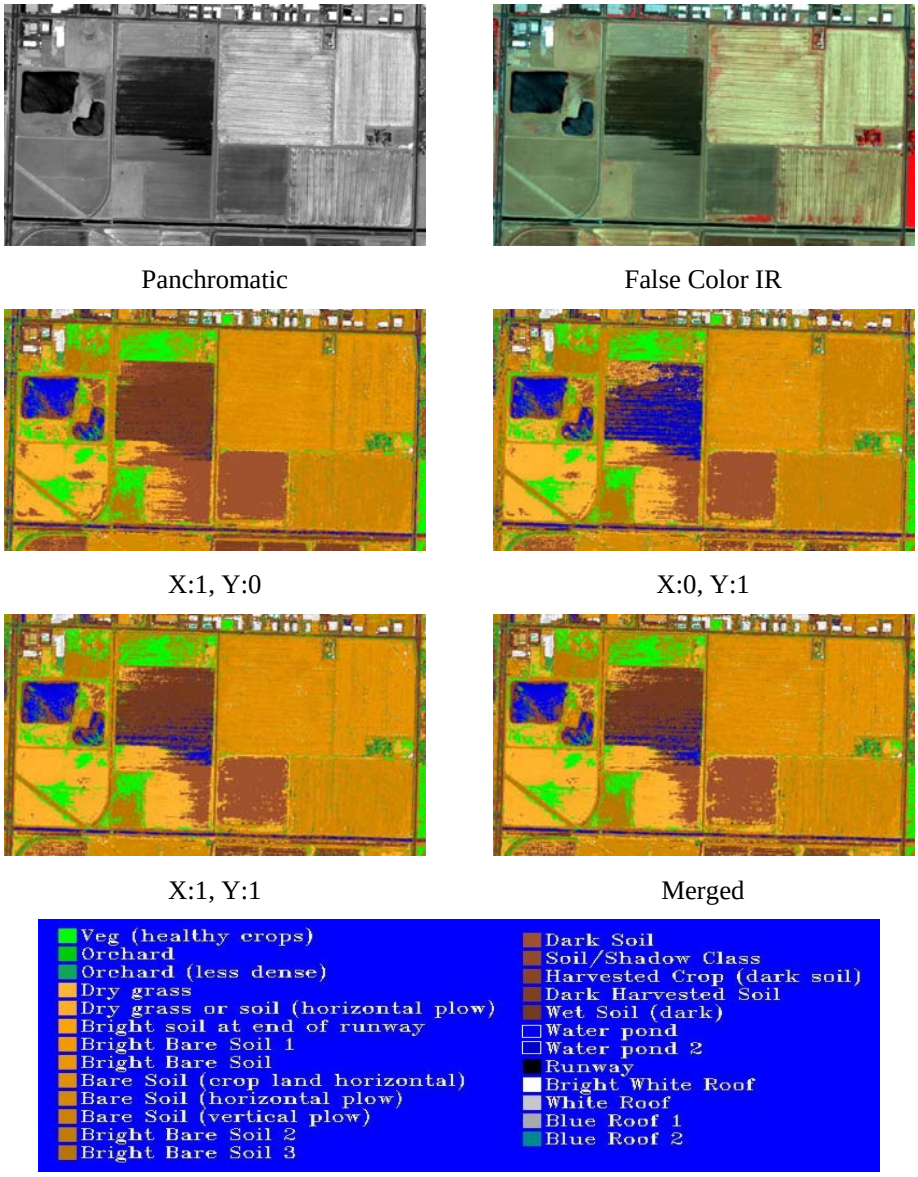

Figure 38. Texture Classification Results

Appendix E shows another premise of the filtered texture classification result. By comparison, these results with the color key and the categories of surface, were reassigned to the neighbor type, from vegetation to orchard, dark soil to wet soil, and so forth. Therefore, the classification result of panchromatic and co-occurrence was not yet captivating. The color scale was deliberately revised in order to enhance the differences of the classification result. Instead of assigning soil classes to the sienna tone as in the conventional color scale, some soil classes were assigned to the blue tone. The classification product with the new color scale presented the fascinating results shown in Figure 39. The bright bare soils, which were once disguised in panchromatic and false color IR, now became noticeable.

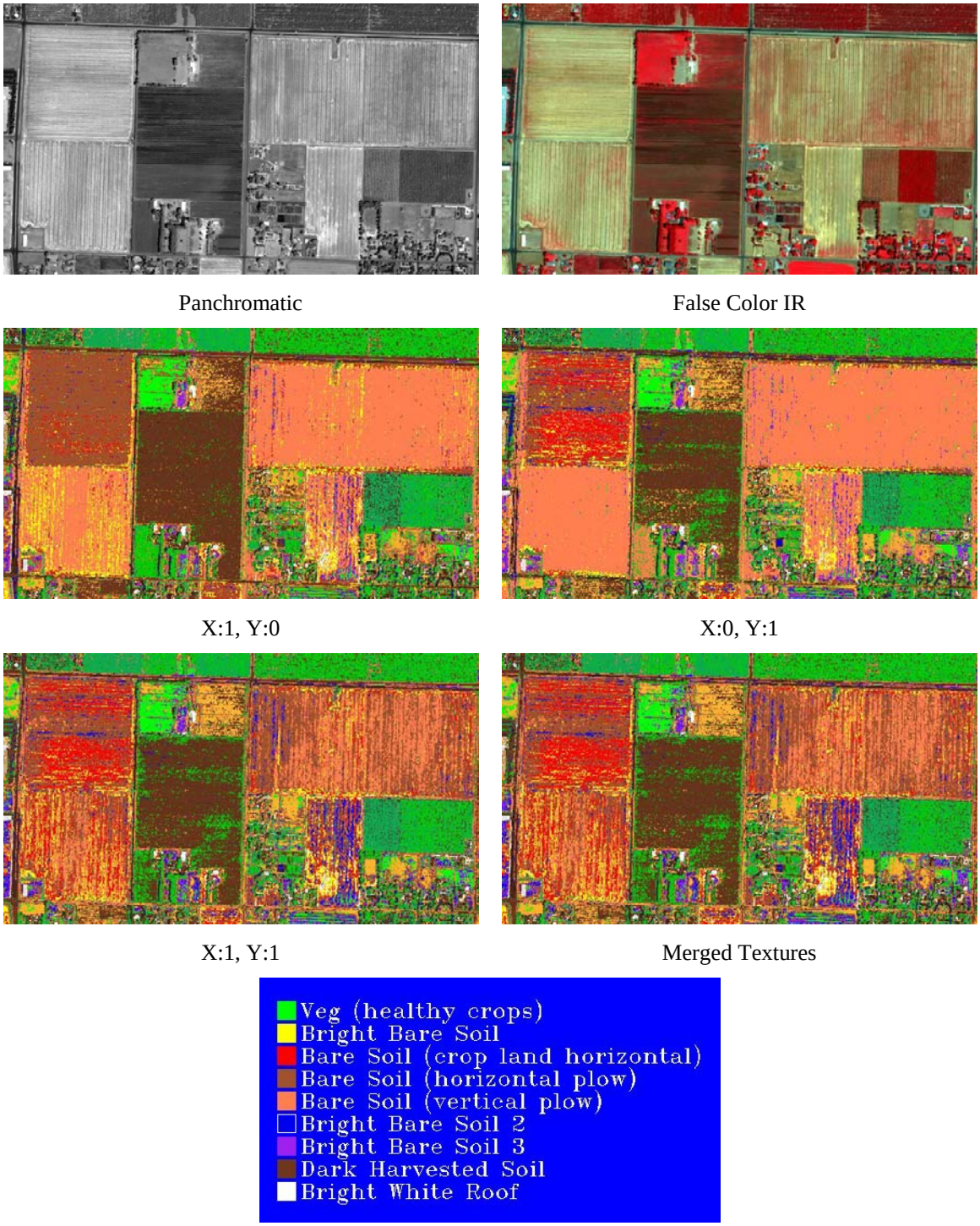

Figure 39. Texture Classification Results with Revised Color Scale

V. CONCLUSIONS

This study has analyzed the consequences of directional reflectance effects in high-spatial resolution imagery, as BDRF effects impact terrain classification. Two major topics were considered for the multi-spectral, multi-angle dataset acquired over Fresno, California, on July 13, 2003 by the QuickBird satellite. First, how does the addition of multiple views to a data collection improve the classification process, and second, how do texture concepts apply in the terrain classification process?

Multiple views (nadir and off-nadir) imagery taken from the panchromatic sensors show Bi-directional Reflectance Distribution Function (BRDF) effects. These variations provide additional information, by comparison to strictly nadir-view multispectral imaging (MSI). Terrain classification using only the panchromatic bands gave results that were very similar to those obtained from the nadir view MSI analysis. Combined analysis using the panchromatic and multispectral data did not produce a noticeably higher accuracy, however. This appears to be an example of the Hughes paradox, where increased dimensionality in the data produced no effective increase in classification accuracy (Hughes, 1968).

Texture analysis in the panchromatic imagery showed the ability to discriminate different surfaces, as previously determined (Haralick, 1973). Texture analysis has a directional component that was dealt with by averaging over direction. The results using texture analysis were comparable to those obtained via spectral and angular classification. Textures did vary with angle in the panchromatic imagery. Put differently, texture did not serve as an invariant with angle.

The dimensionality of the combined data sets, and analysis processes (e.g. texture analysis), has not yet been exploited well. A standard maximum likelihood (ML) classifier was used for this work. This approach does not appear to lend itself well to the redundant information provided by the sensors for this project. A classification technique more appropriate to these redundant datasets is needed.

THIS PAGE INTENTIONALLY LEFT BLANK

APPENDIX A. TEXTURE FILTERED IMAGES

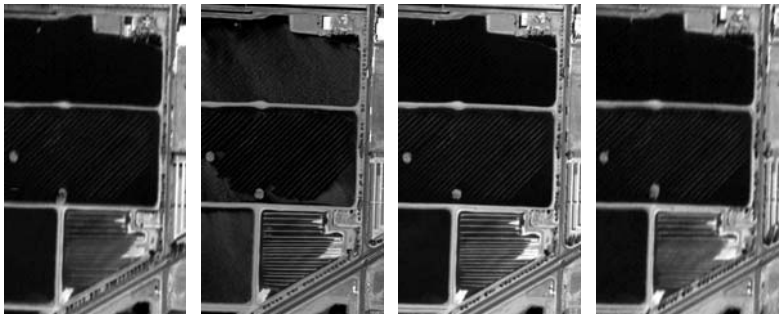

Scene#1, Line 2- Line 8 (Without any texture filter)

Scene#2, Line 2- Line 8 (Without any texture filter)

Scene#1 Line 2- Line 8 Window 5x5 Occurrence Texture Filter

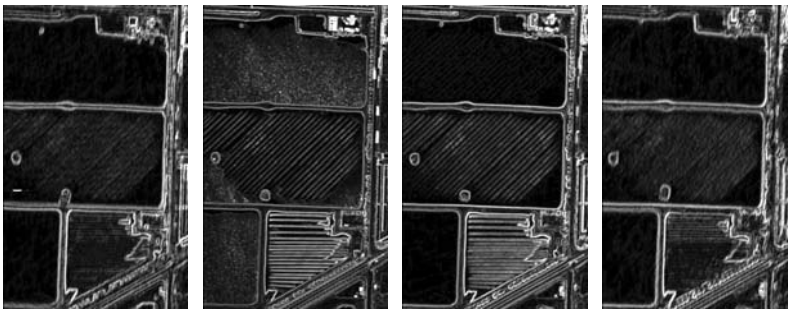

Line 2- Line 8 Window 5x5 Occurrence Texture Filter (Data Range)

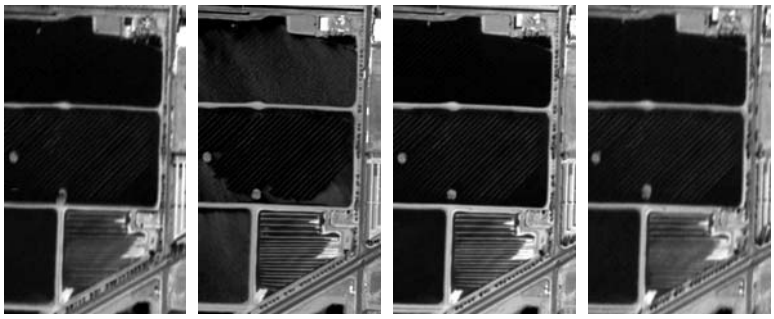

Line 2- Line 8 Window 5x5 Occurrence Texture Filter (Mean)

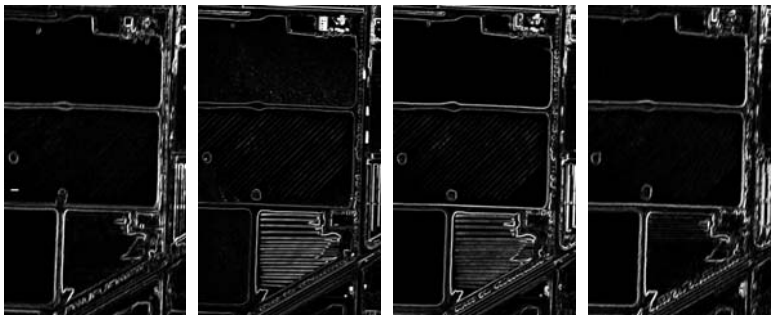

Line 2- Line 8 Window 5x5 Occurrence Texture Filter (Variance)

Line 2- Line 8 Window 5x5 Occurrence Texture Filter (Entropy)

Line 2- Line 8 Window 5x5 Occurrence Texture Filter (Skewness)

Scene#1 Line 2- Line 8 Window 5x5 Co-Occurrence Texture Filter, Shift X=0, Y=1

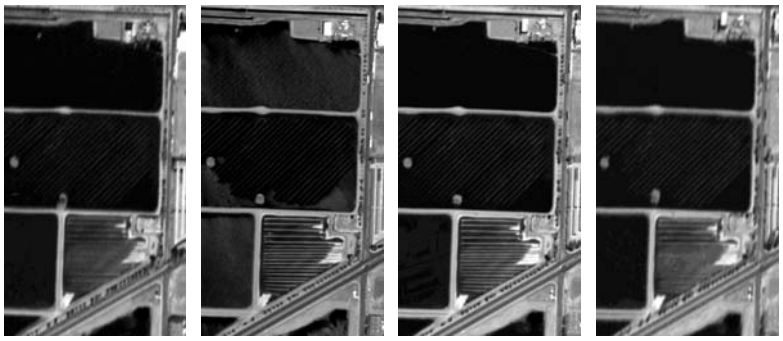

Line 2- Line 8 Window 5x5 Co-Occurrence Texture Filter, Shift X=0, Y=1 (Mean)

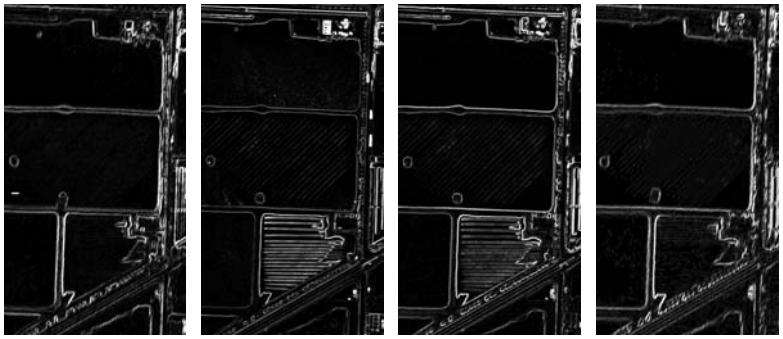

Line 2- Line 8 Window 5x5 Co-Occurrence Texture Filter, Shift X=0, Y=1 (Variance)

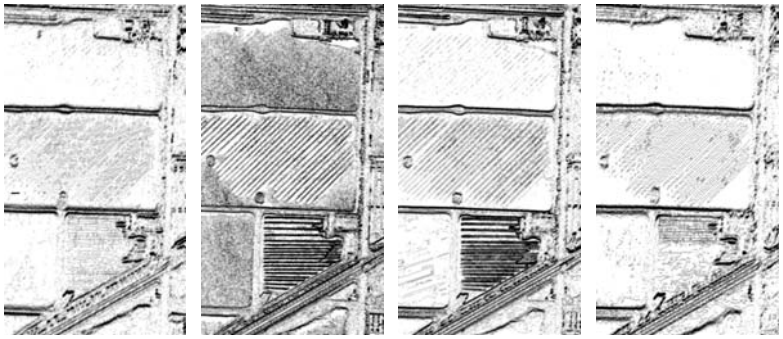

Line 2- Line 8 Window 5x5 Co-Occurrence Texture Filter, Shift X=0, Y=1 (Homogeneity)

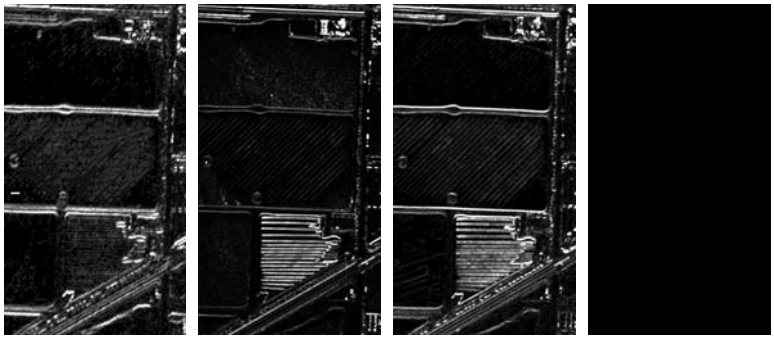

Line 2- Line 8 Window 5x5 Co-Occurrence Texture Filter, Shift X=0, Y=1 (Contrast)

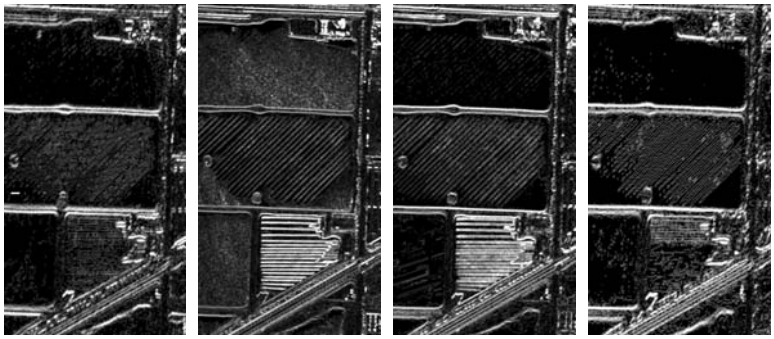

Line 2- Line 8 Window 5x5 Co-Occurrence Texture Filter, Shift X=0, Y=1 (Dissimilarity)

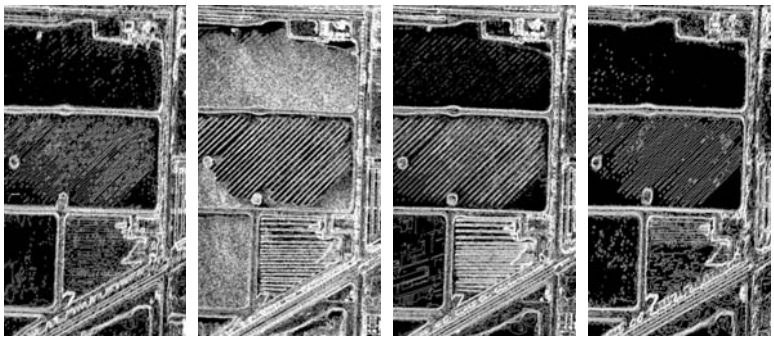

Line 2- Line 8 Window 5x5 Co-Occurrence Texture Filter, Shift X=0, Y=1 (Entropy)

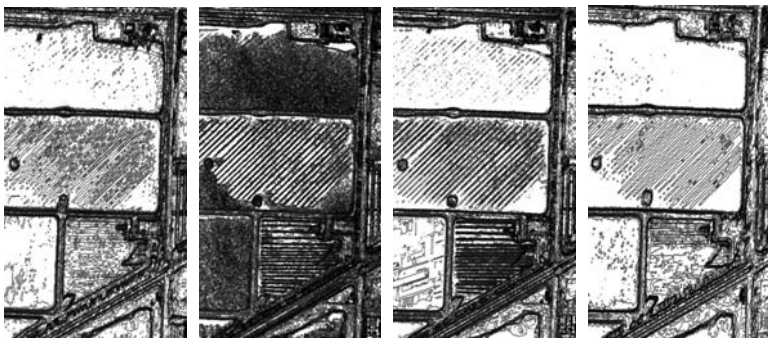

Line 2- Line 8 Window 5x5 Co-Occurrence Texture Filter, Shift X=0, Y=1 (Second Moment)

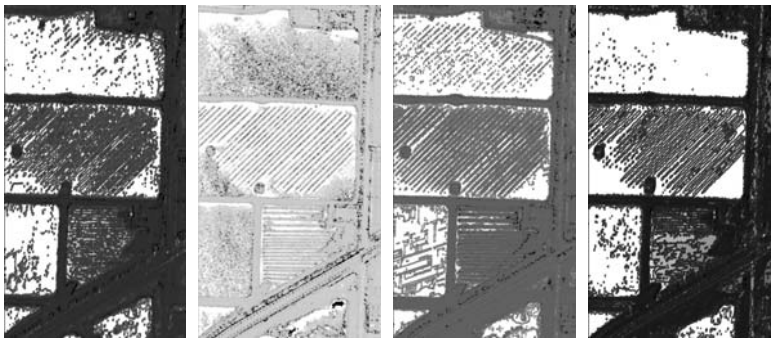

Line 2- Line 8 Window 5x5 Co-Occurrence Texture Filter, Shift X=0, Y=1 (Correlation)

Scene#1 Line 2- Line 8 Window 5x5 Co-Occurrence Texture Filter, Shift X=1, Y=0

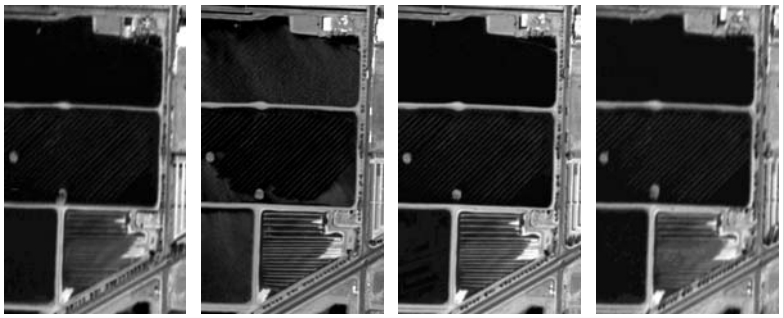

Line 2- Line 8 Window 5x5 Co-Occurrence Texture Filter, Shift X=1, Y=0 (Mean)

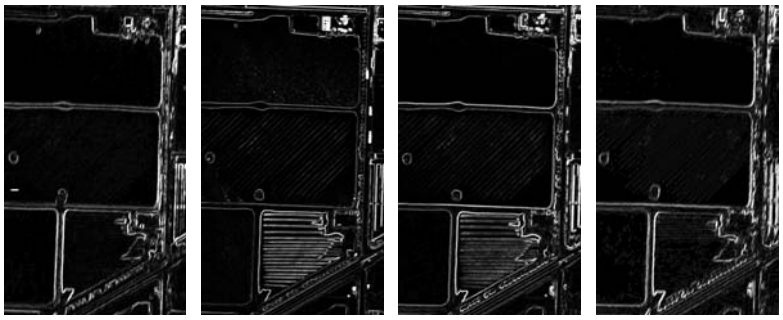

Line 2- Line 8 Window 5x5 Co-Occurrence Texture Filter, Shift X=1, Y=0 (Variance)

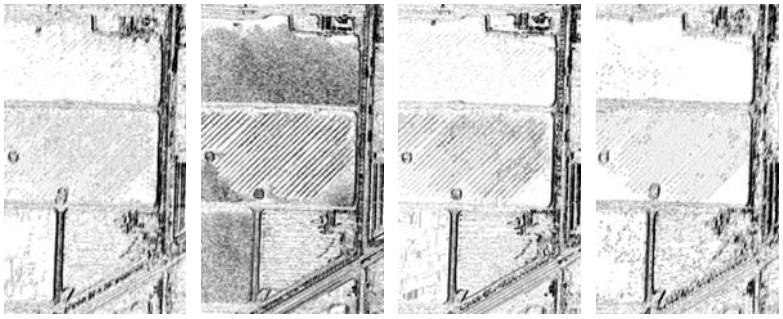

Line 2- Line 8 Window 5x5 Co-Occurrence Texture Filter, Shift X=1, Y=0 (Homogeneity)

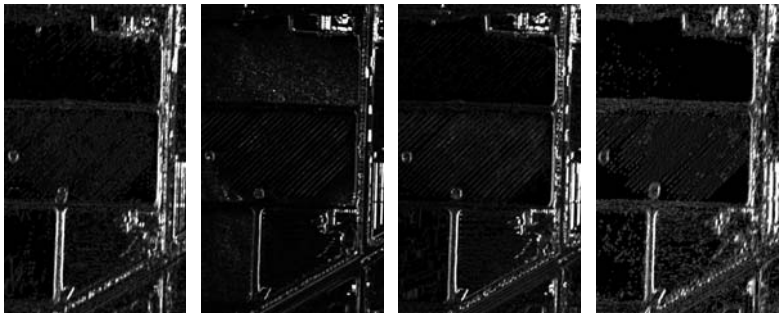

Line 2- Line 8 Window 5x5 Co-Occurrence Texture Filter, Shift X=1, Y=0 (Contrast)

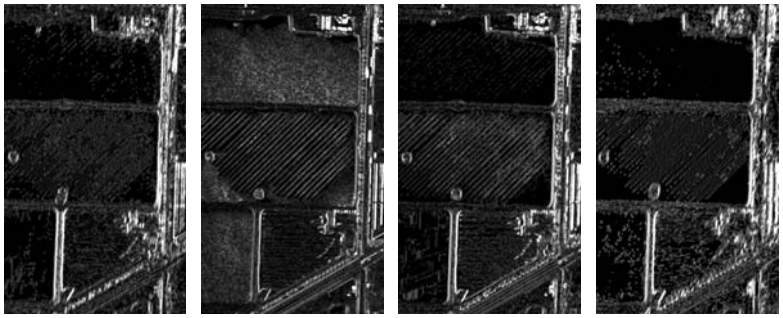

Line 2- Line 8 Window 5x5 Co-Occurrence Texture Filter, Shift X=1, Y=0 (Dissimilarity)

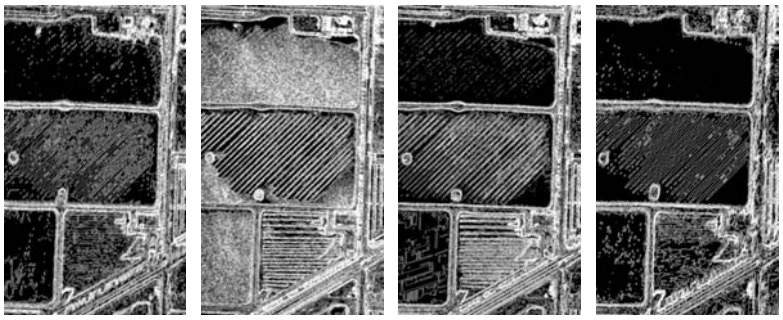

Line 2- Line 8 Window 5x5 Co-Occurrence Texture Filter, Shift X=1, Y=0 (Entropy)

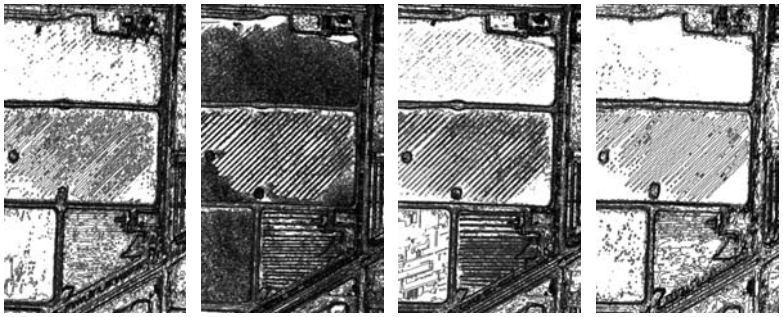

Line 2- Line 8 Window 5x5 Co-Occurrence Texture Filter, Shift X=1, Y=0 (Second Moment)

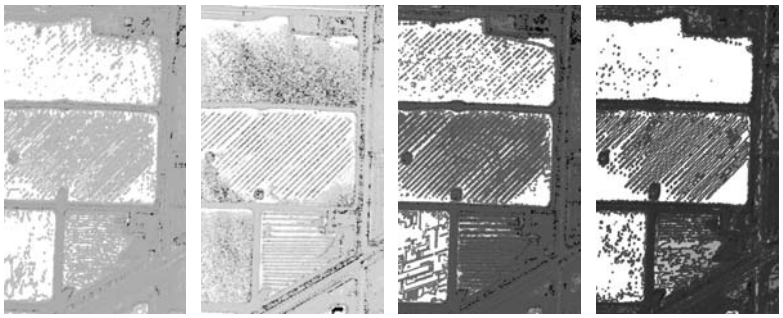

Line 2- Line 8 Window 5x5 Co-Occurrence Texture Filter, Shift X=1, Y=0 (Correlation)

Scene#1 Line 2- Line 8 Window 5x5 Co-Occurrence Texture Filter, Shift X=1, Y=1

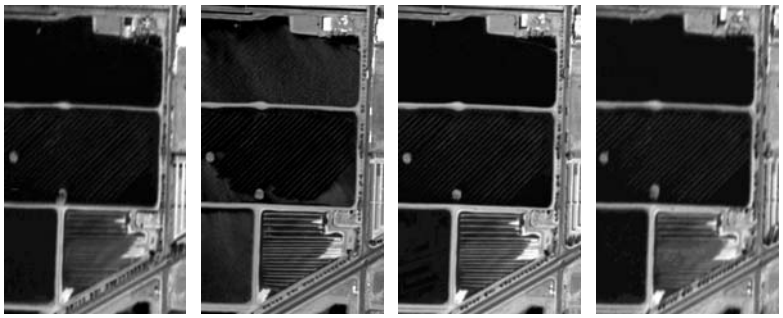

Line 2- Line 8 Window 5x5 Co-Occurrence Texture Filter, Shift X=1, Y=1 (Mean)

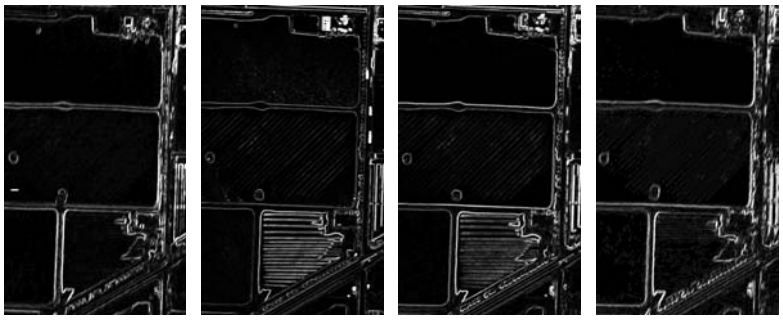

Line 2- Line 8 Window 5x5 Co-Occurrence Texture Filter, Shift X=1, Y=1 (Variance)

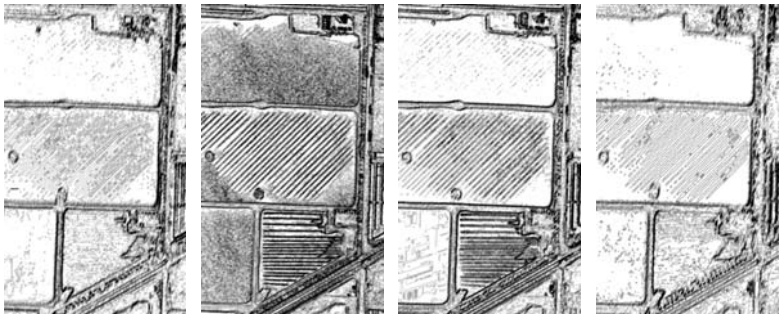

Line 2- Line 8 Window 5x5 Co-Occurrence Texture Filter, Shift X=1, Y=1 (Homogeneity)

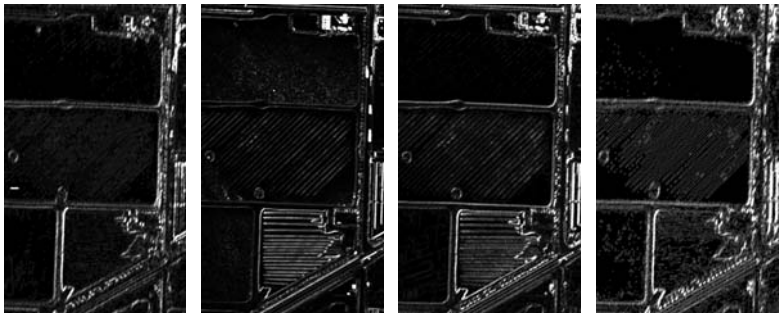

Line 2- Line 8 Window 5x5 Co-Occurrence Texture Filter, Shift X=1, Y=1 (Contrast)

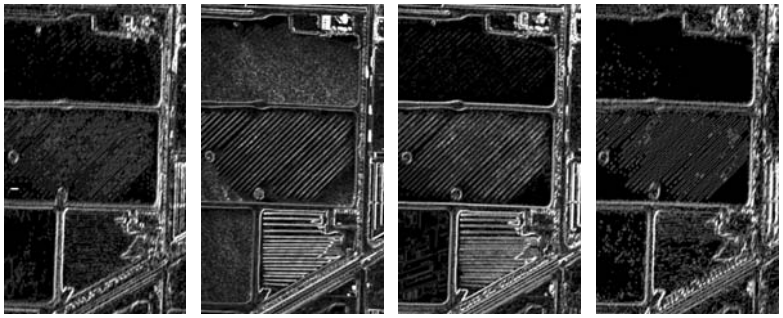

Line 2- Line 8 Window 5x5 Co-Occurrence Texture Filter, Shift X=1, Y=1 (Dissimilarity)

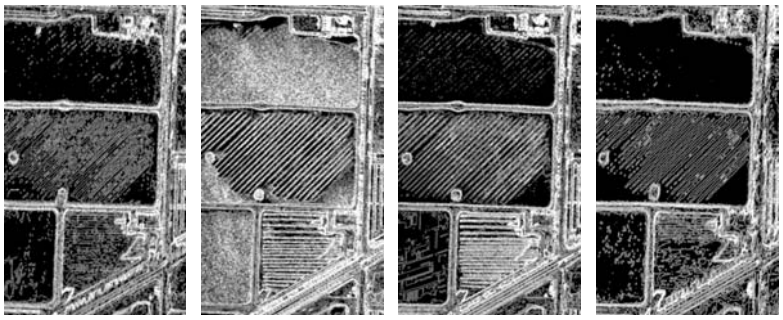

Line 2- Line 8 Window 5x5 Co-Occurrence Texture Filter, Shift X=1, Y=1 (Entropy)

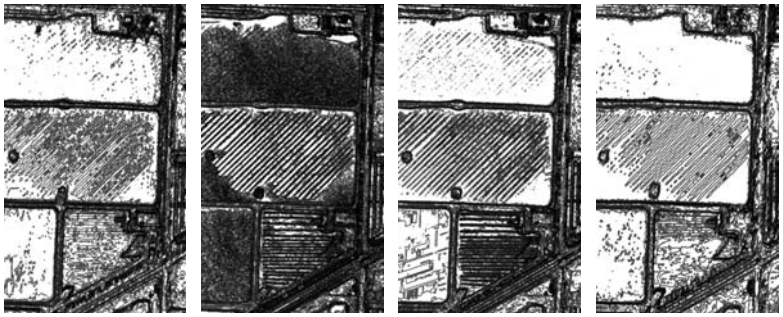

Line 2- Line 8 Window 5x5 Co-Occurrence Texture Filter, Shift X=1, Y=1 (Second Moment)

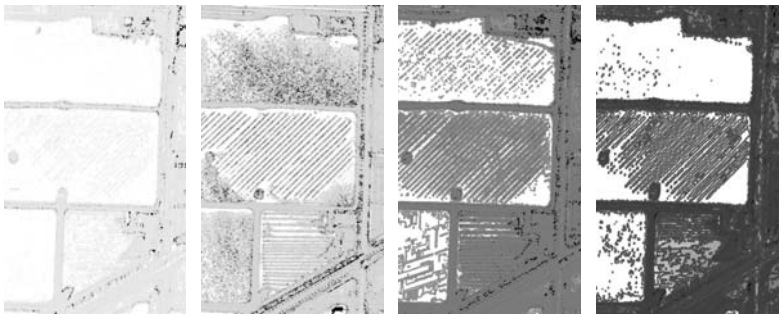

Line 2- Line 8 Window 5x5 Co-Occurrence Texture Filter, Shift X=1, Y=1 (Correlation)

Scene#2 Line 2- Line 8 Window 5x5 Co-Occurrence Texture Filter, Shift X=0, Y=1

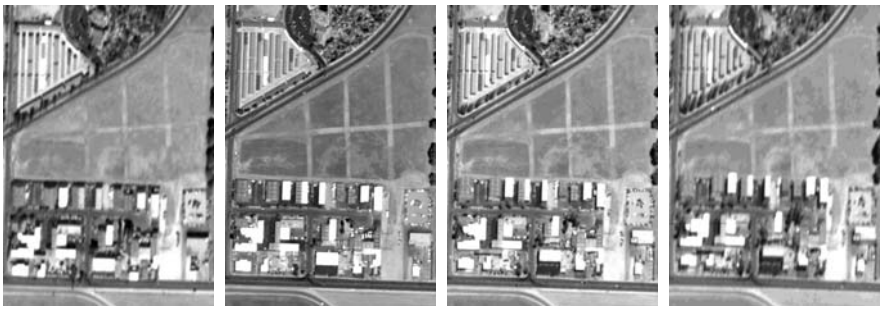

Line 2- Line 8 Window 5x5 Co-Occurrence Texture Filter, Shift X=0, Y=1 (Mean)

Line 2- Line 8 Window 5x5 Co-Occurrence Texture Filter, Shift X=0, Y=1 (Variance)

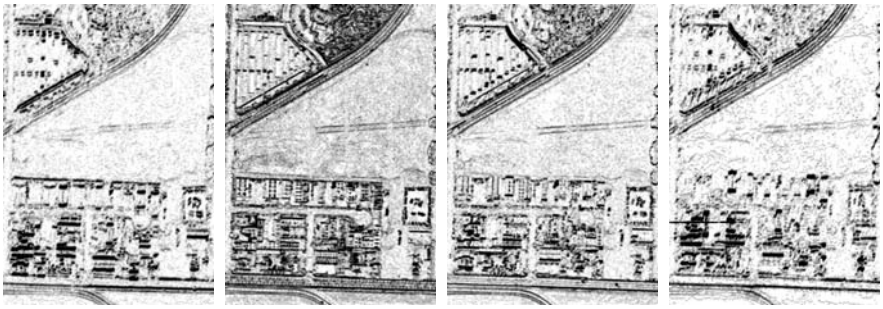

Line 2- Line 8 Window 5x5 Co-Occurrence Texture Filter, Shift X=0, Y=1 (Homogeneity)

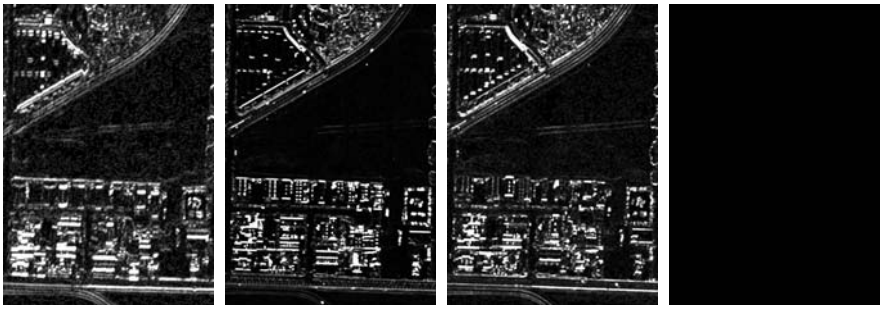

Line 2- Line 8 Window 5x5 Co-Occurrence Texture Filter, Shift X=0, Y=1 (Contrast)

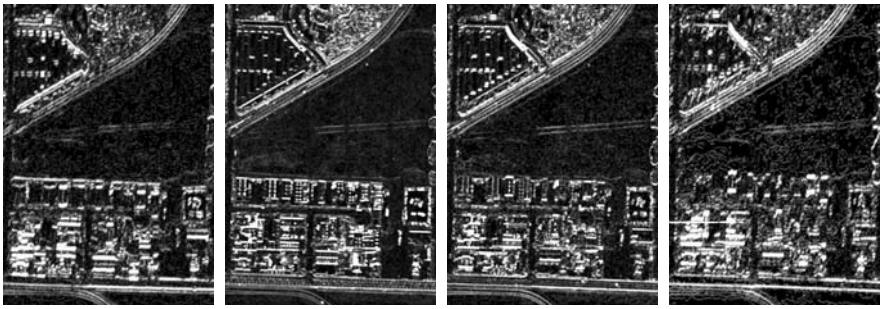

Line 2- Line 8 Window 5x5 Co-Occurrence Texture Filter, Shift X=0, Y=1 (Dissimilarity)

Line 2- Line 8 Window 5x5 Co-Occurrence Texture Filter, Shift X=0, Y=1 (Entropy)

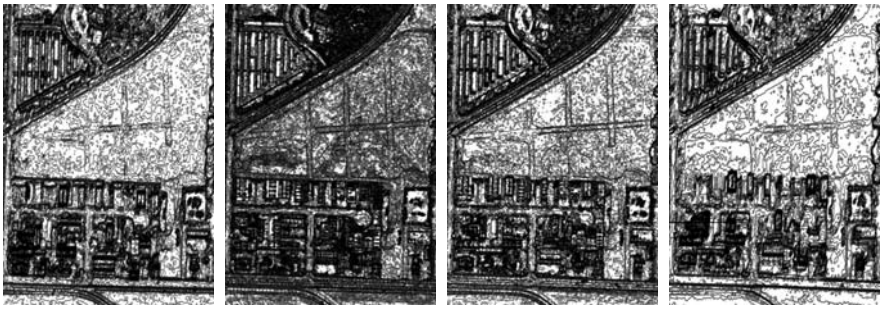

Line 2- Line 8 Window 5x5 Co-Occurrence Texture Filter, Shift X=0, Y=1 (Second Moment)

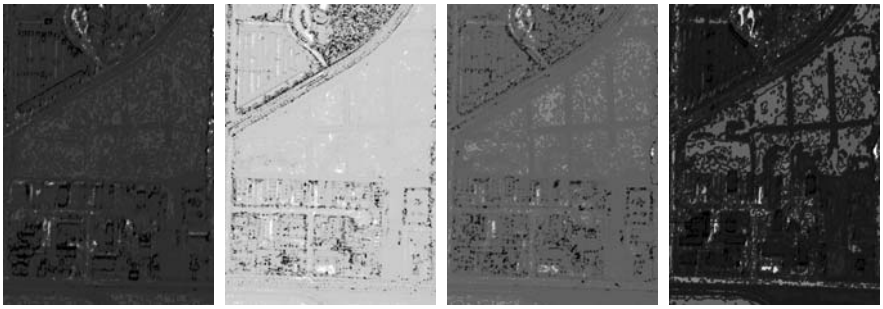

Line 2- Line 8 Window 5x5 Co-Occurrence Texture Filter, Shift X=0, Y=1 (Correlation)

Scene#2 Line 2- Line 8 Window 5x5 Co-Occurrence Texture Filter, Shift X=1, Y=0

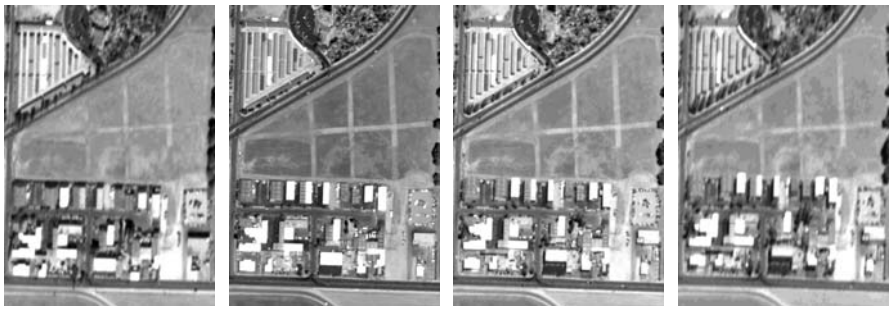

Line 2- Line 8 Window 5x5 Co-Occurrence Texture Filter, Shift X=1, Y=0 (Mean)

Line 2- Line 8 Window 5x5 Co-Occurrence Texture Filter, Shift X=1, Y=0 (Variance)

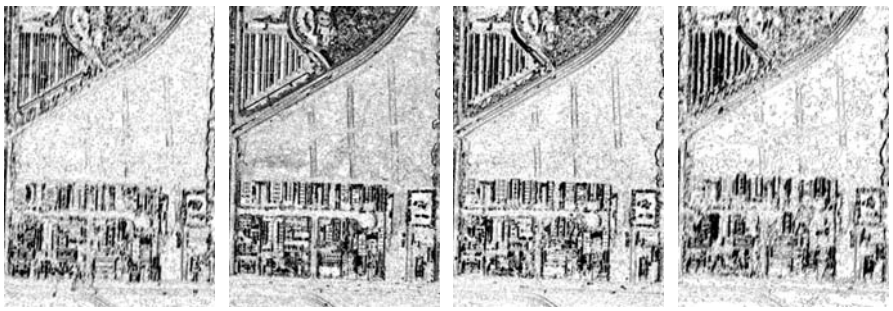

Line 2- Line 8 Window 5x5 Co-Occurrence Texture Filter, Shift X=1, Y=0 (Homogeneity)

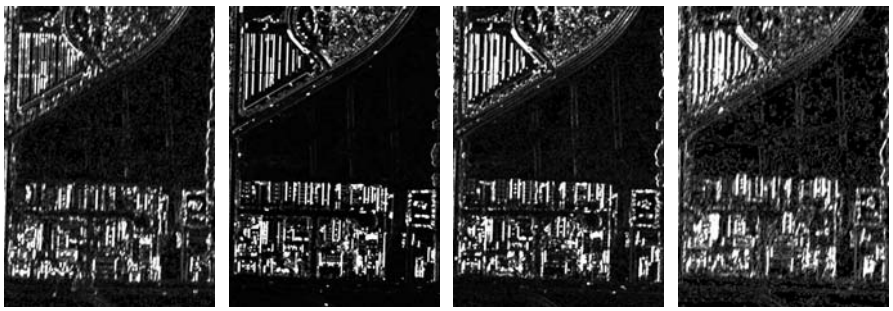

Line 2- Line 8 Window 5x5 Co-Occurrence Texture Filter, Shift X=1, Y=0 (Contrast)

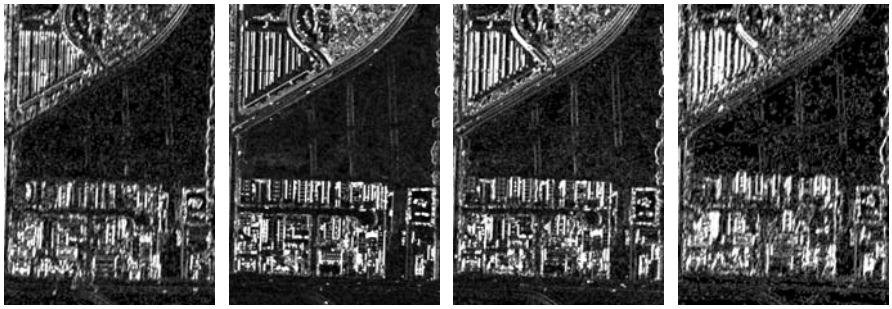

Line 2- Line 8 Window 5x5 Co-Occurrence Texture Filter, Shift X=1, Y=0 (Dissimilarity)

Line 2- Line 8 Window 5x5 Co-Occurrence Texture Filter, Shift X=1, Y=0 (Entropy)

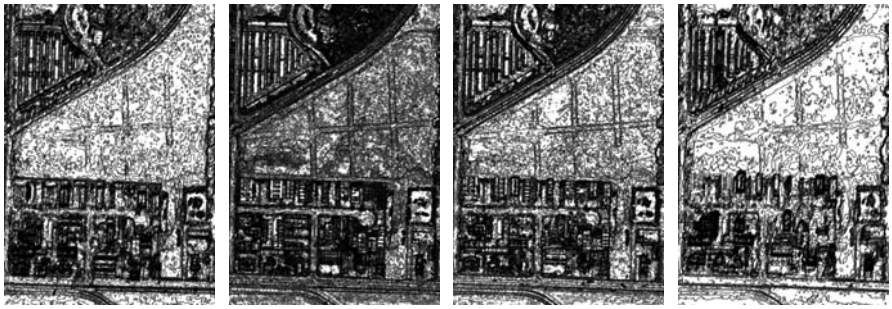

Line 2- Line 8 Window 5x5 Co-Occurrence Texture Filter, Shift X=1, Y=0 (Second Moment)

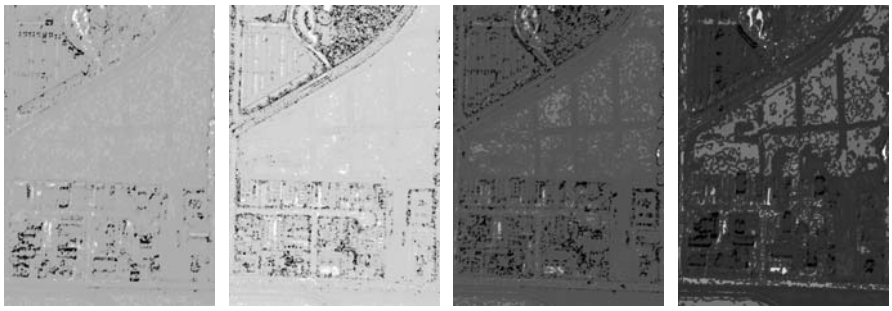

Line 2- Line 8 Window 5x5 Co-Occurrence Texture Filter, Shift X=1, Y=0 (Correlation)

Scene#2 Line 2- Line 8 Window 5x5 Co-Occurrence Texture Filter, Shift X=1, Y=1

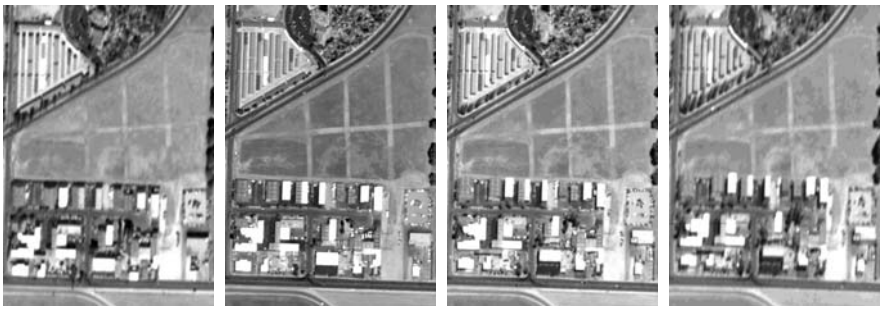

Line 2- Line 8 Window 5x5 Co-Occurrence Texture Filter, Shift X=1, Y=1 (Mean)

Line 2- Line 8 Window 5x5 Co-Occurrence Texture Filter, Shift X=1, Y=1 (Variance)

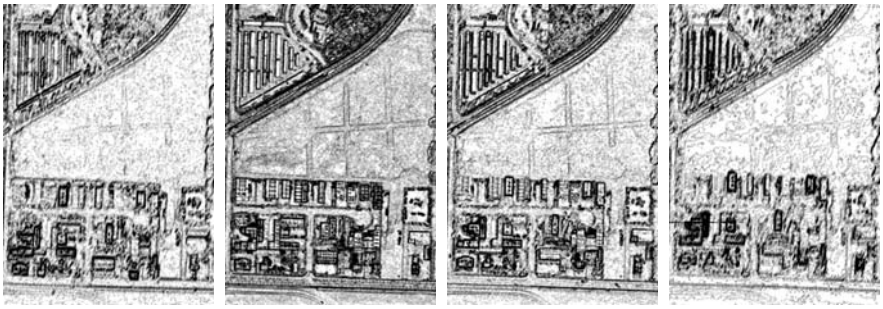

Line 2- Line 8 Window 5x5 Co-Occurrence Texture Filter, Shift X=1, Y=1 (Homogeneity)

Line 2- Line 8 Window 5x5 Co-Occurrence Texture Filter, Shift X=1, Y=1 (Contrast)

Line 2- Line 8 Window 5x5 Co-Occurrence Texture Filter, Shift X=1, Y=1 (Dissimilarity)

Line 2- Line 8 Window 5x5 Co-Occurrence Texture Filter, Shift X=1, Y=1 (Entropy)

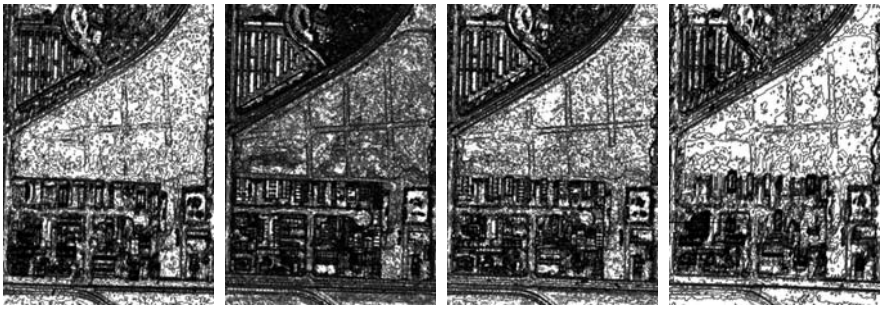

Line 2- Line 8 Window 5x5 Co-Occurrence Texture Filter, Shift X=1, Y=1 (Second Moment)

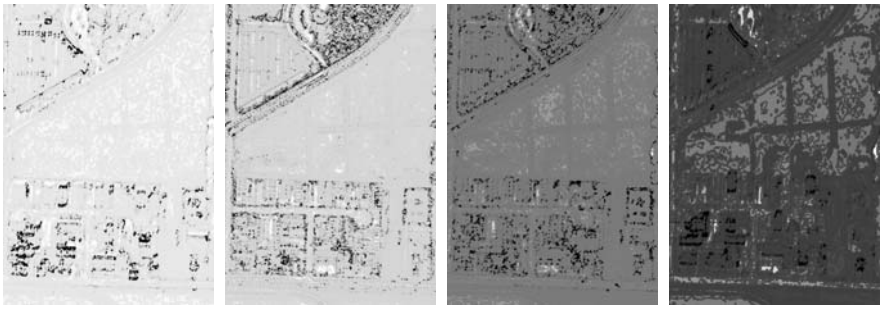

Line 2- Line 8 Window 5x5 Co-Occurrence Texture Filter, Shift X=1, Y=1 (Correlation)

Scene#2 Line 2- Line 8 Window 5x5 Co-Occurrence Texture Filter (Homogeneity)

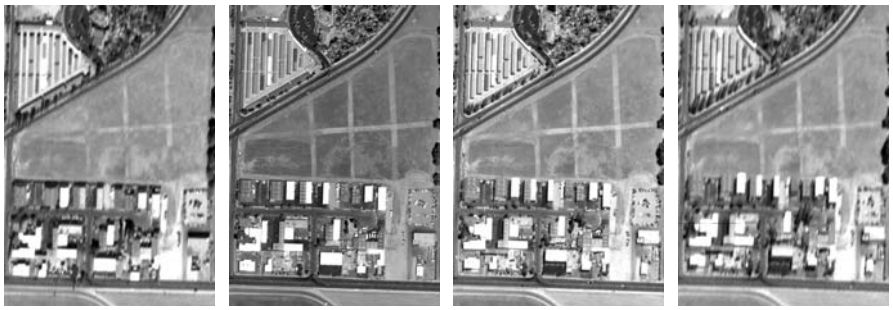

Line 2- Line 8 (Without any texture filter)

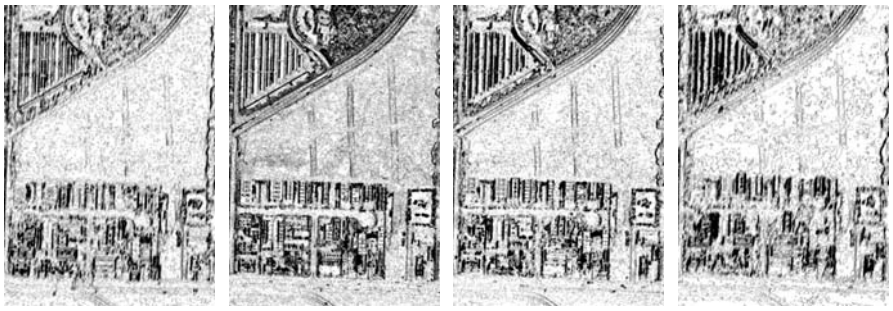

Line 2- Line 8 Window 5x5 Co-Occurrence Texture Filter, Shift X=1, Y=0 (Homogeneity)

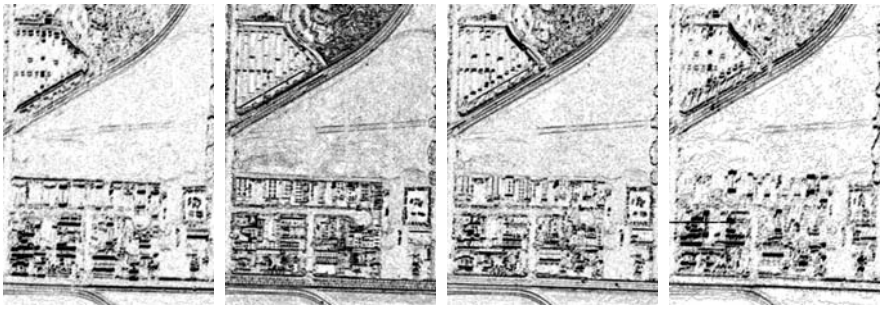

Line 2- Line 8 Window 5x5 Co-Occurrence Texture Filter, Shift X=0, Y=1 (Homogeneity)

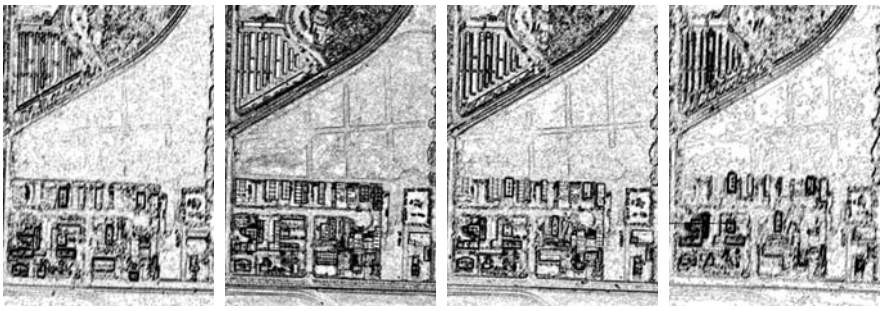

Line 2- Line 8 Window 5x5 Co-Occurrence Texture Filter, Shift X=1, Y=1 (Homogeneity)

Scene#1 Line 2- Line 8 Window 17x17 Occurrence Texture Filter

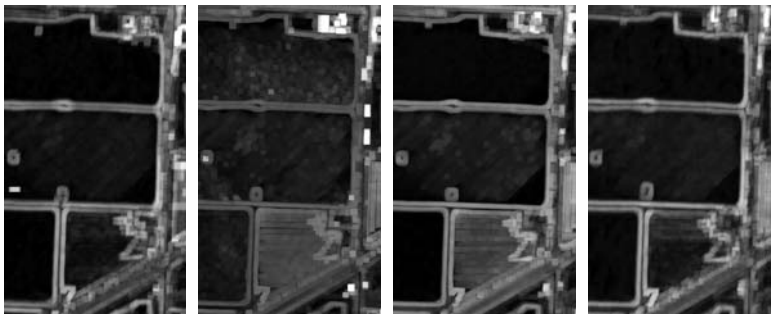

Line 2- Line 8 Window 17x17 Occurrence Texture Filter (Data Range)

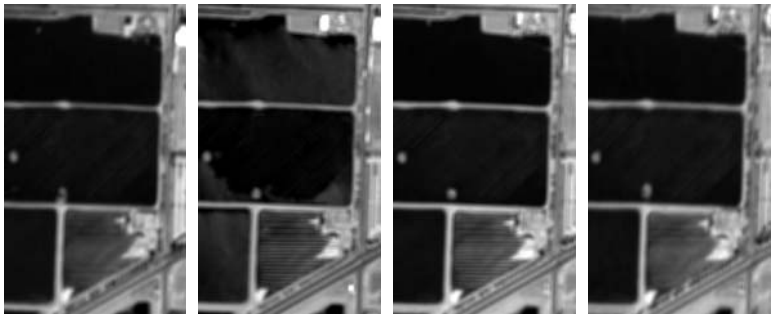

Line 2- Line 8 Window 17x17 Occurrence Texture Filter (Mean)

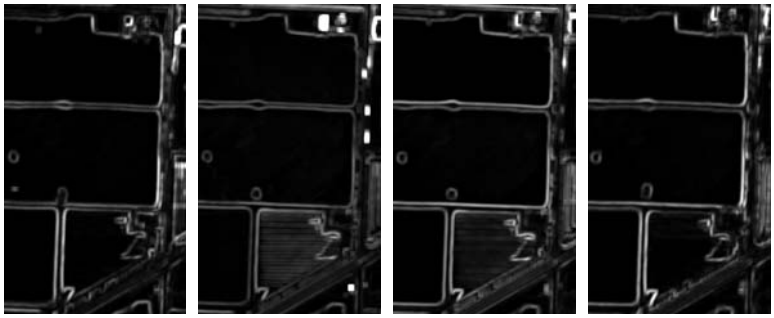

Line 2- Line 8 Window 17x17 Occurrence Texture Filter (Variance)

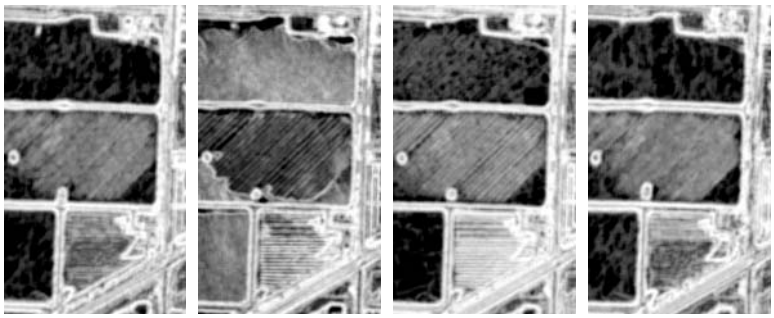

Line 2- Line 8 Window 17x17 Occurrence Texture Filter (Entropy)

Line 2- Line 8 Window 17x17 Occurrence Texture Filter (Skewness)

Scene#1 Line 2- Line 8 Window 17x17 Co-Occurrence Texture Filter, Shift X=0,Y=1

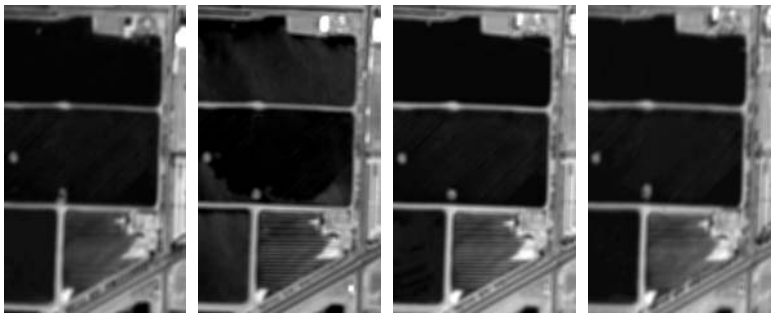

Line 2- Line 8 Window 17x17 Co-Occurrence Texture Filter, Shift X=0, Y=1 (Mean)

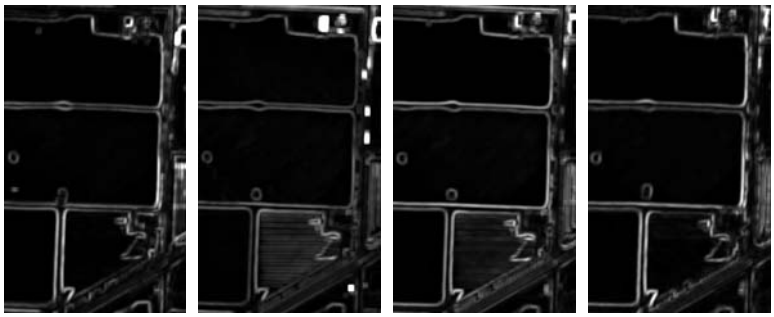

Line 2- Line 8 Window 17x17 Co-Occurrence Texture Filter, Shift X=0, Y=1 (Variance)

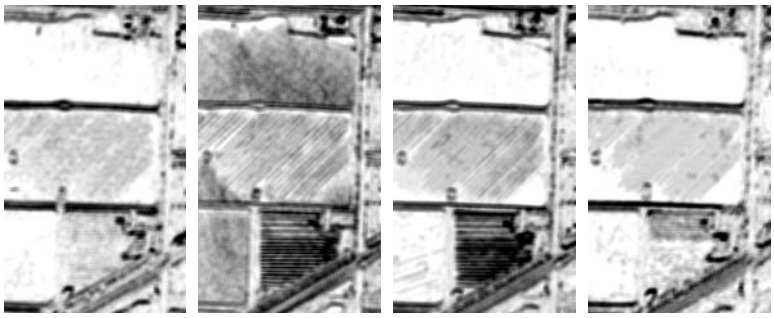

Line 2- Line 8 Window 17x17 Co-Occurrence Texture Filter, Shift X=0, Y=1 (Homogeneity)

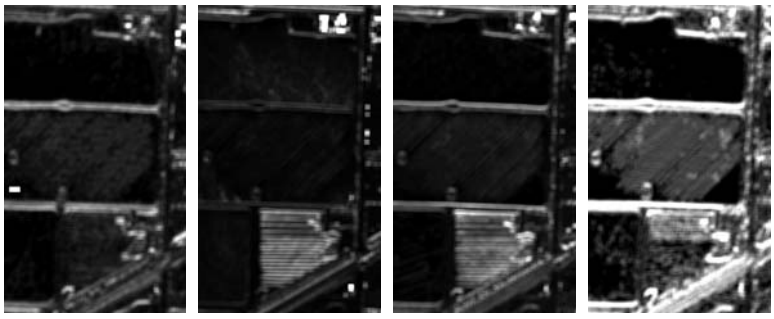

Line 2- Line 8 Window 17x17 Co-Occurrence Texture Filter, Shift X=0, Y=1 (Contrast)

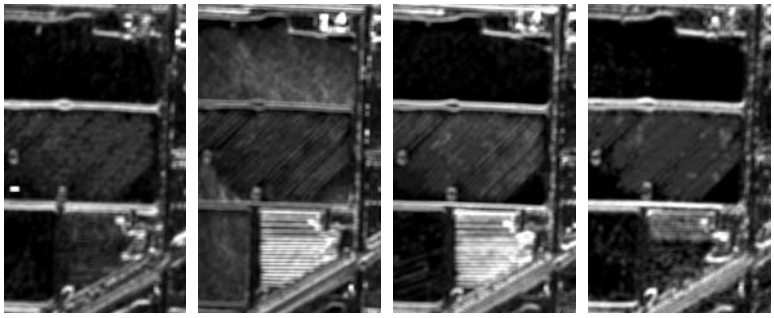

Line 2- Line 8 Window 17x17 Co-Occurrence Texture Filter, Shift X=0, Y=1 (Dissimilarity)

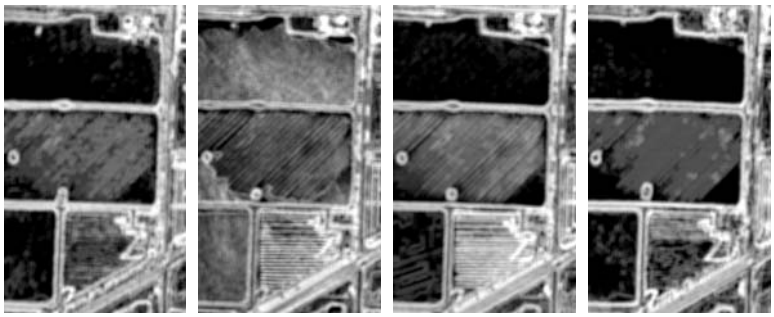

Line 2- Line 8 Window 17x17 Co-Occurrence Texture Filter, Shift X=0, Y=1 (Entropy)

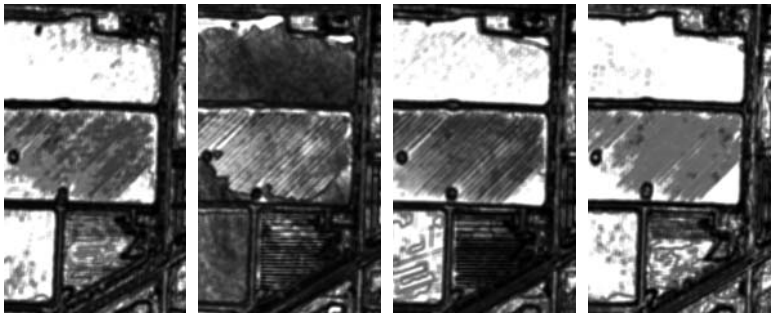

Line 2- Line 8 Window 17x17 Co-Occurrence Texture Filter, Shift X=0, Y=1 (Second Moment)

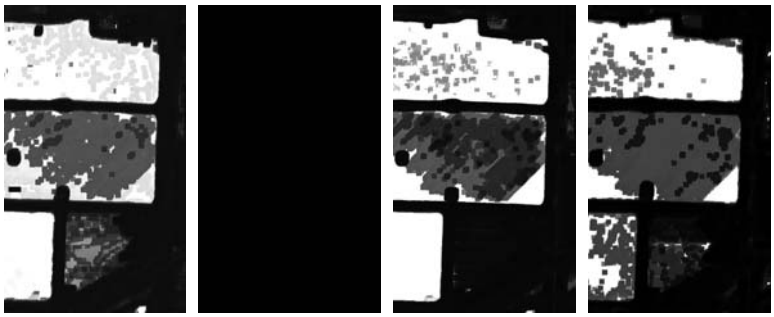

Line 2- Line 8 Window 17x17 Co-Occurrence Texture Filter, Shift X=0, Y=1 (Correlation)

Scene#1 Line 2- Line 8 Window 17x17 Co-Occurrence Texture Filter, Shift X=1,Y=0

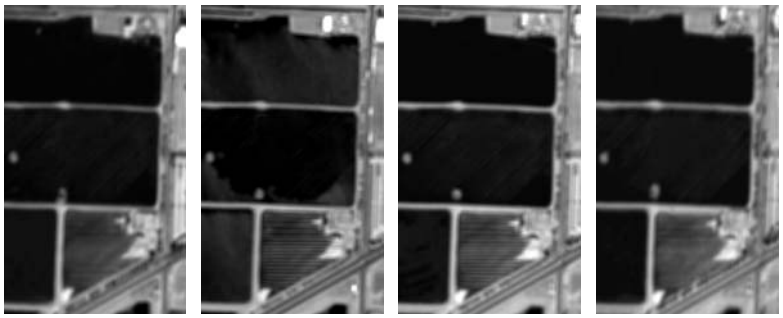

Line 2- Line 8 Window 17x17 Co-Occurrence Texture Filter, Shift X=1, Y=0 (Mean)

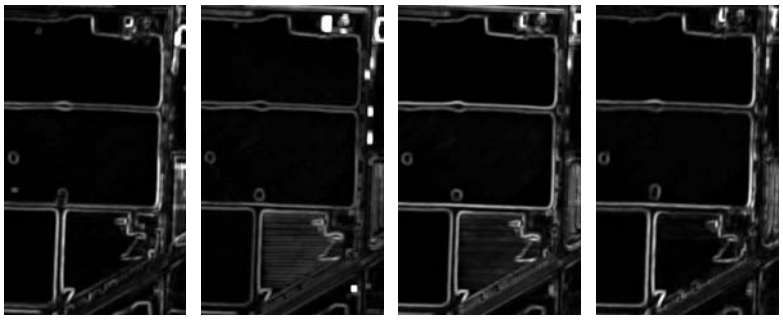

Line 2- Line 8 Window 17x17 Co-Occurrence Texture Filter, Shift X=1, Y=0 (Variance)

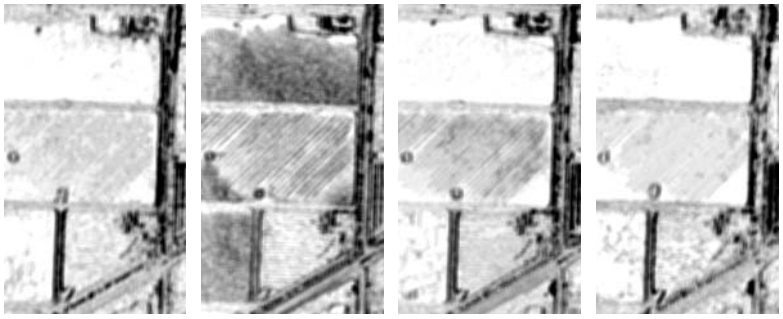

Line 2- Line 8 Window 17x17 Co-Occurrence Texture Filter, Shift X=1, Y=0 (Homogeneity)

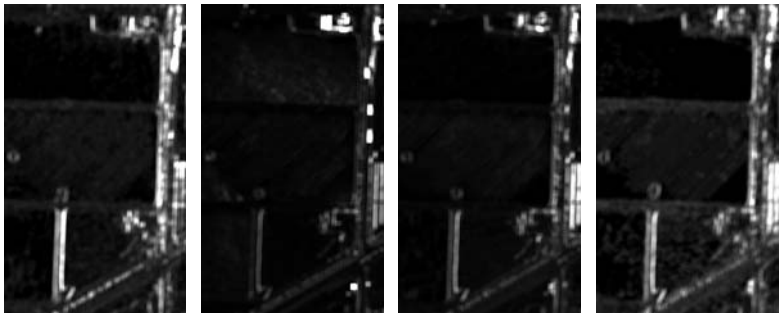

Line 2- Line 8 Window 17x17 Co-Occurrence Texture Filter, Shift X=1, Y=0 (Contrast)

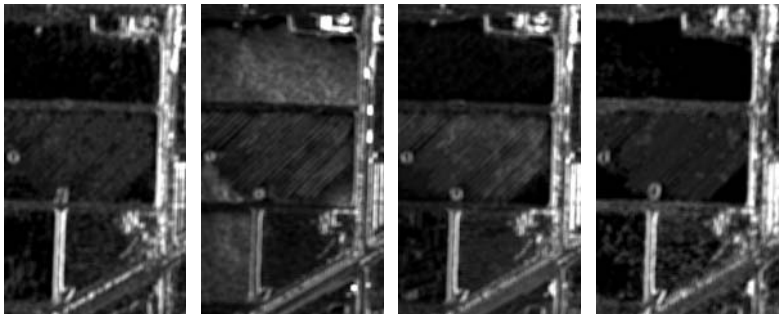

Line 2- Line 8 Window 17x17 Co-Occurrence Texture Filter, Shift X=1, Y=0 (Dissimilarity)

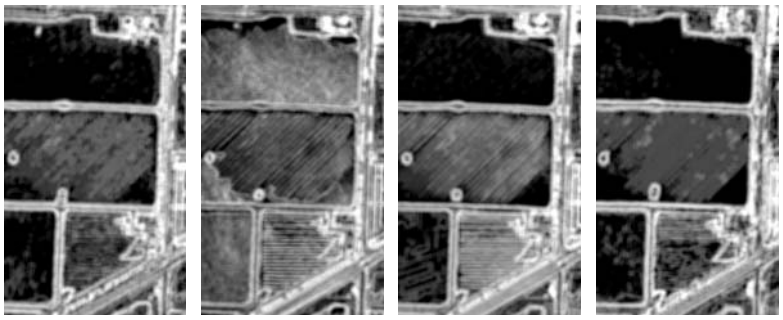

Line 2- Line 8 Window 17x17 Co-Occurrence Texture Filter, Shift X=1, Y=0 (Entropy)

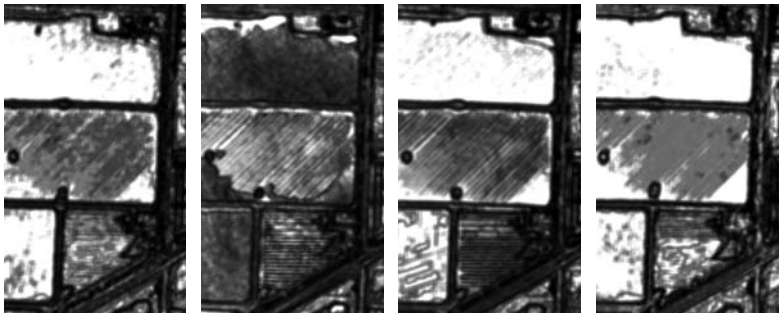

Line 2- Line 8 Window 17x17 Co-Occurrence Texture Filter, Shift X=1, Y=0 (Second Moment)

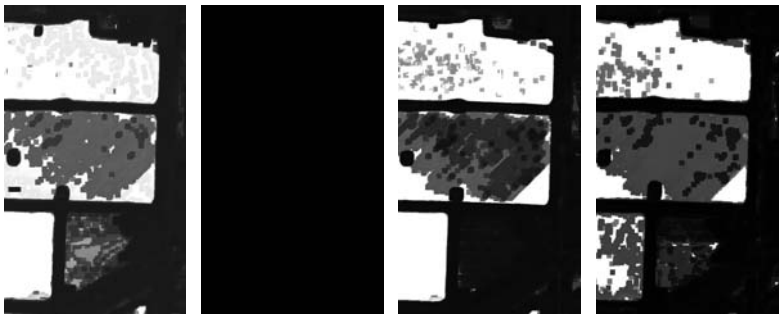

Line 2- Line 8 Window 17x17 Co-Occurrence Texture Filter, Shift X=1, Y=0 (Correlation)

Scene#1 Line 2- Line 8 Window 17x17 Co-Occurrence Texture Filter, Shift X=1,Y=1

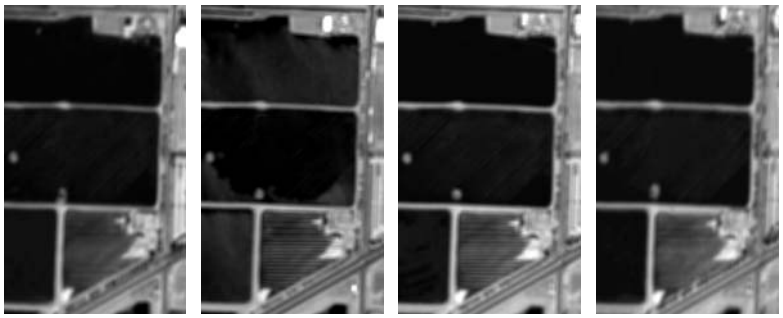

Line 2- Line 8 Window 17x17 Co-Occurrence Texture Filter, Shift X=1, Y=1 (Mean)

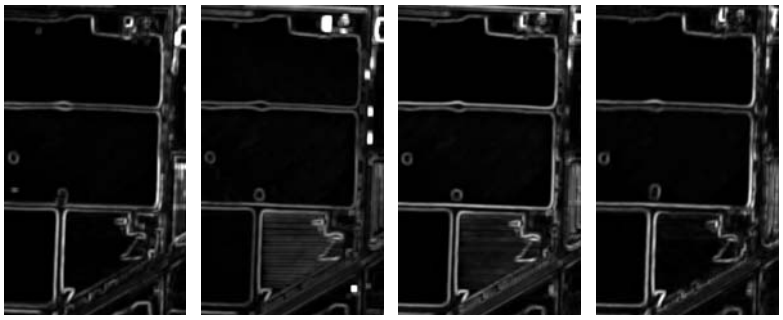

Line 2- Line 8 Window 17x17 Co-Occurrence Texture Filter, Shift X=1, Y=1 (Variance)

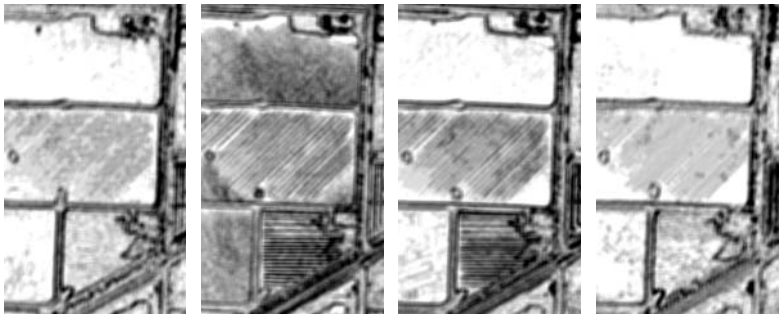

Line 2- Line 8 Window 17x17 Co-Occurrence Texture Filter, Shift X=1, Y=1 (Homogeneity)

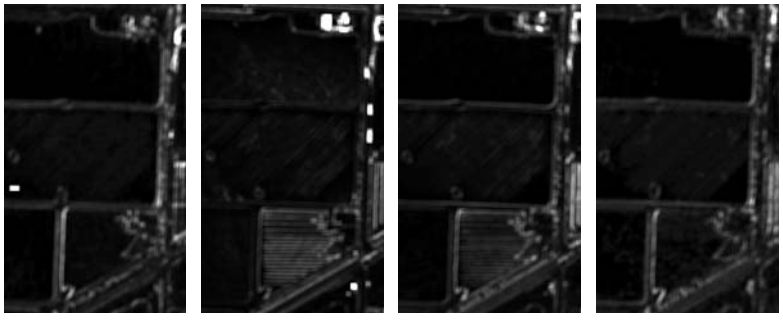

Line 2- Line 8 Window 17x17 Co-Occurrence Texture Filter, Shift X=1, Y=1 (Contrast)

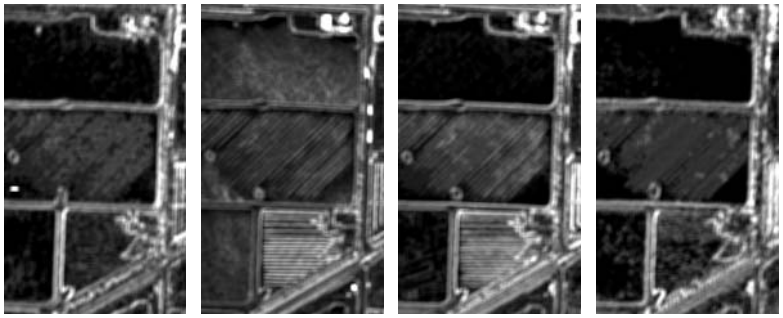

Line 2- Line 8 Window 17x17 Co-Occurrence Texture Filter, Shift X=1, Y=1 (Dissimilarity)

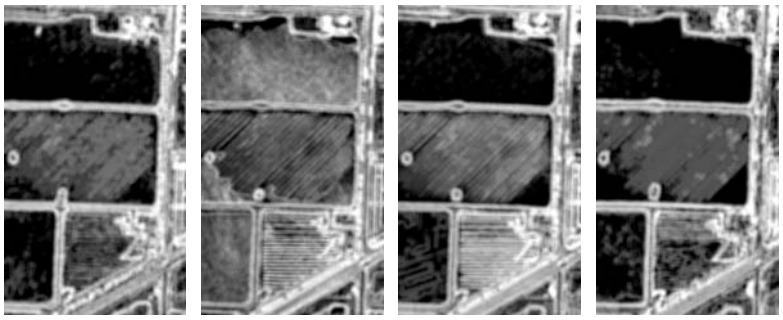

Line 2- Line 8 Window 17x17 Co-Occurrence Texture Filter, Shift X=1, Y=1 (Entropy)

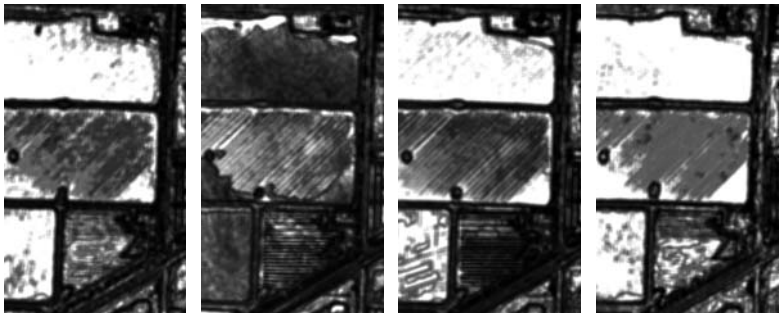

Line 2- Line 8 Window 17x17 Co-Occurrence Texture Filter, Shift X=1, Y=1 (Second Moment)

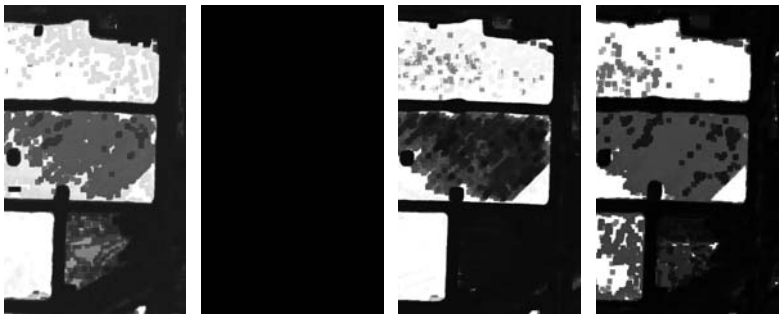

Line 2- Line 8 Window 17x17 Co-Occurrence Texture Filter, Shift X=1, Y=1 (Correlation)

Scene#2 Line 2- Line 8 Window 17x17 Co-Occurrence Texture Filter, Shift X=0,Y=1

Line 2- Line 8 Window 17x17 Co-Occurrence Texture Filter, Shift X=0, Y=1 (Mean)

Line 2- Line 8 Window 17x17 Co-Occurrence Texture Filter, Shift X=0, Y=1 (Variance)

Line 2- Line 8 Window 17x17 Co-Occurrence Texture Filter, Shift X=0, Y=1 (Homogeneity)

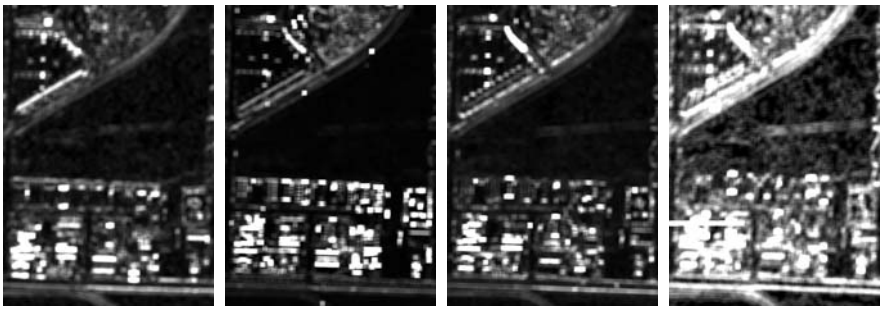

Line 2- Line 8 Window 17x17 Co-Occurrence Texture Filter, Shift X=0, Y=1 (Contrast)

Line 2- Line 8 Window 17x17 Co-Occurrence Texture Filter, Shift X=0, Y=1 (Dissimilarity)

Line 2- Line 8 Window 17x17 Co-Occurrence Texture Filter, Shift X=0, Y=1 (Entropy)

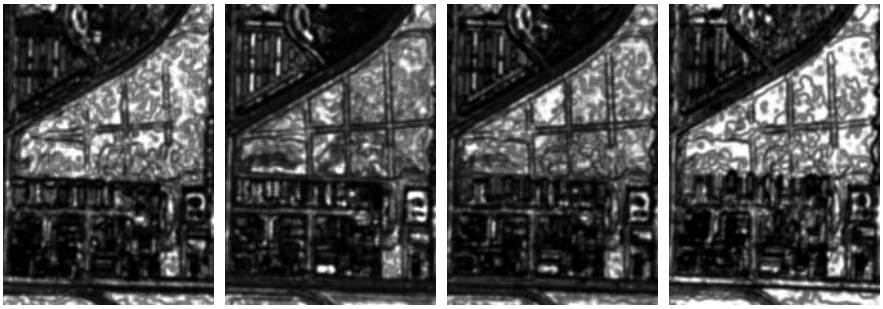

Line 2- Line 8 Window 17x17 Co-Occurrence Texture Filter, Shift X=0, Y=1 (Second Moment)

Line 2- Line 8 Window 17x17 Co-Occurrence Texture Filter, Shift X=0, Y=1 (Correlation)

Scene#2 Line 2- Line 8 Window 17x17 Co-Occurrence Texture Filter, Shift X=1,Y=0

Line 2- Line 8 Window 17x17 Co-Occurrence Texture Filter, Shift X=1, Y=0 (Mean)

Line 2- Line 8 Window 17x17 Co-Occurrence Texture Filter, Shift X=1, Y=0 (Variance)

Line 2- Line 8 Window 17x17 Co-Occurrence Texture Filter, Shift X=1, Y=0 (Homogeneity)

Line 2- Line 8 Window 17x17 Co-Occurrence Texture Filter, Shift X=1, Y=0 (Contrast)

Line 2- Line 8 Window 17x17 Co-Occurrence Texture Filter, Shift X=1, Y=0 (Dissimilarity)

Line 2- Line 8 Window 17x17 Co-Occurrence Texture Filter, Shift X=1, Y=0 (Entropy)

Line 2- Line 8 Window 17x17 Co-Occurrence Texture Filter, Shift X=1, Y=0 (Second Moment)

Line 2- Line 8 Window 17x17 Co-Occurrence Texture Filter, Shift X=1, Y=0 (Correlation)

Scene#2 Line 2- Line 8 Window 17x17 Co-Occurrence Texture Filter, Shift X=1,Y=1

Line 2- Line 8 Window 17x17 Co-Occurrence Texture Filter, Shift X=1, Y=1 (Mean)

Line 2- Line 8 Window 17x17 Co-Occurrence Texture Filter, Shift X=1, Y=1 (Variance)

Line 2- Line 8 Window 17x17 Co-Occurrence Texture Filter, Shift X=1, Y=1 (Homogeneity)

Line 2- Line 8 Window 17x17 Co-Occurrence Texture Filter, Shift X=1, Y=1 (Contrast)

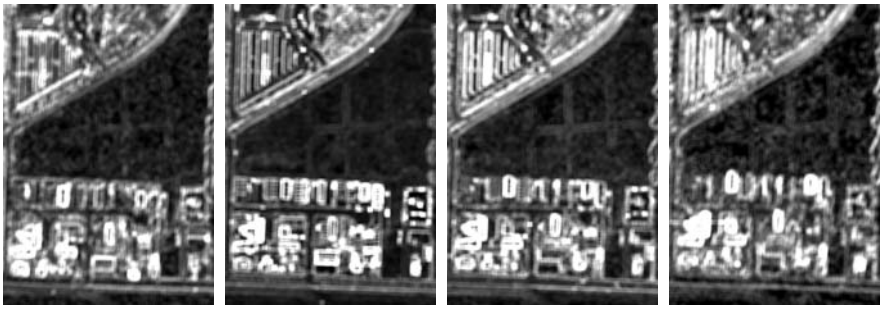

Line 2- Line 8 Window 17x17 Co-Occurrence Texture Filter, Shift X=1, Y=1 (Dissimilarity)

Line 2- Line 8 Window 17x17 Co-Occurrence Texture Filter, Shift X=1, Y=1 (Entropy)

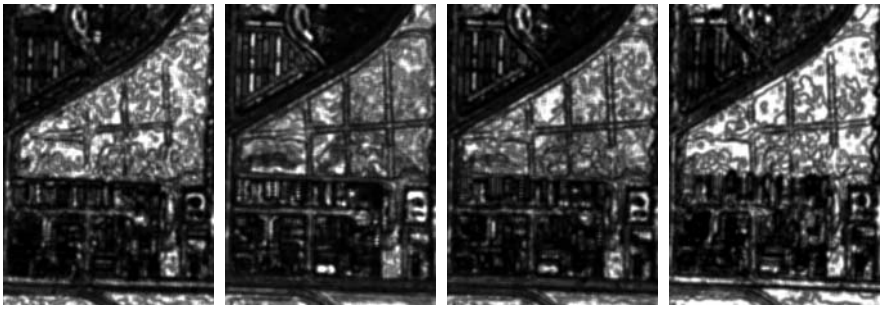

Line 2- Line 8 Window 17x17 Co-Occurrence Texture Filter, Shift X=1, Y=1 (Second Moment)

Line 2- Line 8 Window 17x17 Co-Occurrence Texture Filter, Shift X=1, Y=1 (Correlation)

Scene#2 Line 2- Line 8 Window 17x17 Co-Occurrence Texture Filter (Homogeneity)

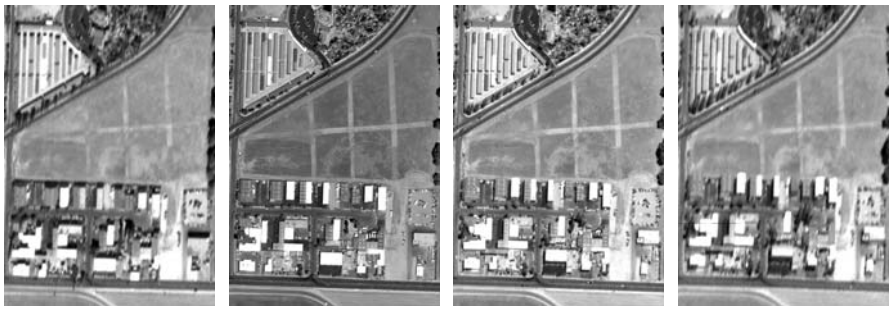

Scene#2, Line 2- Line 8 (Without any texture filter)

Line 2- Line 8 Window 17x17 Co-Occurrence Texture Filter, Shift X=0, Y=1 (Homogeneity)

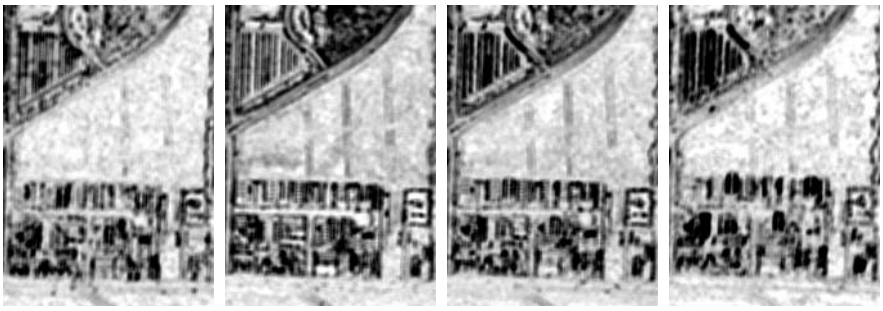

Line 2- Line 8 Window 17x17 Co-Occurrence Texture Filter, Shift X=1, Y=0 (Homogeneity)

Line 2- Line 8 Window 17x17 Co-Occurrence Texture Filter, Shift X=1, Y=1 (Homogeneity)

THIS PAGE INTENTIONALLY LEFT BLANK

APPENDIX B. MAGNIFIED PORTIONS COMPARED WITH TRUE AND FALSE COLOR IR IMAGES

True Color

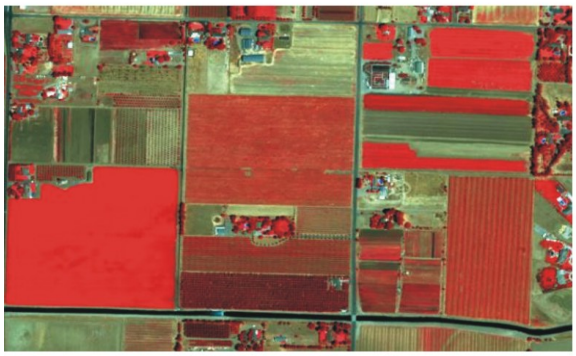

False Color IR

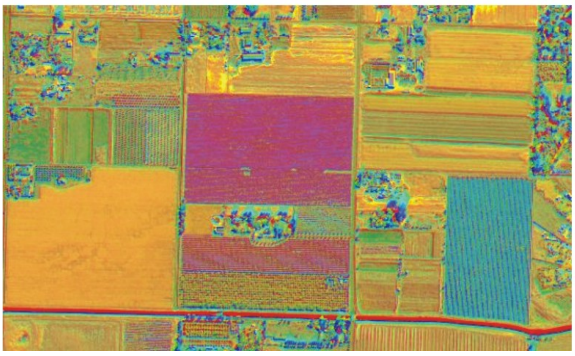

BDRF Lines 8, 6, 4

THIS PAGE INTENTIONALLY LEFT BLANK

APPENDIX C. 25 COLOR KEY

THIS PAGE INTENTIONALLY LEFT BLANK

APPENDIX D. CLASSIFICATION RESULTS

Classification Results

True Color IR

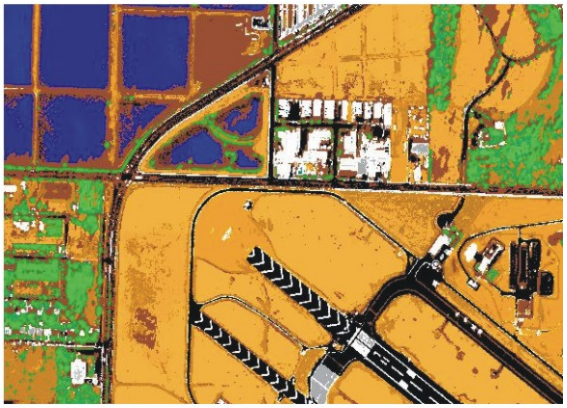

MSI Classification

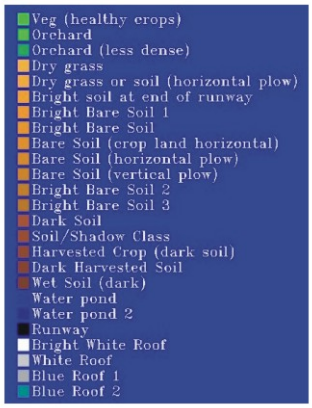

Color Key

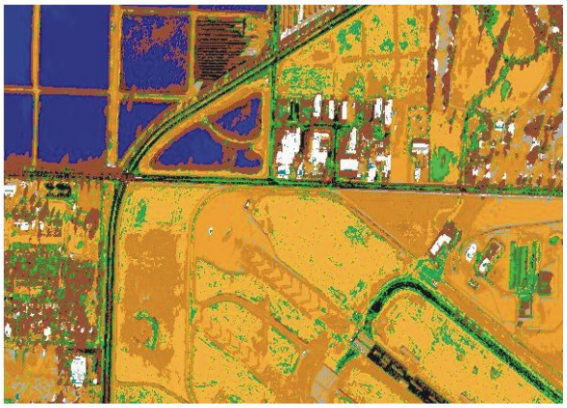

BDRF Classification

THIS PAGE INTENTIONALLY LEFT BLANK

APPENDIX E. TEXTURE CLASSIFICATION RESULTS

Texture Classification Results

Panchromatic

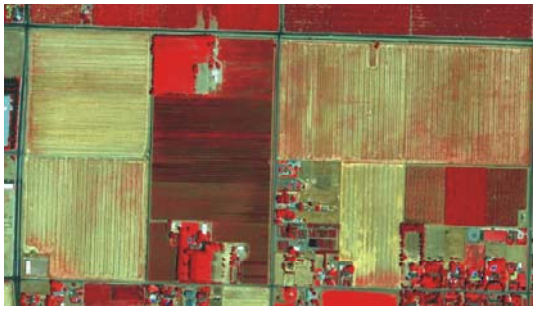

False Color IR

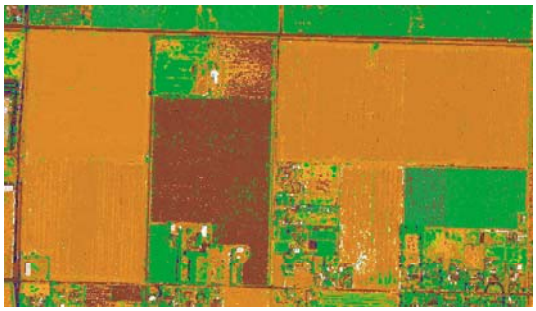

X:1, Y:0

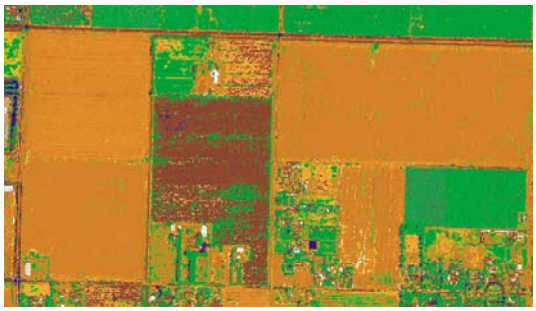

X:0, Y:1

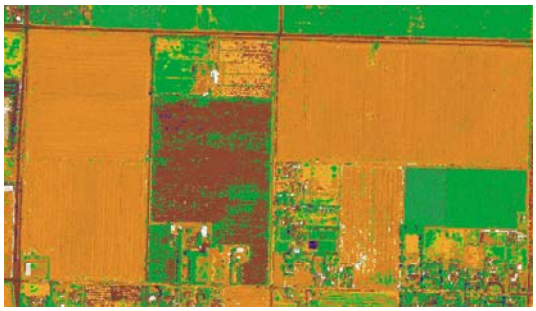

X:1, Y:1

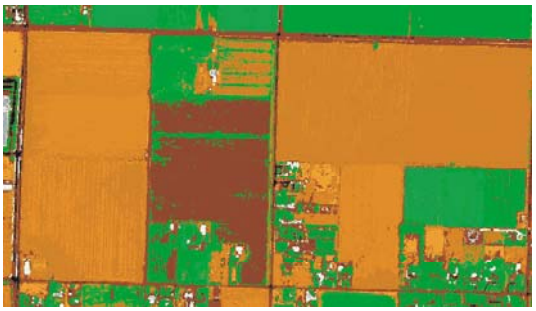

MSI Classification

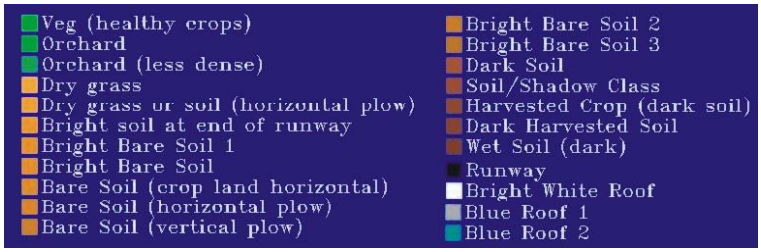

THIS PAGE INTENTIONALLY LEFT BLANK

LIST OF REFERENCES

Avery, Thomas E., and Berlin, Graydon, L. *Fundamentals of Remote Sensing and Airphoto Interpretation, Fifth Edition.* Macmillan Publishing Company, 1992.

Brandt, Tso and Mather, Paul. *Classification Methods for Remotely Sensed Data.* Taylor & Francis, 2001.

Breon, F. M., Deschamps, P. Y., Leroy, M., Podaire, A., Bricaud, A., Buriez, J. C., and Seze, G. "The POLDER Mission: Instrument Characteristics and Scientific Objectives" *IEEE Transactions on Geoscience & Remote Sensing,* Volume 32(3), pp. 598-614, 1994.

Breon, F. M., Maignan, F., Leroy M., and Grant, I. "Analysis of the Hot Spot Directional Signatures Measured from Space" *Journal of Geophysical Research,* 107(D16)(10.1029/2001JD001094), 2002.

Breon, F. M., Vanderbilt, V., Leroy M., Bicheron, P., Walthall, C. L., and Kalshoven, J. E. "Evidence of Hot Spot Directional Signature from Airborne POLDER Measurements", *IEEE Trans. Geosci. Remote Sens.*, Volume 35, pp. 479-484, 1997.

Campbell, James B. *Introduction to Remote Sensing,* Third Edition. The Guilford Press, 2002.

Chen, L. C., and Lee, L. H. "Progressive Generation of Control Frameworks for Image Registration," *Photogrammetric Engineering and Remote Sensing,* Volume 58 (9), pp 1321-1328, 1992.

Department of Defense. *Multispectral User's Guide*. August 1995.

Fernando C. C. "Evaluation of the DISMA Prototyping Algorithm for Vegetation Parameters Retrieval on a Global Scale Using the BRDF PLODER/ADEOS Database" *Eumetat LSA SAF Visiting Scientist Report,* 2003.

Gehrels, T. "Photometric Studies of Asteroids." *Astrophysical Journal,* Volume 123, pp. 331-338. 1956.

Gerstl, S. A. W., and Simmer C. "Radiation Physics and Modeling for off-Nadir Satellite Sensing of Non-Lambertian Surfaces," *Remote Sens. Environ.,* Volume 20, pp. 1-29, 1986.

Hapke, B., DiMucci, D., Nelson, R., and Smythe, W., "The Cause of the Hot Spot in Vegetation Canopies and Soils: Shadow Hiding versus Coherent Backscatter", *Remote Sens. Environ.,* Volume 58, pp. 63-68, 1996.

Haralick, Robert M., Shanmugam, K., and Dinstein, Its'hak. "Textural Features for Image Classification." *IEEE Transactions on Systems, Man, and Cybernetics.* Volume SMC-3, Number 6, pp. 610-621, November 1973.

Hsu, Shin-Yi. “Texture-Tone Analysis for Automated Land-Use Mapping.” *Photogrammetric Engineering and Remote Sensing.* Volume 44, Number 11, pp. 1393-1404, November 1978.

http://math.nist.gov/~FHunt/appearance/brdf.html, 20 August 2004.

http://rst.gsfc.nasa.gov/Sect1/Sect1_19.html, 17 February 2005.

http://smsc.cnes.fr/POLDER/, 21 August 2004.

http://smsc.cnes.fr/POLDER/GP_instrument.htm, 13 October 2004.

http://www.4physics.com/tn3/lambertian.htm, 4 September 2004.

http://www.exportcenter.net/FresnoCountyAgExportsReport20001revised.pdf, 9 October 2004.

http://www.geo.unizh.ch/rsl/research/SpectroLab/goniometry/brdf_intro.shtml, 8 July 2004.

http://www.geo.unizh.ch/rsl/research/SpectroLab/goniometry/brdf_intro.shtml, 8 July 2004.

http://www.mapquest.com, 25 January 2005.

http://www.pixoneer.co.kr/main/ pro/pg_steamer/Education_Module.pdf, 4 September 2004.

http://www.sovereign-publications.com/digitalglobe.htm, 9 October 2004.

Hughes, Gordon F., “On the Mean Accuracy of Statistical Pattern Recognizers.” *IEEE Transactions on Information Theory.* Volume IT-14, Number 1, pp. 55-63, January 1968.

Humphrey, Donald M., “Texture Analysis of High Resolution Panchromatic Imagery for Terrain Classification.” Master’s Thesis, Naval Postgraduate School, 2003.

Jensen, John R. *Introductory Digital Image Processing: A Remote Sensing Perspective, Second Edition*. Prentice Hall, 1996.

Jensen, J. R., Hodgson, M. E., Christensen, E. J., Mackey, H. E., Tinney, L. T., and Sharitz, R. R. “Remote Sensing Inland Wetlands: A Multispectral Approach.” *Photogrammetric Engineering and Remote Sensing.* Volume 52, pp 87-110, 1986.

Jensen, John R. *Remote Sensing of the Environment: An Earth Resource Perspective*. Prentice Hall, 2000.

Lillesand, Thomas M., Keifer, Ralph W., and Chipman Jonathan W. *Remote Sensing and Image Interpretation, Fifth Edition.* John Wiley and Sons, Inc., 2004.

Matter P. M. *Computer Processing of Remotely-Sensed Images: An Introduction.* Wiley, 1999.

Nicodemus, F. E. "Directional Reflectance and Emissivity of an Opaque Surface," *Appl. Opt*., Volume 4, pp. 767-773, 1965.

Nicodemus F. E. "Reflectance Nomenclature and Directional Reflectance and Emissivity." Appl. Opt., Volume 9(6), pp. 1474-1475, 1970.

Olsen, R. C. *Remote Sensing from Air and Space.* August 2003.

Research Systems Incorporated. *ENVI User's Guide. September 2003 Edition,* Research Systems, Inc. September 2003.

Richards, John A., and Xiuping, Jia. *Remote Sensing Digital Image Analysis, Third Edition*. Springer, 1999.

Roujean, J. L., Leroy, M., and Deschamps, P. Y. "A Bidirectional Reflectance Model of the Earth's Surface for the Correction of Remote Sensing Data," *Journal of Geophysical Research*, Volume 97, Number 20, pp. 455-20, 468, 1992.

Sabins, Floyd F. *Remote Sensing Principles and Interpretation, Third Edition*. Freeman and Company, 1996.

Sandmeier, S. R. and Itten, K. I. "Field Goniometer System (FIGOS) for Acquisition of Hyperspectral BRDF Data, "*IEEE Transactions on Geoscience & Remote Sensing*, Volume37(2), pp 978-986, 1999.

Slater P. N. *Remote Sensing: Optics and Optical Systems*. Addison-Wesley, 1980.

THIS PAGE INTENTIONALLY LEFT BLANK

INITIAL DISTRIBUTION LIST

1. Defense Technical Information Center
   Ft. Belvoir, Virginia

2. Dudley Knox Library
   Naval Postgraduate School
   Monterey, California

3. Dr. Richard C. Olsen, Code PH
   Naval Postgraduate School
   Monterey, California

4. William J. Welch, Code IS
   Naval Postgraduate School
   Monterey, California

5. Prof. John Schott
   Rochester Institute of Technology
   Rochester, New York

6. Steve Irish
   DigitalGlobe
   Longmont, Colorado